PHYSICAL REVIEW C **93**, 054321 (2016)

Complete identification of states in ^{208}Pb below $E_x = 6.2$ MeV

A. Heusler*
Gustav-Kirchhoff-Strasse 7/1, D-69120 Heidelberg, Germany

R. V. Jolos
Bogoliubov Laboratory of Theoretical Physics, JINR, Dubna State University, 141980 Dubna, Moscow Region, Russia and Dubna State University, 141980 Dubna, Moscow Region, Russia

T. Faestermann
Lehrstuhl für Physik der Hadronen und Kerne (E12), Technische Universität München, D-85748 Garching, Germany

R. Hertenberger
Fakultät für Physik, Ludwig-Maximilians-Universität München, D-85748 Garching, Germany

H.-F. Wirth
Lehrstuhl für Physik der Hadronen und Kerne (E12), Technische Universität München and Fakultät für Physik, Ludwig-Maximilians-Universität München, D-85748 Garching, Germany

P. von Brentano
Institut für Kernphysik, Universität zu Köln, D-50937 Köln, Germany
(Received 4 December 2015; published 23 May 2016)

The Q3D magnetic spectrograph at the Maier-Leibnitz-Laboratorium of the Ludwig-Maximilians-Universität München and the Technische Universität München (Garching, Germany), was used to study the ^{208}Pb(p,p'), ^{206,207,208}Pb(d,p), and ^{208}Pb(d,d') reactions. One hundred fifty-one states at $E_x < 6.20$ MeV in ^{208}Pb are identified and spin and parity assigned. Four states are newly identified and new spins and/or parities are assigned to 25 states. Tentative spin assignments are done to five states at $5.90 < E_x < 6.10$ MeV. Nearly 50 levels below $E_x = 6.20$ MeV listed by the Nuclear Data Sheets as of 2007 are recognized to be nonexistent or doubly placed. The schematic shell model describing one-particle–one-hole configurations without residual interaction is extended by including two-particle–two-hole configurations. The number of configurations thus predicted at $E_x < 6.20$ MeV nearly agrees with the number of states identified. Several states with dominant two-particle–two-hole configurations are identified. New isobaric analog resonances in ^{209}Bi with two-particle–one-hole structure are discovered at $E^{\rm res} = 17.6$ MeV. The excitation energies of 70 states with unnatural parity at $E_x < 6.20$ MeV are found to agree within about 200 keV with one-particle–one-hole configurations predicted by the extended schematic shell model. In contrast, the excitation energies of about 20 natural parity states are more than 0.5 MeV lower than predicted, demonstrating the residual interaction among the configurations to be much larger for natural parity than for unnatural parity.

DOI: 10.1103/PhysRevC.93.054321

I. INTRODUCTION

Particle-exchange reactions on lead isotopes employing beams of light nuclei excite more than 300 bound states in the doubly magic nucleus ^{208}Pb, as listed by the Nuclear Data Sheets [1] (NDS2007); the particle thresholds are $S(n) = 7368$ keV for neutrons and $S(p) = 8000$ keV for protons. Particle spectroscopy clearly recognizes each state unambiguously, in principle. However, the resolution is insufficient to resolve all states and, in addition, each nuclear level is accompanied by satellites from the simultaneous emission of up to 82 electrons.

In contrast, γ spectroscopy suffers from the need to reconstruct the level scheme from coincidence measurements. Weak levels are often missed and close doublets are not well resolved.

Using the Q3D magnetic spectrograph of the Maier-Leibnitz-Laboratorium (MLL) of the Ludwig-Maximilians-Universät München and the Technische Universät München at Garching (Germany) [2–4], the ^{208}Pb(p,p') and ^{206,207,208}Pb(d,p) reactions have been studied with a mean resolution of 3 keV [5–20]; recently, also the ^{208}Pb(d,d') reaction has been studied.

Inelastic proton scattering via isobaric analog resonances (IARs) is equivalent to a neutron pickup reaction on a target in an excited state or in the ground state [21–30]. Experiments with the ^{208}Pb(p,p') reaction covered seven known IARs in ^{209}Bi [25] and several off-resonance regions [21–26,28,31]. Hence, ten different particle-exchange reactions exciting states in ^{208}Pb were studied.

The high linearity of the Q3D magnetic spectrograph makes it possible to determine excitation energies for states in ^{208}Pb

*a.heusler@mpi-hd.mpg.de

with an absolute uncertainty down to 10 eV by calibration with excitation energies from NDS2007. The precision for about 50 states is better than obtained by NDS2007, but within the statistical uncertainty of 2σ.

Cross sections of 1–1500 μb/sr were determined at scattering angles between 20° and 138° for about 300 levels up to $E_x = 8.0$ MeV. More than 30 doublets with a spacing down to 400 eV are resolved. More than 30 proton bombarding energies were chosen to cover the known IARs [25] in ^{209}Bi and several off-resonance regions in the ^{208}Pb(p,p') reaction; energies of $E_d = 22$ and 24 MeV were chosen for the ^{208}Pb(d,d') and ^{206,207,208}Pb(d,p) reactions.

The ^{207}Pb(d,p) reaction [32–34] and the ^{208}Pb(p,p') reaction via IAR in ^{209}Bi populate the states in ^{208}Pb [21–28] in a highly selective manner. Similarly, the ^{206}Pb(t,p) and ^{210}Pb(p,t) reactions [35–37] and the ^{209}Bi(d,^{3}He) [38–41] and ^{208}Pb(α,α') reactions [33,34,42–44] populate the states selectively. Here, however, the resolution is insufficient and most levels contain more than one state. (The coincidence measurements for the ^{207}Pb(d,$p\gamma$), ^{209}Bi(t,$\alpha\gamma$), and Pb(p,$p'\gamma$) reactions [45–47] improved the resolution.) The ^{208}Pb(e,e') reaction [48–52] is also highly selective. Yet the resolution of 15–60 keV hardly makes it possible to identify a single state amidst the dense sequence of states without the help of other experimental data.

In contrast, the ^{208}Pb(n,$n'\gamma$) [1,53–57] and ^{208}Pb(d,d') reactions excite all states with little selectivity, similar to the ^{208}Pb(p,p') reaction [33,34,58–64], far beyond the known IARs in ^{209}Bi [25]. The cross sections do not much depend on the structure, spin, and parity of the state. Only at forward-scattering angles the diffraction pattern gives a hint to the transferred angular momentum. Yet in our experiments we took data only in a limited range of medium scattering angles (Table V).

The selective excitation by the ^{208}Pb(p,p'), ^{207}Pb(d,p), and ^{209}Bi(d,^{3}He) reactions makes it possible to determine major components of particle-hole configurations with a given particle or hole from excitation functions and angular distributions.

We attempt to gain complete spectroscopy for ^{208}Pb at $E_x < 6.20$ MeV. We rely on the comparison to predictions by the schematic shell model without residual interaction (sSM) [12] extended by including the diagonal part of the surface δ interaction [16,65].

All negative-parity states predicted by the sSM below $E_x^{\rm sSM} = 6361$ keV were recently identified [17,18], as well as many positive-parity states [1,12].

The schematic model is further extended by including the coupling of one-particle–one-hole configurations to the lowest collective states with low spins and to each other and the coupling of the lowest collective states to each other. Similar considerations were presented earlier [35–37,66–71]. The surface δ interaction [16,65] is used to refine the extended schematic model (eSM). It makes it possible to predict both one-particle–one-hole and two-particle–two-hole configurations (Secs. II A and II D) in a reliable manner.

By chance, the eSM predicts a large gap in the sequence of configurations for all spins and both parities for states in ^{208}Pb at $E_x \approx 6.2$ MeV. Spins from 1^+ to 12^+ and from 0^- to 8^- are expected at $E_x < 6.20$ MeV. Indeed, no state is firmly identified in the interval $6.11 < E_x < 6.19$ MeV, while the mean spacing of states at $4.6 < E_x < 6.2$ MeV is 12 keV. The first significant gap opens from $E_x = 4.48$ to $E_x = 4.61$ MeV after the 24 lowest states.

Below $E_x = 6.20$ MeV, 151 states are identified in near agreement with the number of states predicted by the eSM. Since the publication of NDS2007 five new states have been identified and new spin and parity assignments for 59 states have been determined [5,6,10–12,14–18], including four new state identifications and 30 spin and parity assignments discussed in this paper.

Nearly every state is excited by the ^{208}Pb(d,d') reaction and nearly all states are populated by the ^{208}Pb(p,p') reaction via IARs in ^{209}Bi or off-resonance; two-thirds of the states are populated by the ^{207}Pb(d,p) reaction. The ^{209}Bi(d,^{3}He) reaction was performed with a resolution of 12–15 keV [40]; hence, half of the levels are unresolved doublets. The ^{208}Pb(α,α') reaction performed with a resolution of 11 keV [42,43] and 8 keV [33,34,44] populates only natural parity states.

Remarkably, some states with spins 7^-, 8^- and from 1^+ to 6^+ and 12^+ are excited by the ^{207}Pb(d,p) reaction, while no particle-hole configuration is known in the sSM, which may be generated by starting with a $p_{1/2}$ neutron hole coupled to the bare ^{208}Pb core (Sec. V E). Some of these states are populated by newly discovered IARs at $E^{\rm res} = 17.6$ MeV in ^{209}Bi.

The recalibration of the excitation energies from the ^{206}Pb(t,p) and ^{210}Pb(p,t) experiments [36,37] clearly identified many natural parity states. Most of them with large cross sections are explained by the population of two-particle–two-hole configurations with the pairing force [20,67,68].

Although the level density in ^{208}Pb is low, because of the multitude of spins and the two parities (28 values in total at $E_x < 6.5$ MeV), not all states are resolved; about one-fourth of the levels contain states with distances less than 3 keV. Such doublets, even with vanishing distances, are recognized by various different methods (Secs. III F and III G 3).

In Sec. II the description of states by simple models is discussed. In Sec. III the observation of states below $E_x = 6.20$ MeV in ^{208}Pb by different particle-exchange reactions is discussed. In Sec. IV the identification and spin and parity assignments of states are discussed. Shortly, the completeness and peculiar structure information for states in ^{208}Pb are discussed in Sec. V. About one-quarter of the levels below $E_x = 6.20$ MeV shown in NDS2007 are recognized to be nonexistent or doubly placed (Sec. VI).

II. STATES IN ^{208}Pb

A. The schematic shell model

The schematic shell model without residual interaction assumes the same excitation energy for each combination of particles and holes describing a configuration in ^{208}Pb, independent on the total spin I^π.

1. Schematic shell model for particle-hole configurations

The schematic shell model without residual interaction for one-particle–one-hole configurations [12] is a good guideline to find nuclear states in ^{208}Pb. It describes the excitation energies of the particle-hole states in the doubly magic nucleus ^{208}Pb by the sum of the mass differences ΔQ [72,73] between the ground states of the four neighboring nuclei of ^{208}Pb (^{207}Tl, ^{209}Bi, ^{207,209}Pb) and ^{208}Pb itself and the excitation energies of

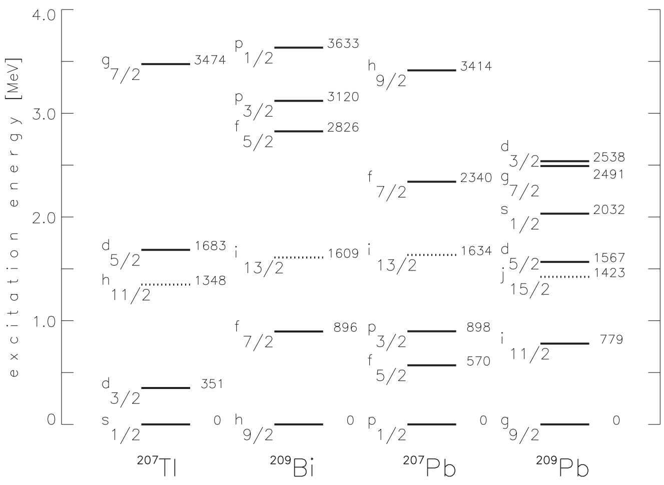

FIG. 1. Level schemes in the four neighbors of the doubly magic nucleus ^{208}Pb, single-hole levels in ^{207}Tl and ^{207}Pb, and single-particle levels in ^{209}Bi and ^{209}Pb. Dotted lines denote intruder orbits (reverse parity).

the particle states [$E_x(LJ)$] and the hole states [$E_x(lj)$] in the four neighboring nuclei [74]:

$$\begin{aligned}&\text{protons } (\tau=\pi) \text{ in the orbits}\\ &\quad lj \text{ for } 50 \leqslant Z \leqslant 82 \quad \text{and } LJ \text{ for } 82 \leqslant Z \leqslant 126\\ &\text{and neutrons } (\tau=\nu) \text{ in the orbits}\\ &\quad lj \text{ for } 82 \leqslant N \leqslant 126 \quad \text{and } LJ \text{ for } 126 \leqslant N \leqslant 184 \end{aligned} \tag{1}$$

are considered. Figure 1 shows the single-particle levels and the single-hole levels in the four neighboring nuclei of ^{208}Pb. By mere chance the excitation energy of the intruder orbit has a similar distance to the ground state in all four nuclei.

The Coulomb interaction between the particle in orbit LJ and the hole in orbit lj is assumed as a constant [12]; for neutrons it vanishes. For the proton configurations in reality, it depends on the configuration; for $h_{9/2}s_{1/2}$, $h_{9/2}d_{3/2}$, $h_{9/2}d_{5/2}$, $h_{9/2}h_{9/2}$, $f_{7/2}s_{1/2}$, $f_{7/2}d_{3/2}$, values are determined from experiment [18]. By using different values for the Coulomb energy in dependence on the angular momentum L of the particle,

$$\begin{aligned} E^{\text{Coul}}(\pi,LJ,lj) &= -350 \text{ keV} \quad \text{for } LJ=i_{13/2},\\ E^{\text{Coul}}(\pi,LJ,lj) &= -300 \text{ keV} \quad \text{for } LJ=h_{9/2},\\ E^{\text{Coul}}(\pi,LJ,lj) &= -200 \text{ keV} \quad \text{for } LJ=f_{7/2}, f_{5/2}, p_{3/2}, p_{1/2},\\ &\qquad\qquad \text{and } lj=s_{1/2}, d_{3/2}, d_{5/2}, g_{7/2}, h_{11/2},\\ E^{\text{Coul}}(\nu,LJ,lj) &= 0 \text{ keV} \quad \text{for all neutron configurations,} \end{aligned} \tag{2}$$

the schematic shell model [12] is refined. In the refined schematic shell model without residual interaction (sSM) the excitation energy is calculated as

$$\begin{aligned} E_x^{sSM}(Lj,lj) &= E_x(LJ)+E_x(lj)+\Delta Q(\tau)+E^{\text{Coul}}(\tau,LJ,lj),\\ &\text{with } \Delta Q(\nu) = 3.431 \text{ MeV},\\ &\text{and } \Delta Q(\pi) = 4.214 \text{ MeV}. \end{aligned} \tag{3}$$

Here L,l are the orbital angular momenta of the valence nucleons and J,j their spins. (The values L and $l = 0, 1, 2, 3, 4, 5, 6, 7$ are usually denoted as s {"sharp"}, p {"peculiar"}, d {"diffuse"} [75], f, g, h, i, j.)

There are $\sum_I (2I+1) = (2j+1)(2j+1)$ substates with magnetic quantum numbers $m_I = -I, \ldots, +I$. Because we work in an environment with vanishing magnetic field all substates have the same energy. Throughout the paper we count each ensemble of the $(2I+1)$ substates for each spin I once only.

In the sSM all configurations $LJ\,lj$ with different total spins I have the same energy. The values LJ,lj differ for neutrons and protons; hence, the names are unique. There is no need to indicate the isospin τ in E_x^{sSM}.

2. Generalized schematic shell model

The sSM can be generalized to describe the excitation of several nucleons in ^{208}Pb with the restriction that the sum of the neutron and proton particles equals the sum of the neutron and proton holes, respectively. Similar to Eq. (3) the excitation energy derives from the masses [72,73] of the neighboring nuclei and ^{208}Pb itself [$M(82,126)$], the Coulomb energy, and the excitation energies of the states in the neighboring nuclei with dominant configurations $\underline{LJ}$ and $\underline{lj}$,

$$\begin{aligned} E_x^{\text{gSM}}([\Delta_Z,\Delta_N],\underline{LJ},\underline{lj}) &= \Delta Q(\Delta_Z,\Delta_N)\\ &\quad + E_{\text{eSM}}^{\text{Coul}}(\tau,\Delta_Z,\Delta_N,\underline{LJ},\underline{lj})\\ &\quad + E_x(+\Delta_Z,+\Delta_N,\underline{LJ})\\ &\quad + E_x(-\Delta_Z,-\Delta_N,\underline{lj}),\\ \text{with} \quad [\Delta_Z,\Delta_N] &= [0,0],[1,0],[0,1],[1,1],\ldots,\\ \text{and} \quad \Delta Q(\Delta_Z,\Delta_N) &= M(82+\Delta_Z,126+\Delta_N)c^2\\ &\quad + M(82-\Delta_Z,126-\Delta_N)c^2\\ &\quad - 2M(82,126)c^2, \end{aligned} \tag{4}$$

where c is the speed of light. Here $+\Delta_Z, +\Delta_N, \underline{LJ}$ denote a configuration in the nucleus with $82+\Delta_Z$ protons and $126+\Delta_N$ neutrons and similarly for $-\Delta_Z, -\Delta_N, \underline{lj}$. Equation (3) is the special case of Eq. (4) with $[\Delta_Z,\Delta_N] = [1,0]$ and $[0,1]$.

The Coulomb energy is estimated similar to Eq. (2),

$$\begin{aligned} E_{\text{eSM}}^{\text{Coul}}(\pi,\Delta_Z,\Delta_N,\underline{LJ},\underline{lj}) &= 0 && \text{for } \Delta_Z = 0,\\ &= E^{\text{Coul}}(\pi,LJ,lj) && \text{for } \Delta_Z = 1,\\ &\approx -1.2 \text{ MeV} && \text{for } \Delta_Z = 2,\\ &&& \text{and any } \Delta_N,\\ E_{\text{eSM}}^{\text{Coul}}(\nu,\Delta_Z,\Delta_N) &= 0 && \text{for any } \Delta_Z \text{ and any } \Delta_N. \end{aligned} \tag{5}$$

We especially consider two classes of the generalized schematic shell model:

(i) the modified schematic shell model (mSM, Sec. II A 3) describing one-particle–one-hole configurations as an extension of the sSM (Sec. II A 1); and

(ii) the extended schematic shell model (Secs. II D 1–II D 7) describing two-particle–two-hole configurations and including the mSM one-particle one-hole configurations.

3. The modified schematic shell model

The mSM is a modification of the sSM by including the diagonal matrix elements of the surface δ interaction (SDI). The mSM has a single parameter C^{SDI} derived from the splitting of the ground-state multiplet in ^{210}Po [16,65]. The excitation energies are calculated as

$$E_x^{\mathrm{mSM}}(LJ,lj,I) = E_x^{\mathrm{sSM}}(LJ,lj) + C^{\mathrm{SDI}} g^{\mathrm{SDI}}(J,j,I). \quad (6)$$

Here $g^{\mathrm{SDI}}(J,j,I)$ are geometrical factors derived from the recoupling of the isospin and the spins.

The sSM including the diagonal part of the SDI is referred to as mSM. It describes the excitation energies of the particle-hole states in the doubly magic nucleus ^{208}Pb better than the sSM up to the neutron threshold $S(n) = 7368$ keV and the proton threshold $S(p) = 8000$ keV and beyond [16,19].

The excitation energy E_x^{mSM} is reigned by two geometrical qualities, the nature of parity,

$$U_p(I,L,l) = (-1)^{I+L+l}, \quad (7)$$

and the Nordheim number [77,78],

$$N_h(LJ,lj) = (-1)^{1+L+J+l+j}. \quad (8)$$

The two parameters U_p and N_h define four classes of the multiplet splitting [16].

The multiplet splitting in each class follows a parabolic dependence on the classical angle θ defined [79] as

$$\theta(J,j,I) = \arccos\left[\frac{I(I+1) - J(J+1) - j(j+1)}{2\sqrt{J(J+1)j(j+1)}}\right]. \quad (9)$$

The members with the lowest spin and the highest spin are often substantially separated from all other members of a given multiplet. For certain Nordheim numbers, the members with natural and unnatural parity form distinct multiplets separated by several tens of keV [16]. The multiplet splitting may become up to 1 MeV in either direction. In Table I the energies E_x^{mSM} for the case of the configuration $f_{7/2}h_{11/2}$ are shown.

The difference of the excitation energies E_x^{mSM} [Eq. (6)] from E_x^{sSM} [Eqs. (2) and (3)] becomes large if the orbits are nearly parallel ($\Theta = 0^\circ$) or antiparallel ($\Theta = 180^\circ$) [Eq. (9)]. The mSM predicts the excitation energies of states in ^{208}Pb within about 100 keV, similar to the precision of calculations with realistic forces [80–86]. It also indicates which configurations might mix more strongly in the case where the excitation energies of two configurations approach each other by less than the average matrix element of the residual interaction of about 100 keV [87–89].

Tables I and II list energies E_x^{sSM} for negative- and positive-parity sSM configurations. Figures 3–16 (Sec. III C 1) show level schemes for configurations and states with spins from 0^- to 8^-, 14^-, and from 1^+ to 12^+. The energies $E_x^{\mathrm{sSM}}(Lj,lj)$ [Eq. (3)], $E_x^{\mathrm{mSM}}(LJ,lj,I)$ [Eq. (6)], and the experimental energies (the energy labels $\tilde{E}_x$ [Eq. (10)]) are shown. The level scheme for the lowest excited 0^+ states is included for completeness (Fig. 8).

TABLE I. Particle-hole configurations $LJ\,lj$ in ^{208}Pb predicted by the sSM [Eqs. (2) and (3)] with protons in orbits $50 \leqslant Z \leqslant 126$ and neutrons in orbits $82 \leqslant N \leqslant 184$ [Eq. (1)] for positive parity at $E_x^{\mathrm{sSM}} < 6.65$ MeV. Configurations are printed boldface if the state with the corresponding dominant configuration is identified [1,12,18]; see also Sec. IV C.

$LJ\,lj$	I^π												E_x^{sSM} (keV)
$j_{15/2}p_{1/2}$							**7^+**	**8^+**					4854
$g_{9/2}i_{13/2}$		**2^+**	**3^+**	**4^+**	**5^+**	**6^+**	**7^+**	**8^+**	**9^+**	**10^+**	**11^+**		5064
$h_{9/2}h_{11/2}$	**1^+**	**2^+**	**3^+**	**4^+**	**5^+**	**6^+**	**7^+**	**8^+**	**9^+**	**10^+**			5262
$j_{15/2}f_{5/2}$					**5^+**	**6^+**	**7^+**	**8^+**	**9^+**	**10^+**			5424
$i_{13/2}s_{1/2}$						**6^+**	**7^+**						5472
$j_{15/2}p_{3/2}$						**6^+**	**7^+**	**8^+**	**9^+**				5752
$i_{13/2}d_{3/2}$					**5^+**	**6^+**	**7^+**	**8^+**					5823
$i_{11/2}i_{13/2}$	1^+	**2^+**	**3^+**	**4^+**	**5^+**	**6^+**	**7^+**	**8^+**	**9^+**	**10^+**	**11^+**	**12^+**	5843
$f_{7/2}h_{11/2}$		**2^+**	3^+	**4^+**	5^+	**6^+**	7^+	**8^+**	9^+				6259[a]
$d_{5/2}i_{13/2}$				4^+	5^+	6^+	7^+	8^+	9^+				6631

[a]The mSM [16] yields the energies $E_x^{\mathrm{mSM}} = 6081$, 6089, 6122, and 6147 keV for spins 2^+, 4^+, 6^+, 8^+, with $U_p = +1$, and 6328, 6315, 6333, and 6464 keV for spins 3^+, 5^+, 7^+, and 9^+, with $U_p = -1$ [Eq. (7)]; the Nordheim number is $N_h = -1$ [Eq. (8)].

TABLE II. Similar to Table I for negative-parity states. All states with configurations predicted by the sSM below $E_x^{\mathrm{sSM}} = 6361$ keV are identified [18] as well as a few more [1,10,19]; Sec. IV C 1.

$LJ\,lj$	I^π											E_x^{sSM} (keV)
$g_{9/2}p_{1/2}$					**4^-**	**5^-**						3431
$h_{9/2}s_{1/2}$					**4^-**	**5^-**						3914
$g_{9/2}f_{5/2}$			**2^-**	**3^-**	**4^-**	**5^-**	**6^-**	**7^-**				4001
$i_{11/2}p_{1/2}$						**5^-**	**6^-**					4210
$h_{9/2}d_{3/2}$				**3^-**	**4^-**	**5^-**	**6^-**					4265
$g_{9/2}p_{3/2}$				**3^-**	**4^-**	**5^-**	**6^-**					4329
$i_{11/2}f_{5/2}$				**3^-**	**4^-**	**5^-**	**6^-**	**7^-**	**8^-**			4780
$f_{7/2}s_{1/2}$				**3^-**	**4^-**							4911
$d_{5/2}p_{1/2}$			**2^-**	**3^-**								4998
$i_{11/2}p_{3/2}$					**4^-**	**5^-**	**6^-**	**7^-**				5108
$f_{7/2}d_{3/2}$			**2^-**	**3^-**	**4^-**	**5^-**						5262
$s_{1/2}p_{1/2}$	**0^-**	**1^-**										5463
$d_{5/2}f_{5/2}$	**0^-**	**1^-**	**2^-**	**3^-**	**4^-**	**5^-**						5568
$h_{9/2}d_{5/2}$			**2^-**	**3^-**	**4^-**	**5^-**	**6^-**	**7^-**				5597
$g_{9/2}f_{7/2}$		**1^-**	**2^-**	**3^-**	**4^-**	**5^-**	**6^-**	**7^-**	**8^-**			5771
$d_{5/2}p_{3/2}$		**1^-**	**2^-**	**3^-**	**4^-**							5896
$g_{7/2}p_{1/2}$				**3^-**	**4^-**							5922
$d_{3/2}p_{1/2}$		**1^-**	**2^-**									5969
$s_{1/2}f_{5/2}$			**2^-**	**3^-**								6033
$s_{1/2}p_{3/2}$		**1^-**	**2^-**									6361
$j_{15/2}i_{13/2}$		**1^-**	**2^-**	**3^-**	4^-	**5^-**	6^-	7^-	8^-	9^-[a]	**14^-**	6487
$g_{7/2}f_{5/2}$		**1^-**	**2^-**	**3^-**	4^-	**5^-**	6^-					6492
$d_{3/2}f_{5/2}$		**1^-**	**2^-**	**3^-**	4^-							6539
$i_{11/2}f_{7/2}$			**2^-**	**3^-**	4^-	5^-	6^-	7^-	8^-	9^-		6550
$f_{7/2}d_{5/2}$		**1^-**	**2^-**	**3^-**	4^-	**5^-**	6^-					6594

[a]States with spin 10^-, 11^-, 12^-, and 13^- are not yet firmly identified.

Positive-parity one-particle–one-hole configurations show up because of the lowering of the intruder orbits, $i_{13/2}$, $h_{11/2}$ for protons and $j_{15/2}$, $i_{13/2}$ for neutrons (Fig. 1). The separation of the orbits $h_{9/2}$, $h_{11/2}$, and $i_{11/2}$, $i_{13/2}$, and $j_{13/2}$, $j_{15/2}$ from each other becomes more than 5 MeV (Figs. 2-30 and 3-3 in Ref. [90]). This phenomenon is the main difference between the shell models for nuclei [91] and atoms.

B. Description of states

The physical states in ^{208}Pb with spin I and parity π are described by a mixture of configurations. In the space of mSM configurations, a physical state is given by the superposition

$$\left|\tilde{E}_x, I^\pi_M\right\rangle = \sum_i c^{I^\pi}_{M,i} \left|E^{\rm mSM}_x(i), I^\pi_i\right\rangle, \tag{10}$$

with amplitudes $-1 < c^{I^\pi}_{M,i} < +1$.

Instead of the index i often the configuration $LJ\,lj$ is given, thus denoting the amplitudes by $c^{I^\pi_M}_{LJ,lj}$.

Each state is uniquely labeled with an integer $\tilde{E}_x$ with four digits corresponding to the excitation energy listed by NDS2007 within about 2 keV. Newly identified states are labeled similarly.

An order number M is defined by counting the states with increasing excitation energies for each spin I and either parity π; hence, a state is uniquely identified by I^π_M. For negative parity, all states predicted by the sSM at $E^{\rm sSM}_x < 6361$ keV are identified [18]. For positive parity, the identification of all states at $E_x < 6.20$ MeV is sometimes doubtful (Sec. IV C 3).

Table VI defines the energy label $\tilde{E}_x$ [Eq. (10)]; spin I, parity π, and order number M are given for each state. In the text most states are denoted by showing the energy label $\tilde{E}_x$, spin I, and parity π. In Figs. 3–16 the energy label $\tilde{E}_x$ is shown (each figure shows the level scheme for one value I^π), in Figs. 17–21 the energy label $\tilde{E}_x$, spin I, order number M, and parity π are shown.

In contrast to reality [Eq. (10)], both the schematic shell model (sSM, Sec. II A 1) itself and modified by including the diagonal matrix elements of the surface δ interaction (mSM, Sec. II A 3) do not include any configuration mixing.

In the sSM the excitation energy of the configurations does not depend on the spin. Similarly to the order number M of the states, we define an order number m for each spin and either parity by counting the configurations with increasing excitation energies, I^π_m. The order of the mSM configurations sometimes differs from the order of the sSM configurations, but we adhere to the numbering of the sSM configurations for clarity. By including two-particle–two-hole configurations, the basis is extended and order numbers are defined similarly in the extended shell model [Eq. (36)].

The sSM configurations are shown in Figs. 3–16 to alleviate the comparison of level schemes for different spins. Often states with a certain spin I^π have most configurations in common with states for the spin of $(I+1)^\pi$; only few values $LJ\,lj$ appear in addition or are absent for either spin.

The different behaviors of natural parity and unnatural parity states can thus be compared more easily. The order of the mSM configurations aggravates the comparison owing to the multiplet splitting with shifts by up to 900 keV in either direction.

C. Residual interaction among particle-hole configurations

1. *Off-diagonal matrix elements from experiment*

The final goal of the investigation of nuclear states in ^{208}Pb is the determination of the residual interaction among particle-hole configurations. It is defined as the difference between the action of the Hamiltonian $\mathbf{H}^{\rm exp}$ in the space of the experimental states and the Hamiltonian $\mathbf{H}^{\rm mod}$ in the space of the configurations,

$$\mathbf{v} = \mathbf{H}^{\rm exp} - \mathbf{H}^{\rm mod}. \tag{11}$$

The method presented by two of us (A.H. and P. von B.) [87] allows to derive off-diagonal matrix elements from experimental data under the condition that an ensemble of states consists of an equal number of configurations nearly entirely,

$$v_{ij} = \sum_l c_{il} c_{jl} \left\{ E^{\rm exp}_x(l) - \frac{1}{2}\left[E^{\rm mod}_x(i) + E^{\rm mod}_x(j)\right]\right\}; \tag{12}$$

see Eq. (17a) in Ref. [87].

The simplest case is the mixing between two well-isolated configurations. By neglecting the influence of other configurations, the matrix element is given by the mixing amplitude c_{12} corresponding to the value $c^{I^\pi}_{M,i}$ in Eq. (10) with some spin I^π and the difference between the energies $E^{\rm exp}_x(i)$ of the two states,

$$v_{12} = c_{12} c_{11} E^{\rm exp}_x(1) + c_{21} c_{22} E^{\rm exp}_x(2). \tag{13}$$

The assumption of a complete subspace yields $c_{21} = -c_{12}$ and $c_{11} = c_{22} = \sqrt{1 - c^2_{21}}$.

The off-diagonal matrix element of the residual interaction between the two lowest 0^- configurations in ^{208}Pb was thus determined [6] as $|v_{12}| = 110 \pm 10(\text{exp.}) \pm 15(\text{syst.})$ keV.

2. *Dense ensembles of configurations*

Another extreme case is the appearance of a highly collective state if many configurations are crowded together.

As shown by Brown in an analytical model [92], one state out of an ensemble of configurations is shifted far away if the spacing $\Delta E^{\rm mod}_x$ of the model configurations is much less than the mean matrix element of the residual interaction $v^{\rm mean}$,

$$\begin{aligned} E^{\rm mod}(i) &= E^{\rm mod}(i-1) + \Delta E^{\rm mod}_x, \quad i = 2,3,\ldots, \\ E(0) &= \Delta E^{\rm mod}_x + \lambda \sum_{m,i} v_{mi}, \\ |E(0)| &\gg \Delta E^{\rm mod}_x, \\ v^{\rm mean} &= \frac{1}{N^2} \sum_{m=1}^{N} \sum_{i=1}^{N} v_{mi}, \end{aligned} \tag{14}$$

where λ is some constant with negative sign; see Fig. 10 and Eq. IV(7.4) in Ref. [92]. The collective state with energy $E(0)$ is described by a multitude of weak particle-hole configuration fragments in a coherent manner.

D. Multi-particle-hole models

Many states in ^{208}Pb are well described by the mSM [16]. Here particles and holes are coupled to the 0^+ ground state (Sec. II A). The configuration mixing depends on the nature of parity [Eq. (7)]. While unnatural parity configurations separated by more than 100 keV are generally little mixed, natural parity configurations are strongly mixed if the distance is less than 200 keV.

The large number of 1^- and 3^- configurations together with the stronger residual interaction explains the collective nature of the corresponding yrast states (2615 3^- and 4841 1^-; Table VI), as shown by Brown in an analytical model [92]; see Eq. (14). The 2^+ yrast state ($\tilde{E}_x = 4086$) is similarly explained as there are many two-particle–two-hole configurations starting at the very low energy $E_x = 5.2$ MeV (Fig. 3; Table VI).

We call the 1_1^-, 2_1^+, and 3_1^- states low-spin yrast configurations. The coupling of low-spin yrast configurations together is discussed in Sec. II D 1, the coupling of one-particle–one-hole configurations to low-spin yrast configurations in Sec. II D 4, and the coupling of one-particle–one-hole configurations to each other in Sec. II D 3.

The pairing of nucleons lowers the excitation energy of the configuration with small spins (0^+, 2^+) by up to 2 MeV [6,65]. The multiplet splitting of configurations containing a pair of nucleons thus becomes exceedingly large. The coupling of pairing vibration states [20,35–37,67,68] is discussed in Sec. II D 2. Two-particle–one-hole configurations and their isobaric analogs with the proton decay are discussed in Sec. II D 5 and four-particle–four-hole configurations in Sec. II D 6.

In the following the two-particle–two-hole configurations are described by showing the single nucleon LJ or lj outside ^{208}Pb (denoting neutrons with ν and protons with π), the coupling to the lowest yrast states 3_1^- and 2_1^+ in ^{208}Pb, and the coupling of two-nucleon states in six neighboring nuclei of Pb. Equivalent abbreviations shown in curly parentheses in Secs. II D 1–II D 5 are used in Figs. 3–16.

1. Coupling of low-spin yrast configurations

Quite generally, the low-spin yrast configurations may couple together owing to their collectivity, yielding higher excited states in ^{208}Pb,

$$E_x^{\rm eSM}(I^\pi,3_1^-\otimes 3_1^-) \equiv \{3^-3^-\} = 5229\ \text{keV},\quad I^+ = 0^+,2^+,4^+,6^+; \tag{15}$$

$$E_x^{\rm eSM}(I^\pi,3_1^-\otimes 2_1^+) \equiv \{3^-2^+\} = 6700\ \text{keV},\quad I^+ = 1^-,2^-,3^-,4^-,5^-. \tag{16}$$

Equations (15) and (16) correspond to Eq. (4) with $[\Delta_Z,\Delta_N] = [0,0]$.

The coupling of two 3^- yrast states predicts a multiplet with spins 0^+, 2^+, 4^+, and 6^+, the double octupole excitations [53] (Table III). These states are known [54–57,76] except for the 6^+ configuration which is strongly mixed with eight close-lying sSM configurations (Fig. 5).

The coupling of the 3^- yrast state to the 2^+ yrast state predicts a multiplet with spins from 1^- to 5^-; these states have the lowest excitation energies for multi-particle-hole configurations with negative parity (Table III). Other couplings of low-spin yrast configurations are expected at excitation energies $E_x > 7$ MeV.

2. Pairing vibration configurations

Pairing vibration configurations were first described by Bohr [67]. The neutron pairing vibration state was identified in 1968 [35–37], the proton pairing vibration state in 2015 [20,68]. They are predicted [67,93,94] as

$$E_x^{\rm eSM}[\nu,0_1^+(206)\otimes 0_1^+(210)] \equiv \{0_\nu^+\}, \tag{17}$$

$$E_x^{\rm eSM}[\pi,0_1^+(206)\otimes 0_1^+(210)] \equiv \{0_\pi^+\}. \tag{18}$$

Table III shows the values, Fig. 8 the level scheme. Equation (17) corresponds to Eq. (4) with $[\Delta_Z,\Delta_N] = [0,2]$, Eq. (18) to Eq. (4) with $[\Delta_Z,\Delta_N] = [2,0]$. Corresponding to the prediction of the neutron pairing vibration state [67,94], the coupling of the 0^+ yrare state in ^{206}Pb to the 0^+ yrast state in ^{210}Pb predicts the configuration

$$E_x^{\rm eSM}[\nu,0_2^+(206)\otimes 0_1^+(210)] \equiv \{0_2^+0^+\}. \tag{19}$$

The coupling of $2^+,4^+,6^+,8^+$ yrast states to the pairing vibration state yields configurations at $E_x > 5.7$ MeV. For neutrons the predictions are

$$\begin{aligned}
&E_x^{\rm eSM}[\nu,I^+,0_1^+(206)\otimes I_1^+(210)] \equiv \{0^+I^+\},\\
&I_1^+ = I^+ = 2^+,4^+,6^+,8^+;\\
&E_x^{\rm eSM}[\nu,I^+,2_1^+(206)\otimes I_1^+(210)] \equiv \{2^+I_1^+\},\\
&I^+ = 0^+,2^+,\ldots,10^+,\\
&I_1^+ = 0^+,2^+,4^+,6^+,8^+;\\
&E_x^{\rm eSM}[\nu,4^+,4_1^+(206)\otimes 0_1^+(210)] \equiv \{4^+0^+\}.
\end{aligned} \tag{20}$$

By chance, the 2^+ yrast states in ^{206}Pb and ^{210}Pb have almost the same excitation energy of 0.80 MeV [74]. The lowest $0^+,2^+,4^+,6^+,8^+$ states in ^{210}Pb are described by the pairing of two $g_{9/2}$ neutrons [9,16,65]. Table III shows some values. Similar combinations are considered in Table IV.

Experimentally, the purity of the $g_{9/2}$ pairs is confirmed by the g factors of the 6^+ and 8^+ states in ^{210}Pb, which are equal to that of the $g_{9/2}$ ground state of ^{209}Pb with values of $g = -0.312(15)$ [95], $g = -0.313(8)$ [95], and $g = -0.3274(4)$ [96], respectively.

Predictions for protons equivalent to Eq. (20) are

$$\begin{aligned}
&E_x^{\rm eSM}[\pi,I_1^+,2_1^+(206)\otimes I^+(210)] \equiv \{\pi\ 2^+I^+\},\\
&I_1^+ = 0^+,2^+,\ldots,10^+,\\
&I^+ = 2^+,4^+,6^+,8^+;\\
&E_x^{\rm eSM}[\pi,I^+,0_1^+(206)\otimes I^+(210)] \equiv \{\pi\ 0^+I^+\},\\
&I_1^+ = 2^+,4^+,6^+,8^+.
\end{aligned} \tag{21}$$

Here the lowest $0^+,2^+,4^+,6^+,8^+$ states in ^{210}Po are described by the pairing of two $h_{9/2}$ protons [9,16,65].

TABLE III. Excitation energies of two-particle–two-hole configurations predicted by the extended shell model (Sec. II D). Configurations with correspondence to identified states at $E_x < 6.20$ MeV are printed in boldface.

Dominant configuration			Eq(s).	E_x (keV) 0^+	1^+	2^+	3^+	4^+	5^+	6^+	7^+	8^+	9^+	10^+	11^+	12^+	: I^π
3_1^-	⊗	3_1^-	(15)	**5229**[a]		**5229**[b]		**5229**[c]		**5229**[d]							
^{206}Pb(0_1^+)	⊗	^{210}Pb(I_1^+)[e]	(17),(20)	**4983**[f]		**5783**		**6081**		6178		6261					
^{206}Hg(0_1^+)	⊗	^{210}Po(I_1^+)[e]	(18),(21)	**5873**[g]		7054		7300		7346		7429					
^{206}Hg(2_1^+)	⊗	^{210}Po(0_1^+)	(19)			6941											
^{206}Pb(0_2^+)	⊗	^{210}Pb(0_1^+)	(19)	6149													
^{206}Pb(I_1^+)[h]	⊗	^{210}Pb(0_1^+)	(20)			**5786**		6667									
^{206}Pb(2_1^+)	⊗	^{210}Pb(2_1^+)	(20)	6585	6585	6585	6585	6585									
^{206}Tl(I_1^+)	⊗	^{210}Bi(I_2^+)	(22)[i]	6198	6152	6463	6499	6591	6524	6702	6585	6689	6423	6689	6689	**7225**[j]	
$g_{9/2}p_{1/2}$	⊗	3_1^-	(27)		**6125**	6125	6125	6125	6125	6125	6125						
						5980	**5980**	**5980**	**5980**	**5980**	**5980**	**5980**					
$g_{9/2}f_{5/2}$	⊗	3_1^-	(27)[k]	6615	6615	6615	6615	6615	6615	6615	6615	6615	6615	6615			
$g_{9/2}{}^2$	⊗	$f_{5/2}p_{3/2}$	(31)[k]	8330	8330	8330	8330	8330	8330	8330	8330	8330	8330	8330	8330	8330	
^{204}Hg(0_1^+)	⊗	^{212}Po(0_1^+)	(35)	7200													
				0^-	1^-	2^-	3^-	4^-	5^-	6^-	7^-	8^-	9^-	10^-	11^-		: I^π
3_1^-	⊗	2_1^+	(16)		6700	6700	6700	6700	6700								
$j_{15/2}p_{1/2}$	⊗	3_1^-	(29)[k]					7468	7468	7468	7468	7468	7468	7468	7468		

[a]The 5241 state is assumed to contain the dominant strength [54,57].
[b]The 5286 state is assumed to contain the dominant strength [54,57].
[c]The 5216 state is assumed to contain the dominant strength [54,57].
[d]Strength mixed with eight sSM configurations.
[e]$I^\pi = 0^+, 2^+, 4^+, 6^+, 8^+$.
[f]The 4868 state contains the dominant strength [35–37].
[g]The 5667 state contains the dominant strength [20,68].
[h]$I_1^+ = 2^+, 4^+$.
[i]Only the lowest value is shown. The Coulomb energy is assumed with $E_{\rm eSM}^{\rm Coul} = -200$ keV; see Eq. (5).
[j]More configurations are tabulated in Table IV. The 6101 state is assumed to contain major parts of the configuration (Sec. IV B 3).
[k]For simplicity the energies are calculated by the sSM and not by the mSM, but for most spins more than one state exists.

Again, the purity of the $h_{9/2}$ pairs is confirmed by the g factors of the 6^+ and 8^+ states in ^{210}Po; they agree with that of the $h_{9/2}$ ground state of ^{209}Bi with values of $g = 0.913(8)$ [97], $g = 0.919(6)$ [97], and $g = 0.913\,47(4)$ [98], respectively. Because of the large excitation energies, $E_x > 7.0$ MeV, the configurations Eq. (21) are of no interest to this paper.

3. Coupling of neutron particle-hole to proton particle-hole configurations

Coupling of ^{206}Tl *to* ^{210}Bi *and* ^{208}Tl *to* ^{208}Bi. The excitation energies of configurations with pairs of neutrons or protons coupled to spin $I^\pi = 0^+$ or 2^+ are lowered considerably by the pairing force, as described in the previous section (Sec. II D 2). In contrast, excitation energies of configurations with unpaired nucleons are much higher.

The coupling of nucleon configurations in the odd-odd nuclei ^{206}Tl and ^{210}Bi yields two-particle–two-hole configurations,

$$E_x^{\rm eSM}[I^+, {}^{206}{\rm Tl}(I_1^-) \otimes {}^{210}{\rm Bi}(I_2^-)] \equiv \{{}^{206}{\rm Tl} \otimes {}^{210}{\rm Bi}\}$$
$$I^+ = 0^+, 1^+, \ldots, \quad I_1^- = 0^-, 1^-, \ldots, \quad I_2^- = 0^-, 1^-, \ldots, \tag{22}$$

corresponding to Eq. (4) with $[\Delta_Z, \Delta_N] = [1,1]$.

The constituent configurations derive from the coupling of a neutron to a proton,

$$^{206}{\rm Tl}(LJ, lj, I_1^-), \quad LJ\,lj = s_{1/2}p_{1/2}, s_{1/2}f_{5/2}, \ldots,$$
$$^{210}{\rm Bi}(LJ, lj, I_2^-), \quad LJ\,lj = h_{9/2}g_{9/2}, h_{9/2}i_{11/2}, \ldots. \tag{23}$$

The lowest states in ^{206}Tl and ^{210}Bi consist mostly of the configurations $s_{1/2}p_{1/2}$ and $g_{9/2}h_{9/2}$, yielding $I^+ = 0^+, \ldots, 10^+$. Higher configurations in ^{206}Tl contain $s_{1/2}f_{5/2}$ and $s_{1/2}p_{3/2}$ and $d_{3/2}p_{1/2}$, $d_{3/2}f_{5/2}$, and $d_{3/2}p_{3/2}$. Table III shows some values.

The excitation energies of corresponding configurations from the coupling of the odd-odd nuclei ^{208}Tl and ^{208}Bi corresponding to Eq. (4) with $[\Delta_Z, \Delta_N] = [-1,1]$ are predicted with $E_x > 7.5$ MeV and hence are of no interest to this paper.

Configurations with spin 12^+. Among the configurations ^{206}Tl ⊗ ^{210}Bi [Eq. (22)], only those with the spin 12^+ are relevant in this paper. The excitation energies can be predicted for three configurations because in ^{206}Tl only few spins are known [74].

More interesting configurations can be described in another schematic manner. Namely, in ^{206}Tl there are neutron-hole–proton-hole configurations and in ^{210}Bi neutron-particle–proton-particle configurations. Alternatively, the coupling

TABLE IV. Excitation energies of configurations with spin 12^+ predicted by the extended shell model.

m	Configuration					Equation	$E_x^{\mathrm{e*SM}}$ (keV)	E_x^{SDI} (keV)	E_x^{eSM} (keV)
1	$i_{11/2}i_{13/2}$					(6)	5776		
2	$\nu g_{9/2}f_{5/2}$	7^-	$\otimes$	$\pi h_{9/2}s_{1/2}$	5^-	(26)	7225	7932	7225
3	$\nu g_{9/2}f_{5/2}$	7^-	$\otimes$	$\pi h_{9/2}d_{3/2}$	6^-	(26)	7635	8342	7767
4	$\nu g_{9/2}f_{5/2}$	6^-	$\otimes$	$\pi h_{9/2}d_{3/2}$	6^-	(26)	7661	8368	7820
5	$\nu i_{11/2}f_{5/2}$	7^-	$\otimes$	$\pi h_{9/2}s_{1/2}$	5^-	(26)	7810	8517	
6		4_1^+	$\otimes$		8_1^+	(20)	7944		
7	$\nu i_{11/2}p_{1/2}$	6^-	$\otimes$	$\pi h_{9/2}d_{3/2}$	6^-	(26)	7987	8694	
8	$\nu i_{11/2}f_{5/2}$	8^-	$\otimes$	$\pi h_{9/2}s_{1/2}$	5^-	(26)	8101	8808	
9	$\nu i_{11/2}f_{5/2}$	8^-	$\otimes$	$\pi h_{9/2}s_{1/2}$	4^-	(26)	8246	8953	
10		4_2^+	$\otimes$		8_1^+	(20)	8258		
11	$j_{15/2}h_{9/2}$					(6)	8267		
12	$\nu g_{9/2}{}^2$	8^+	$\otimes$	$\pi f_{5/2}p_{3/2}$	4^+	(31)	8330		
13	$j_{15/2}i_{13/2}$	9^-	$\otimes$		3_1^-	[a]	8353		
14	$j_{15/2}i_{13/2}$	11^-	$\otimes$		3_1^-	[a]	8372		
15	$j_{15/2}i_{13/2}$	13^-	$\otimes$		3_1^-	[a]	8390		
16	$\nu i_{11/2}f_{5/2}$	8^-	$\otimes$	$\pi h_{9/2}d_{3/2}$	5^-	(26)	8403	9110	
17	$\nu i_{11/2}f_{5/2}$	6^-	$\otimes$	$\pi h_{9/2}d_{3/2}$	6^-	(26)	8535	9242	
18	$\nu i_{11/2}f_{5/2}$	8^-	$\otimes$	$\pi h_{9/2}d_{3/2}$	4^-	(26)	8548	9255	
19	$j_{15/2}i_{13/2}$	10^-	$\otimes$		3_1^-	[a]	8566		
20	$j_{15/2}i_{13/2}$	12^-	$\otimes$		3_1^-	[a]	8601		
21	$\nu i_{11/2}f_{5/2}$	8^-	$\otimes$	$\pi h_{9/2}d_{3/2}$	6^-	(26)	8656	9363	
22	$j_{15/2}i_{13/2}$	14^-	$\otimes$		3_1^-	[a]	8769		
23	$j_{15/2}p_{1/2}$	8^+	$\otimes$		4_1^+	(29)	9107		
24	$j_{15/2}p_{1/2}$	8^+	$\otimes$		6_1^+	(29)	9207		
25	$j_{15/2}p_{1/2}$	7^+	$\otimes$		6_1^+	(29)	9358		
26	$\pi h_{11/2}s_{1/2}$	5^-	$\otimes$	$\pi h_{9/2}i_{13/2}$	11^-	(26)			10 824
27	$\pi h_{11/2}{}^2$	8^+	$\otimes$	$\pi h_{9/2}{}^2$	4^+	(26)			10 923

[a]Similar to Eq. (29).

of neutron particle-hole configurations in ^{208}Pb to proton configurations in ^{208}Pb can be considered.

By using Eq. (4), the excitation energy of the lowest configuration in Eq. (22) is denoted as

$$\begin{aligned} E_x^{\mathrm{eSM}}(12_a^+) &\equiv E_x^{\mathrm{eSM}}[12^+, {}^{206}\mathrm{Tl}(3_1^-) \otimes {}^{210}\,\mathrm{Bi}(9_1^-)] \\ &= \Delta Q(1,1) + E_{\mathrm{eSM}}^{\mathrm{Coul}}(\pi,1,0,271\,9^-,801\,3^-) \\ &\quad + E_x({}^{210}\mathrm{Bi},271,9^-) + E_x({}^{206}\mathrm{Tl},801,3^-) \\ &= 7225\ \mathrm{keV}. \end{aligned} \tag{24}$$

Regrouping the nucleons yields the equivalent particle-hole configurations $\pi h_{9/2}s_{1/2} \otimes \nu g_{9/2}f_{5/2}$, $\pi h_{9/2}d_{3/2} \otimes \nu g_{9/2}f_{5/2}$, $\pi h_{9/2}d_{3/2} \otimes \nu i_{11/2}p_{1/2}$, and $\pi h_{9/2}s_{1/2} \otimes \nu i_{11/2}f_{5/2}$ in ^{208}Pb.

The energies of particle-hole configurations can be rather precisely calculated by the mSM. We thus obtain the eSM energies

$$\begin{aligned} &E_x^{\mathrm{SDI}}(12^+,\nu LJ\,lj,I_1^-,\pi LJ\,lj,I_2^-) \\ &\quad = E_x^{\mathrm{mSM}}(LJ,lj,I_1^-) + E_x^{\mathrm{mSM}}(LJ,lj,I_2^-), \end{aligned} \tag{25}$$

where $I_1^- \otimes I_2^-$ yields 12^+. The difference between the lowest configuration $E_x^{\mathrm{eSM}}(12_a^+)$ [Eq. (24)] and the lowest SDI configuration $h_{9/2}s_{1/2}g_{9/2}f_{5/2}$ with $E_x^{\mathrm{SDI}} = 7932$ keV is 707 keV (Table IV). It is explained by the interaction between the four nucleons.

In the alternate method the eSM excitation energies are then calculated with the adjustment of $E_x^{\mathrm{eSM}}(12_a^+)$ [Eq. (24)] as

$$\begin{aligned} &E_x^{\mathrm{e*SM}}(12^+,\nu LJ\,lj,\pi LJ\,lj) \\ &\quad = E_x^{\mathrm{SDI}}(12^+,\nu LJ\,lj,I_1^-,\pi LJ\,lj,I_2^-) \\ &\qquad - E_x^{\mathrm{SDI}}(12^+,\nu g_{9/2}f_{5/2},7^-,\pi h_{9/2}s_{1/2},5^-) + E_x^{\mathrm{eSM}}(12_a^+). \end{aligned} \tag{26}$$

By including other eSM configurations we obtain the predicted excitation energies shown in Table IV and Fig. 9. At $7.7 < E_x < 8.8$ MeV, the mean spacing between the configurations is 55 keV.

4. Coupling of particle-hole configurations to low-spin yrast configurations

Similar to the coupling of a particle and a hole to the 0^+ ground state in ^{208}Pb, the coupling to the low-spin yrast states (Sec. II D 4) and to the pairing vibration states (Sec. II D 2) can be imagined. First evidence for the coupling of a particle to the 3_1^- state was obtained by ^{207}Pb$(d,p\gamma)$ experiments [66]. The coupling of particle-hole configurations to the pairing vibration states yields high excitation energies, $E_x > 8.3$ MeV, and hence is of no interest to this paper.

The coupling of sSM configurations to the low-spin yrast states yields positive-parity configurations starting with

$$\begin{aligned} &E_x^{\rm eSM}(I^+, g_{9/2}p_{1/2} \otimes 3_1^-) \\ &= E_x(3_1^-) + E_x^{\rm mSM}(I_m^\pi, g_{9/2}, p_{1/2}) \equiv \{g_{9/2}p_{1/2}\ 3_1^-\} \\ I_m^\pi &= 4^- \quad \text{and } I^+ = 1^+, \ldots, 7^+, \\ I_m^\pi &= 5^- \quad \text{and } I^+ = 2^+, \ldots, 8^+. \end{aligned} \tag{27}$$

Negative-parity configurations start with

$$\begin{aligned} &E_x^{\rm eSM}(I^-, g_{9/2}p_{1/2} \otimes 2_1^+) \\ &= E_x(2_1^+) + E_x^{\rm mSM}(I_m^\pi, g_{9/2}p_{1/2}) \equiv \{g_{9/2}p_{1/2}\ 2_1^+\}, \\ I_m^\pi &= 4^- \quad \text{and } I^+ = 2^+, \ldots, 6^+, \\ I_m^\pi &= 5^- \quad \text{and } I^+ = 3^+, \ldots, 7^+; \end{aligned} \tag{28}$$

$$\begin{aligned} &E_x^{\rm eSM}(I^-, j_{15/2}p_{1/2} \otimes 3_1^-) \\ &= E_x(3_1^-) + E_x^{\rm mSM}(I_m^\pi, j_{15/2}p_{1/2}) \equiv \{j_{15/2}p_{1/2}\ 3_1^-\}, \\ I_m^\pi &= 7^+ \quad \text{and } I^- = 4^-, \ldots, 10^-, \\ I_m^\pi &= 8^+ \quad \text{and } I^- = 5^-, \ldots, 11^-. \end{aligned} \tag{29}$$

Equations (27)–(29) correspond to Eq. (4) with $[\Delta_Z, \Delta_N] = [0,0]$.

The coupling of sSM configurations among themselves yields positive-parity configurations starting with ${g_{9/2}}^2\, {p_{1/2}}^2$, which is the essential configuration described by the pairing vibration model (Sec. II D 2). Interesting configurations of this type are

$$\begin{aligned} &E_x^{\rm eSM}(I^+, {g_{9/2}}^2 \otimes p_{1/2}f_{5/2}) \equiv \{{g_{9/2}}^2\ p_{1/2}f_{5/2}\} \\ &= E_x^{\rm sSM}(g_{9/2}p_{1/2}) + E_x^{\rm sSM}(g_{9/2}f_{5/2}), \\ I^+ &= 0^+, \ldots, 11^+; \end{aligned} \tag{30}$$

$$\begin{aligned} &E_x^{\rm eSM}(I^+, {g_{9/2}}^2 \otimes f_{5/2}p_{3/2}) \equiv \{{g_{9/2}}^2\ f_{5/2}p_{3/2}\} \\ &= E_x^{\rm sSM}(g_{9/2}f_{5/2}) + E_x^{\rm sSM}(g_{9/2}p_{3/2}), \\ I^+ &= 0^+, \ldots, 12^+. \end{aligned} \tag{31}$$

Here, for simplicity, we do not specify the number of states for each spin I because they are of little interest in this paper. Equations (30) and (31) correspond to Eq. (4) with $[\Delta_Z, \Delta_N] = [0,2]$.

The configurations are not strictly orthogonal to those described by Eqs. (15), (16), (21), and (22). However, they are considered as a reasonable guide to find corresponding states. Similar to the one-particle–one-hole configurations [Eq. (3)], there are $(2J+1)(2j+1)(2I_C+1)$ different magnetic substates, where J is the spin of the particle, j the spin of the hole, and I_C the spin of the core.

5. Special multi-particle-hole configurations

Two-particle–one-hole configurations in ^{209}Pb. The lowest $15/2^-$ state in ^{209}Pb is no pure single-particle state and, hence, all particle-hole configurations excited in the proton decay of the $j_{15/2}$ IAR are already mixtures of one-particle–one-hole and two-particle–two-hole configurations.

The lowest $9/2^+$ and $15/2^-$ states in ^{209}Pb are described by Bohr and Mottelson (Eq. (6-457) in Ref. [94]) as

$$\begin{aligned} |\hat{g}_{9/2}\rangle &= 0.97|0^+_{\rm g.s.} \otimes g_{9/2}\rangle + 0.24|3_1^- \otimes j_{15/2}\rangle, \\ |\hat{j}_{15/2}\rangle &= 0.85|0^+_{\rm g.s.} \otimes j_{15/2}\rangle + 0.52|3_1^- \otimes g_{9/2}\rangle, \end{aligned} \tag{32}$$

involving the coupling to the ground state (g.s.) or the lowest excited state (2615 3_1^-). Similar calculations were made by Hamamoto and Siemens [99].

Therefore, the coupling of the configurations $\hat{g}_{9/2}$ and $\hat{j}_{15/2}$ in ^{209}Pb to holes lj in ^{207}Pb contain multi-particle-hole configurations described by Eq. (29). Configurations complementary to Eq. (32) are expected 2.6 MeV higher in energy,

$$E_x(I^-, 3_1^- \otimes g_{9/2}) = 2.6 \text{ MeV}, \quad I^- = \tfrac{3}{2}^-, \ldots, \tfrac{15}{2}^-. \tag{33}$$

Several states in the same region are shown to contain two-particle–one-hole configurations with either dominant $LJ\,L'J'\,p_{1/2}$ or ${g_{9/2}}^2\ lj$ structure [74]. ^{207}Pb$(d,p\gamma)$ experiments revealed weakly excited states where the dominant component consists of the coupling of particles to the 3_1^- state [66]. Dünnweber *et al.* [100] studied ^{208}Pb$(d,p\gamma)$ again and identified some members of the multiplet. Further studies suggested similar couplings of particles to the 3_1^- state in ^{209}Pb [101].

Excitation of two-particle–two-hole configurations in ^{208}Pb *by* ^{207}Pb(d,p). Starting from the ground state of ^{207}Pb with the dominant configuration $p_{1/2}$, the simultaneous excitation of the 3_1^- state and the transfer of a neutron with angular momentum $L = 7$ populates states in ^{208}Pb with spins from 4^+ to 11^+. Without the excitation of the 3_1^- state, the ^{207}Pb(d,p) reaction can excite only states with spin 7^+ or 8^+.

Similarly, the transfer with $L = 4$ with simultaneous excitation of the 3_1^- state makes it possible to populate states with spins from 1^- to 8^- described by Eq. (27) while without the excitation of the 3_1^- state only spins 4^- and 5^- in the final states are possible.

Proton decay of IARs based on two-particle–one-hole configurations. Isobaric analog resonances with parent states in ^{209}Pb having dominant two-particle–one-hole configurations decay by the emission of protons to two-particle–two-hole configurations in ^{208}Pb.

An important configuration of this type is described by Eq. (33); the correspondent overlapping resonances are expected at $E_p \approx 17.5$ MeV close to the $g_{7/2}$ and $d_{3/2}$ doublet IAR. (By chance, the states with dominant particle configurations $g_{7/2}$ and $d_{3/2}$ have similar excitation energies in ^{209}Pb as the predicted energy $E_x = 2.6$ MeV, $E_x =$ 2491 and 2539 keV, respectively.)

The coupling with the $p_{1/2}$ hole creates states in ^{208}Pb with dominant configurations described by Eq. (27). Because the single-particle width from the emission of a $p_{1/2}$ proton is rather large [28], a considerable cross section can be expected even with a weak excitation of the relevant IARs.

6. α vibrations

The α vibration can be considered as the simultaneous excitation of the neutron-pairing vibration and the proton-pairing vibration [Eqs. (17) and (18)]. The masses [72,73] yield

$$\Delta Q(2,2) = [M(^{206}\mathrm{Hg}) + M(^{210}\mathrm{Po}) - 2M(^{208}\mathrm{Pb})]c^2$$
$$= 8.4\ \mathrm{MeV} \quad (34)$$

from Eq. (4), with $[\Delta_Z,\Delta_N] = [2,2]$ for the lowest four-particle–four-hole configuration. Broglia and Bortignon [102] calculate the Coulomb energy and other corrections, yielding an estimate,

$$E_x(0^+,[2,2],0^+_{\mathrm{g.s.}},0^+_{\mathrm{g.s.}}) = 7.2\ \mathrm{MeV}. \quad (35)$$

We do not consider four-particle–four-hole configurations because we limit our discussion to states at $E_x < 6.20$ MeV.

7. The extended schematic shell model

We subsume all configurations discussed in Secs. II D 1–II D 5 as eSM configurations. We define the order number of eSM configurations by ordering both the sSM configurations (Tables I and II) and the configurations shown in Table III in a common set,

$$E_x^{\mathrm{eSM}}(i_{m+1}) > E_x^{\mathrm{eSM}}(i_m), \quad m = 1,2,\ldots. \quad (36)$$

Although not all configurations are strictly orthogonal to each other (Sec. II D 4), the eSM configurations may be considered as a reasonable guide for the description of states at $E_x \lesssim 7$ MeV.

E. Limits of investigation

1. Gaps among the configurations and complete systems

The mSM predicts several large gaps among the particle-hole configurations. The gaps are large with respect to the mean matrix element of the residual interaction of around 100 keV [87]. The gaps depend on the spin and parity. The first common gap is at $E_x \approx 4.5$ MeV; the next two gaps are at $E_x \approx 5.4$ and 6.1 MeV (Fig. 2). For some spins very large gaps show up (Figs. 3–16). By chance, a large gap shows up at $E_x \approx 6.1$ MeV for all spins as especially shown by Figs. 18 and 23; see also Sec. III C 5.

For a sufficiently large gap, all states below the gap are described by an orthogonal transformation of the corresponding configurations [87]. In Sec. III G 1 an example of three states described by three configurations is discussed.

Indeed, at $4.49 < E_x < 4.68$ MeV no negative-parity state is observed; solely the 4611 8^+ state shows up (Fig. 21). This gap made it possible to determine the structure of 20 negative-parity states with spins from 2^- to 7^- by assuming a complete subspace of configurations [87–89]. The analysis by Rejmund *et al.* [103] confirm the determination of many wave functions in an astonishing detail.

At $5.39 < E_x < 5.47$ MeV no negative-parity state is observed; only two positive-parity states show up (5419 6^+, 5474 7^+, Fig. 22). At $6.11 < E_x < 6.19$ MeV no state of either parity is clearly identified (Table VI). All spectra for particle-exchange reactions reveal the gap (Figs. 18 and 23 and Fig. 1 in Ref. [10]). The assumption of a complete system is verified by investigating the deviation matrices; in Sec. III G 1 the example of a three-level system is discussed [Eqs. (42)–(44)].

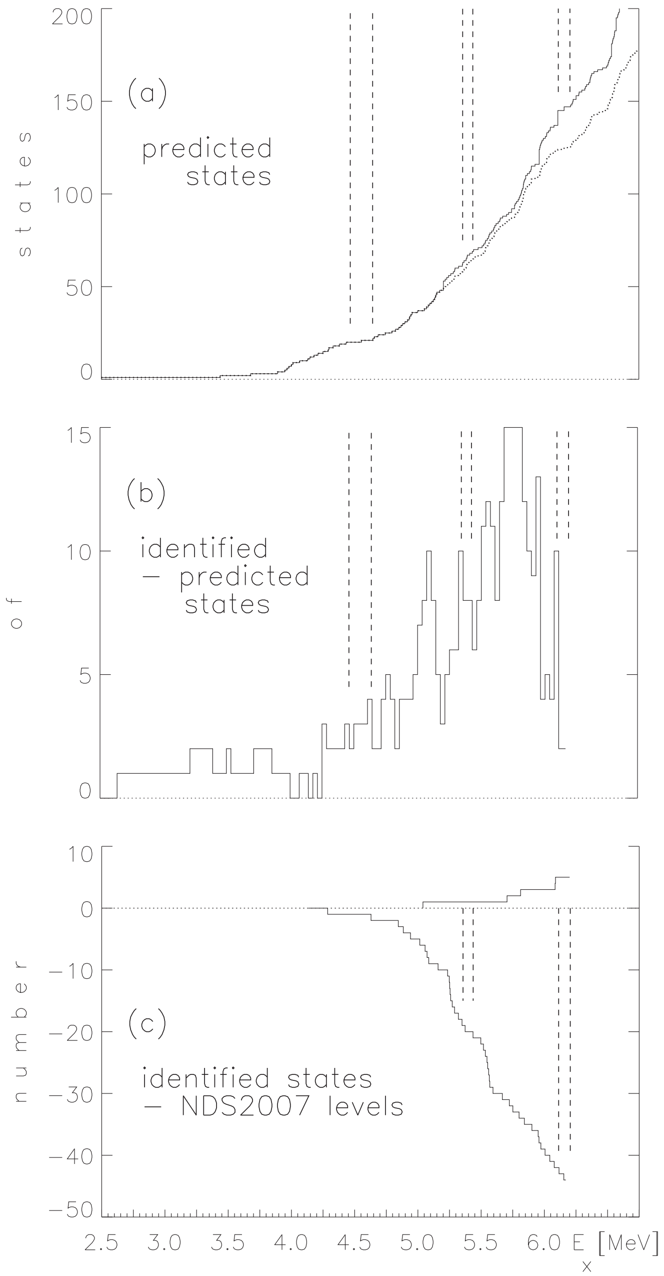

FIG. 2. Statistics of levels listed by NDS2007 and of identified states in ^{208}Pb for $E_x < 7.0$ MeV. At $E_x < 6.20$ MeV 151 states are identified (Sec. IV). Above 6.2 MeV spin and parity for only few states are known; consequently, no states are shown. Three large gaps (Sec. II E) in the mSM are denoted by vertical dashed lines. The deep minimum in panel (b) near the gap at $E_x \approx 6.2$ MeV corresponds to the difference $N^{\mathrm{predict}}(2) - N^{\mathrm{ident}}(2)$ [Eqs. (38) and (52)]. (a) Number of configurations predicted by the mSM (dotted line, Sec. II A) and by the eSM (solid line; Secs. II D 1–II D 7); (b) difference between the number of identified states and of configurations predicted by the eSM; (c) the number of NDS2007 levels recognized as "spurious" (Sec. VI) and the appearance of newly identified states.

In many cases, especially for unnatural parity states, the sequence of states can be divided into groups separated by a rather large gap. These groups of states may be considered as nearly complete systems. The clearest example consists of the five pairs of 4^- states with order numbers $M = 2$ and 3, 4 and 5, 6 and 7, 8 and 9, 10 and 11, and the three states with $M = 12$, 13, and 14 together with the isolated yrast state (Fig. 13). Each of the seven groups consists of more than 90% of an equivalent number of configurations. Similar examples are with the nine lowest 2^- states (Fig. 11), the eight lowest 6^- states (Fig. 15), and the five lowest 9^+ states (Fig. 7).

Figures 3–16 show compartments with small groups of states which may be considered as rather complete subsystems; Table IX shows the centroid energies. In a complete system the centroid energy of the eSM configurations is expected to coincide with the centroid energy of the states. In Sec. V B 1 we verify this assumption.

In this paper we do not discuss the configuration mixing in detail; we just want to compare the number of identified states for each spin and either parity with model predictions. Therefore, in Figs. 3–16 each identified state is connected with the eSM configuration one to one: M [Eq. (10)] $=$ m [Eq. (36)]. [Above $E_x = 6.20$ MeV states identified by NDS2007 with a firm spin assignment are shown with an energy label defined by Eq. (10).]

In several cases, the dominant configuration is known (Sec. II A 3), but more often no dominant configuration can be defined, especially for most positive-parity states. The number of states below a large gap should agree with the number of configurations as discussed in Sec. V A 1 [Eqs. (37), (38) and (51), (52)].

2. *Uncertainty of model excitation energies*

The mSM excitation energies are reliably calculated [16]; the energies of the two-particle–two-hole models are less certain [Eqs. (15)–(29)] because of the uncertain Coulomb energy [Eq. (5)]. However, at $E_x < 7$ MeV the number of eSM configurations is rather low (Table III). Therefore, the number of expected states can be judged convincingly.

The sSM predicts 70 states with negative parity at $E_x^{\rm sSM} \leqslant$ 6033 keV (Table II); the mSM energies are less than 6.20 MeV. The sSM predicts 50 states with positive parity at $E_x^{\rm sSM} \leqslant$ 5973 keV (Table I). Several mSM energies differ considerably from the sSM energies. The $i_{11/2}i_{13/2}$ 1^+ member is predicted at $E_x^{\rm mSM} = 6543$ keV (Fig. 3). The members of the configuration $f_{7/2}h_{11/2}$ with odd spin have energies above 6.30 MeV, while the members with even spin have energies below 6.15 MeV (Table I).

Two pairing vibration 0^+ states, 4 double octupole members ($0^+, 2^+, 4^+, 6^+$), 14 members of the $g_{9/2}p_{1/2} \otimes 3^-$ multiplet, and 3 other positive-parity states are expected at $E_x \lesssim 6.2$ MeV (Table III).

In total, all one-particle–one-hole and two-particle–two-hole models together predict the number of states (by including the ground state) as

$$N^{\rm predict}(1) = 72 \qquad \text{at } E_x < 5.45 \text{ MeV}, \tag{37}$$

$$N^{\rm predict}(2) = 146 \pm 3 \text{ at } E_x < 6.20 \text{ MeV}. \tag{38}$$

Some calculated eSM energies are close to $E_x =$ 6.20 MeV; therefore, the number $N^{\rm predict}(2)$ is shown with an uncertainty.

3. *Knowledge of spins and identification of states*

Just at $E_x > 6.20$ MeV, the knowledge of spins and the identification of states drops tremendously. Especially in the region $6.2 < E_x < 6.5$ MeV more than 30 levels are known [1]; many of them clearly exhibit admixtures of the configurations $g_{7/2}f_{5/2}$ and $d_{3/2}f_{5/2}$ [25,28]. Yet less than five spin assignments are firm.

Therefore, we discuss only states and restrict the discussion of "complete spectroscopy" to excitation energies $E_x <$ 6.20 MeV. Yet of equal importance is the presence of an extremely large gap at $E_x \approx 6.1$ MeV (Secs. II E 1 and III D).

(1) At $E_x \leqslant 5.87$ MeV all states with negative parity and dominant one-particle–one-hole configurations in ^{208}Pb are identified with high certitude [18]. Almost all states with positive parity and spins from 5^+ to 10^+ [12], all states with spin 0^+ [1,20], all states with spins 1^+, 3^+ (Sec. IV B 1), 11^+, and 12^+ (Sec. IV B 2), and probably also all states with spins 2^+ and 4^+ (Sec. IV C) are identified.

(2) In the region $5.80 < E_x < 6.20$ MeV, the states with configurations $d_{5/2}p_{3/2}$, $g_{7/2}p_{1/2}$, and $d_{3/2}p_{1/2}$, which produce extremely large cross sections, are present. However, positive-parity states with the configurations $i_{11/2}i_{13/2}$ and $i_{13/2}d_{3/2}$ are barely visible and weak $s_{1/2}f_{5/2}$ admixtures in negative-parity states may be hardly detected. Below $E_x \approx 6.2$ MeV, all states are assumed to be completely described by the mSM, except for few additional eSM configurations (Table III).

(3) The stronger configuration mixing for natural parity tends to spread the states across a larger energy region while for unnatural parity many states stay rather pure. For this reason the gap at $E_x \approx 6.1$ MeV may vanish. Yet in reality it seems to be still present (Secs. II E 1 and III D).

III. EXPERIMENTS

A. Experiments performed on the ^{208}Pb(p,p'), ^{208}Pb(d,d'), and ^{206,207,208}Pb(d,p) reactions

We used the Q3D magnetic spectrograph of the MLL at Garching (Germany) [2–4] to study states in ^{208}Pb in the range $3.0 < E_x < 8.1$ MeV. When we started the work in 2003, the final detector was just finished [4]. We had several beam times in 2003–2013 with the ^{206,207,208}Pb(d,p) and ^{208}Pb(d,d') reactions and with the resonant and nonresonant proton scattering on ^{208}Pb; see Table V.

Original data and some trials of fitting spectra by GASPAN [104] are stored at the Max-Planck Institute for Nuclear Physics at Heidelberg, Germany (MPIK) and the MLL (Garching) [31].

The ^{208}Pb(p,p') reaction is equivalent to the neutron pickup reaction on a target of ^{209}Pb in an excited state or in the ground state. It excites states with components of the neutron particle-hole configurations $LJ\,lj$ with particles in orbits $LJ = g_{9/2}$,

TABLE V. Experiments performed in 2003–2013 with the Q3D magnetic spectrograph of the MLL at Garching (Germany). The table shows (1) the reaction; (2) E^{beam}, beam energy; (3) Q value; (4) IAR in ^{209}Bi; (5) Θ, range of scattering angles; (6) N^{targ}, number of targets; (7) e^{isotop}, isotopic enrichment; (8) E_x, range of excitation energies; and (9) N^{run}, useful runs.

Reaction	E^{beam} (MeV)	Q value (MeV)	IAR in ^{209}Bi	Θ	N^{targ}	e^{isotop} (percent)	E_x (MeV)	N^{run}
^{208}Pb(d,d')	22			15°–45°	2	99.98	3.1–7.3	40
^{208}Pb(d,d')	24			47°–90°	1	99.98	3.9–5.8	6
^{207}Pb(d,p)	22	−2397.5		15°–38°	3	78.8, 99.1, 99.81, 99.96	3.1–7.8	40
^{207}Pb(d,p)	24	−2397.5		47°–112°	3	99.81	3.7–7.4	20
^{206}Pb(d,p)	22	−3758		15°–70°	2	99.96	4.5–7.7[a]	7
^{208}Pb(d,p)	24	+644.4		65°–96°	2	99.98	4.1–6.1[a]	7
^{208}Pb(p,p')	14.82–15.07		$g_{9/2}$	25°–115°, 138°	6	99.98	3.6–6.1	73
^{208}Pb(p,p')	15.72		$i_{11/2}$	20°–115°	5	99.98	4.1–6.0	42
^{208}Pb(p,p')	16.26–16.41		$j_{15/2}$	25°–115°, 138°	3	99.98	4.5–6.6	54
^{208}Pb(p,p')	16.43–16.63		$d_{5/2}$	30°–115°, 138°	10	99.98	3.1–8.0	80
^{208}Pb(p,p')	16.95		$s_{1/2}$	45°–84°	4	99.98	4.0–7.8	20
^{208}Pb(p,p')	17.30–17.72		$g_{7/2}$, $d_{3/2}$	20°–115°, 138°	3	99.98	4.2–7.8	24
^{208}Pb(p,p')	17.90–18.14		Off resonance	45°–90°, 138°	2	99.98	3.9–6.3	16

[a]The energies E_x^{contam} [Eq. (50)] are shown.

$i_{11/2}, j_{15/2}, d_{5/2}, s_{1/2}, g_{7/2}, d_{3/2}$ and holes in orbits $lj = p_{1/2}, p_{3/2}, f_{5/2}, i_{13/2}, f_{7/2}, h_{9/2}$.

Experiments covered all known IARs [25] and several off-resonance regions, especially $17.8 < E_p < 18.2$ MeV. Together with the ^{208}Pb(d,d') and ^{207}Pb(d,p) reactions, we investigated in effect ten different particle-exchange reactions exciting states in the doubly magic nucleus ^{208}Pb (Table V). In addition, we used published data from the ^{209}Bi($t,\alpha\,\gamma$), ^{207}Pb($d,p\,\gamma$), ^{208}Pb($p,p'\,\gamma$), and ^{207}Pb(d,p) experiments with polarized deuterons and ^{208}Pb(α,α') experiments (Sec. III B).

The 3^- yrast state was not studied; a single spectrum was taken for calibration purposes. Early observations of the ^{208}Pb(p,p') reaction reveal the collective octupole excitation [24]. Most higher excited states are described by one-particle–one-hole configurations [21–26]. Studies of the ^{207}Pb(d,p) reaction with polarized deuterons using the Q3D magnetic spectrograph at MLL, but with an older detector of lower resolution determined the strengths of two particle-hole configurations with the $p_{1/2}$ neutron hole in many states [33,34].

Several parts of the data were analyzed and results already published [5,6,10–12,14–18]; see also Ref. [105]. For this paper, all available Q3D data for ^{208}Pb at $4.60 < E_x < 6.20$ MeV are reanalyzed and discussed. The ^{208}Pb(d,d') reaction has been only recently performed; Figs. 17–20 show spectra covering the region $3.10 < E_x < 6.20$ MeV. All known states (Table VI) are shown. For clarity, the order number M and the parity π are shown above the spin I; the energy label $\tilde{E}_x$ [Eq. (10)] is shown below the spin (Sec. III C 4).

The peak shape in particle spectroscopy is highly asymmetric because of the interaction of both the incoming and outgoing particles with the atomic electrons [12,13,20]. A half-width at half-maximum (HWHM) of 1.5 keV on the low-energy side is achieved in many spectra. The mean distance between any two states at $3.90 < E_x < 6.20$ MeV is 15 keV; at $5.45 < E_x < 6.11$ MeV it is only 9 keV.

Hence, about one-third of all levels show up in doublets with a spacing of 2–6 keV (Sec. III F 3) and less than 2.5 keV (Sec. III F 4).

B. Other experiments described in the literature: ^{208}Pb(α,α'), ^{208}Pb(e,e'), and ^{208}Pb(p,p') with low resolution, ^{208}Pb(p,p') at high proton energies, ^{207}Pb(d,p) with polarized deuterons, ^{209}Bi($d,{}^3$He), ^{209}Bi($t,\alpha\,\gamma$), ^{207}Pb($d,p\,\gamma$), ^{208}Pb($p,p'\,\gamma$), and ^{208}Pb($n,n'\,\gamma$)

The amount of data on ^{208}Pb increased with every publication of Nuclear Data Sheets, from 72 levels in 1971 [106] at $E_x < 6.20$ MeV to about 140 levels in 1986 [107] and about 200 in 2007 [1]. The knowledge of ^{208}Pb states in 1971 was sparse [106]; the calibration of excitation energies varied by up to 6 keV.

The 1^-, 8^-, and 14^- and 1^+, 3^+, 5^+, 9^+, 10^+, 11^+, and 12^+ yrast states were unknown; the 2^-, 6^-, and 7^- and the 6^+, 7^+, and 8^+ yrast states were only suggested. Only the 0^-, 2^+, 3^-, 4^-, 4^+, and 5^- yrast states were already identified with an uncertainty from 0.1 to 0.5 keV. The knowledge on states with spins from 1^- to 7^- and 0^+ to 10^+ was limited; almost no γ data were available. (The 9^-, 10^-, 11^-, 12^-, and 13^- yrast states are still unknown today; the claimed assignments in NDS2007 are doubted.)

The most important source of other experimental data derives from the Nuclear Data Sheets in 2007 [1]. Valuable information derives from the experiments on ^{209}Bi($t,\alpha\,\gamma$), ^{207}Pb($d,p\,\gamma$), ^{208}Pb($p,p'\,\gamma$), and ^{208}Pb($n,n'\,\gamma$) with high-resolution γ spectroscopy. NDS2007 investigated these experiments in detail; the comments are highly appreciated.

Information on ^{208}Pb(α,α'), ^{208}Pb(e,e'), and ^{208}Pb(p,p') experiments at high proton energies, earlier ^{208}Pb(p,p') experiments via IAR in ^{209}Bi with low resolution, and experiments on ^{207}Pb(d,p) with polarized deuterons and ^{209}Bi($d,{}^3$He) were also discussed in NDS2007.

The most precise excitation energies were determined by the ^{208}Pb($n,n'\,\gamma$) reaction. Yet, except for few specific publications [53–56], no original ^{208}Pb($n,n'\,\gamma$) data are

TABLE VI. Levels in ^{208}Pb below $E_x = 6.20$ MeV. For details, see Sec. III C 6.

N^o	$\tilde{E}_x$	t,p p,t	Assignment I^π_M	Assignment Ref.	NDS2007 [1] I^π	NDS2007 [1] E_x (keV)	^{208}Pb(p,p') E_p = 14–18 (MeV) E_x [a] (keV)	^{208}Pb(p,p') Dominant IAR	^{208}Pb(d,d') E_d = 22 (MeV) E_x [a] (keV)	$d\sigma/d\Omega(\Theta^{avg})$ (d,d') [a] $[\frac{\mu b}{sr}]$	$d\sigma/d\Omega(\Theta^{avg})$ (p,p') [34] E_p = 22 (MeV) $[\frac{\mu b}{sr}]$	$d\sigma/d\Omega(\Theta^{avg})$ (α,α') [34] E_α = 40 (MeV) $[\frac{\mu b}{sr}]$	$d\sigma/d\Omega(\Theta^{avg})$ (d,p) [b] $[\frac{\mu b}{sr}]$	^{207}Pb(d,p) E_d = 22 (MeV) E_x [a] (keV)
		[c]		[d]										
1	0		0^+_1	[1]	0^+	0	0	[e]	0					0
2	2615	T,t	3^-_1	[1]	3^-	2614.522±0.010	2614.50±0.20	[e]	[f]		1000	7500	70	[f]
3	3198	T,t	5^-_1	[g]	5^-	3197.711±0.010	3197.70±0.10	$g_{9/2}$	3197.72±0.15	40	440	700	1400	[f]
4	3475		4^-_1	[g]	4^-	3475.078±0.011	3475.80±0.15	$g_{9/2}$	3474.90±0.15	15	42		1500	3475.30±0.15
5	3708	T	5^-_2	[h]	5^-	3708.451±0.012	3708.05±0.70	$g_{9/2}$	3708.25±0.10	30	780	<20	300	3708.50±0.70
6	3920		6^-_1	[h]	6^-	3919.966±0.013	3920.14±0.02	$g_{9/2}$	3920.05±0.10	4	125		1	3920.25±0.55
7	3947		4^-_2	[h]	4^-	3946.578±0.014	3946.73±0.05	$g_{9/2}$	3946.50±0.30	1	4		25	3946.25±0.30
8	3961	T,t	5^-_3	[h]	5^-	3961.162±0.013	3961.05±0.03	$g_{9/2}$	3961.30±0.15	6	35	42		[k]
9	3995		4^-_3	[h]	4^-	3995.438±0.013	3995.44±0.04	$g_{9/2}$	3995.65±0.15	4	35		25	3995.88±0.12
10	4037	T	7^-_1	[g]	7^-	4037.443±0.014	4037.40±0.02	$g_{9/2}$	4037.65±0.07	15	68	148		[k]
11	4051		3^-_2	[g]	3^-	4051.134±0.013	4051.11±0.05	$g_{9/2}$	4051.40±0.25	5	22	<20	1	4051.48±0.70
12	4086	T,t	2^+_1	[1]	2^+	4085.52±0.04	4085.50±0.04	[e]	4085.67±0.03	250	270	848	1	4085.55±0.25
13	4125		5^-_4	[h]	5^-	4125.347±0.012	4125.28±0.02	$g_{9/2}$	4125.35±0.15	7	15	37	60	4124.95±0.65
	(4144)				+	4144 ±5								
14	4180	T,t	5^-_5	[h]	5^-	4180.414±0.014	4180.33±0.03	$g_{9/2}$	4180.43±0.05	3	23	<20	100	4180.16±0.20
15	4206		6^-_2	[g]	6^-	4206.277±0.014	4206.28±0.02	$i_{11/2}$	4206.12±0.10	2	12		300	4206.44±0.08
16	4230		2^-_1	[g]	2^-	4229.590±0.017	4229.50±0.05	$g_{9/2}$	4229.47±0.10	4	30		90	4229.04±0.16
17	4255	T,t	3^-_3	[g]	3^-	4254.795±0.017	4254.64±0.05	$g_{9/2}$	4254.55±0.20	8	22	36	2	4254.15±0.50
18	4262		4^-_4	[g]	4^-	4261.871±0.013	4261.74±0.02	$g_{9/2}$	4262.00±0.20	6	8		30	4262.00±0.65
19	4297	T,t	5^-_6	[g]	5^-	4296.560±0.013	4296.39±0.05	$g_{9/2}$	4296.40±0.05	6	9	30	20	4296.00±0.40
20	4324	T,t	4^+_1	[1]	4^+	4323.946±0.014	4323.83±0.15	[e]	4323.74±0.16	100	195	255	1	4323.30±0.70
21	4359		4^-_5	[g]	4^-	4358.670±0.013	4358.59±0.05	$g_{9/2}$	4358.45±0.17	20	24		60	4357.88±0.46
22	4383		6^-_3	[g]	6^-	4383.285±0.017	4383.21±0.05	$g_{9/2}$	4383.07±0.13	4	12		10	4382.47±0.35
23	4424	T,t	6^+_1	[1]	6^+	4423.647±0.015	4423.53±0.16	[e]	4423.45±0.20	70	130	268		[k]
	(4447)				−	4447 ±5								
24	4481		6^-_4	[g]	6^-	4480.746±0.016	4480.84±0.04	$g_{9/2}$	4480.50±0.10	30	26	<20	1	4480.13±0.50
25	4611	T	8^+_1	[1]	8^+	4610.748±0.016	4610.81±0.05	$j_{15/2}$	4610.98±0.25	12	26	144	100	4610.33±0.05
26	4680		7^-_2	[5]	7^-	4680.266±0.022	4680.23±0.08	$i_{11/2}$	4680.27±0.03	2	8	<20		[k]
27	4698	T,t	3^-_4	[g]	3^-	4698.323±0.017	4698.32±0.02	$d_{5/2}$	4698.40±0.04	50	57	242	650	4698.30±0.03
28	4709		5^-_7	[5]	5^-	4708.727±0.021	4708.95±0.08	$i_{11/2}$	4709.34±0.06	15	5	30	20	4709.05±1.20
29	4712		4^-_6	[5]	4^-	4711.817±0.021	4711.70±0.06	$i_{11/2}$	4711.80±0.40	1	[i]		10	4711.42±0.15
30	4762		6^-_5	[5]	6^-	4761.956±0.023	4761.99±0.02	$i_{11/2}$	4761.93±0.10	3	8		4	4761.70±0.40
	(4830)				(8,9,10)	4830								
31	4842	t	1^-_1	[1]	1^-	4841.60±0.05	4841.63±0.16	[e]	4841.55±0.03	60	52	224	20	4841.72±0.17

TABLE VI. (Continued.)

N^o	$\tilde{E}_x$	t,p p,t	Assignment I^π_M	Assignment Ref.	NDS2007 [1] I^π	NDS2007 [1] E_x	^{208}Pb(p,p') $E_p = 14$–18 (MeV) E_x	^{208}Pb(p,p') Dominant IAR	^{208}Pb(d,d') $E_d = 22$ (MeV) E_x	$d\sigma/d\Omega(\Theta^{avg})$ (d,d') [a]	$d\sigma/d\Omega(\Theta^{avg})$ (p,p') [34] $E_p = 22$ (MeV)	$d\sigma/d\Omega(\Theta^{avg})$ (α,α') [34] $E_\alpha = 40$ (MeV)	$d\sigma/d\Omega(\Theta^{avg})$ (d,p) [b]	^{207}Pb(d,p) $E_d = 22$ (MeV) E_x [a]
		[c]		[d]		(keV)	(keV) [a]		(keV) [a]	[$\frac{\mu b}{sr}$]	[$\frac{\mu b}{sr}$]	[$\frac{\mu b}{sr}$]	[$\frac{\mu b}{sr}$]	(keV)
32	4861	T,t	8^+_2	[12]	8^+	4860.78±0.06	4860.83±0.04	$j_{15/2}$	4860.24±0.06	2	8	20	50	4860.75±0.26
33	4867		7^+_1	[12]	7^+	4867.91±0.04	4867.74±0.04	$j_{15/2}$	4867.73±0.23	6	12	< 20	150	4867.69±0.17
34	4868	T,t	0^+_2	[1]	0^+	4868.35±0.05	4868.25±0.10	[e]	4868.11±0.05	[i]	[i]			[k]
	(4878)					4878 ±2								
35	4895		10^+_1	[12]	10^+	4895.23±0.05	4895.10±0.10	$j_{15/2}$	4895.75±0.10	1	12	< 20		[k]
	(4909)					4909.5±0.3								
36	4911		4^-_7	[1]	4^-	4911.343±0.020	4911.37±0.06	$d_{5/2}$	4911.38±0.15	3	5		5	4911.66±0.15
37	4919		8^-_1	[5]	8^-	4918.8±0.4	4918.86±0.05	$i_{11/2}$	4918.73±0.07	2	12			[k]
38	**4928**		$\mathbf{6^+_2}$	[a]	2^+	4928.1±1.5	4928.85±0.15	$j_{15/2}$	4928.98±0.05	4	8			[k]
39	4937	T,t	3^-_5	[1]	3^-	4937.19±0.04	4937.11±0.06	$d_{5/2}$	4937.05±0.04	10	16	35	30	4937.17±0.04
40	4953		3^+_1	[18]	3^-	4953.302±0.017	4953.17±0.12	$d_{5/2}$	4953.24±0.06	3	6	< 20		[k]
41	**4962**		$\mathbf{5^+_1}$	[a]	$4^{(-)},5^{(+)}$	4962.428±0.21	4962.20±0.10	[e]	4962.18±0.08	3	[f]			[k]
42	4974	T	3^-_6	[1]	3^-	4973.918±0.19	4973.87±0.04	$d_{5/2}$	4973.79±0.08	40	35	156	1200	4973.76±0.04
	(4992)				$(2)^-$	4992.5±0.6								
43	4995		7^+_2	[12]	$\geqslant 7$	4994.7±0.6	4994.54±0.15	[e]	4993.38±0.20	2	6		1	4995.62±0.20
44	5010		9^+_1	[12]	9^+	5010.43±0.14	5010.70±0.03	$j_{15/2}$	5010.32±0.10	2	5			[k]
45	5038		2^-_2	[15]	3^-	5037.536±0.018	5037.45±0.04	$d_{5/2}$	5037.28±0.04	30	41		1000	5037.59±0.10
46	**5040**	T	$\mathbf{2^+_2}$	[l]		[j]	5039.40±0.30	[e]	5039.01±0.30	[i]	[i]	34		[k]
	(5056)					5056.1±0.3								
47	5069		10^+_2	[12]	10^+	5069.31±0.10	5069.00±0.08	$j_{15/2}$	5069.22±0.10	1	9	< 20	1	5070.15±0.90
48	5075	t	5^-_8	[5]	5^-	5074.81±0.06	5074.79±0.04	$i_{11/2}$	5075.58±0.08	20	19	48	2	5075.13±0.22
	(5076)				$-$	5075.78±0.18								
49	5080		6^-_6	[5]	6^-	5079.912±0.020	5080.00±0.06	$i_{11/2}$	5080.15±0.09	10	[i]		2	5080.14±0.25
50	5085		7^-_3	[5]	7^-	5085.470±0.024	5085.45±0.10	$i_{11/2}$	5085.29±0.05	20	26	50	2	5085.05±0.20
	(5087)				3^-	5087.9±0.15								
51	5093		8^+_3	[12]	8^+	5092.99±0.03	5093.26±0.05	$j_{15/2}$	5093.44±0.15	1	[i]	< 20	8	5093.00±0.13
	(5103)					5103.3±1.5								
52	5127		2^-_3	[15]	$2^-,3^-$	5127.356±0.016	5127.36±0.02	$d_{5/2}$	5127.21±0.06	25	14		600	5127.27±0.40
53	5162		9^+_2	[12]	9^+	5162.05±0.05	5162.40±0.03	$j_{15/2}$	5162.50±1.50	1	[f]			[k]
54	5193		5^+_2	[1]	5^+	5193.428±0.025	[i]	[i]	5193.83±0.05	[i]	[f]			[k]
55	5195		3^-_7	[18]	$3^-,4^-$	5195.054±0.023	5194.12±0.10	$d_{5/2}$	5194.42±0.08	2	[f]		15	5194.77±0.10
56	5196		7^+_3	[12]	7^+	5195.37±0.10	5195.35±0.08		5195.75±0.50	[i]	[f]		[i]	5195.48±0.25
57	5213	T,t	6^+_3	[12]	6^+	5213.007±0.021	5213.50±0.06		5213.15±0.18	[i]	[i]		[i]	5213.82±0.25
58	5214	T,t	5^-_9	[18]	(5^-)	5213.98±0.03	5214.04±0.08	$d_{5/2}$	5213.95±0.04	15	10	61	50	5214.00±0.25
59	5216		4^+_2	[1]	4^+	5216.214±0.018	5216.10±0.15	[e]	5215.76±0.45	20	21			[k]

TABLE VI. (*Continued.*)

N^o	$\tilde{E}_x$	t,p p,t	Assignment		NDS2007 [1]		^{208}Pb(p,p') $E_p = 14$–18 (MeV)		^{208}Pb(d,d') $E_d = 22$ (MeV)	$d\sigma/d\Omega(\Theta^{avg})$				^{207}Pb(d,p) $E_d = 22$ (MeV)
		[c]	I^π_M	Ref. [d]	I^π	E_x (keV)	E_x [a] (keV)	Dominant IAR	E_x [a] (keV)	(d,d') [a] $[\frac{\mu b}{sr}]$	(p,p') [34] $E_p = 22$ (MeV) $[\frac{\mu b}{sr}]$	(α,α') [34] $E_\alpha = 40$ (MeV) $[\frac{\mu b}{sr}]$	(d,p) [b] $[\frac{\mu b}{sr}]$	E_x [a] (keV)
	(5234)				+	5234 ±5								
60	*5235*		11^+_1	[70]	$(11)^+$	5235.37±0.11	5235.56±0.10	$j_{15/2}$	5235.31±0.20	3	6			[k]
61	5239		4^-_8	[5]	4^-	5239.3±0.4	5239.55±0.10	$i_{11/2}$	5239.79±0.22	5	[i]		5	5238.40±0.65
62	5241	T,t	0^+_3	[1]	0^+	5241.1±0.3	5241.00±0.10	[e]	5240.93±0.12	5	10	< 20		[k]
63	5245	t	3^-_8	[1]	3^-	5245.246±0.021	5245.23±0.02	$d_{5/2}$	5245.07±0.20	25	20	25	600	5245.15±0.28
	(5254)					5254.12±0.15								
	(5260)				9^+	5260								
	(5261)					5261.2±0.8								
	(5266)					5266.6±0.9								
	(5270)				$(11)^+$	5270								
64	5276		4^-_9	[5]	4^-	5276.418±0.024	5276.29±0.03	$i_{11/2}$	5276.47±0.10	2	5		70	5275.46±0.10
65	5280		0^-_1	[6]	0^-	5280.47±0.04	5280.58±0.03	$s_{1/2}$	5280.53±0.42	2	2		300	5280.25±0.60
66	**5286**	T,t	$\mathbf{2^+_3}$	[a]	$2,3^-$	5286.484±0.017	5286.42±0.10	[e]	5286.33±0.30	5	6	< 20		[k]
	(5291)				11^+	5291 ±6								
67	5292	T,t	1^-_2	[6]	1^-	5291.90±0.12	5292.19±0.07	$s_{1/2}$	5292.13±0.03	8	13	244	1200	5292.05±0.40
	(5307)					5307.6±1.5								
68	*5317*		3^+_2	[a]	$(3)^+$	5317.041±0.018	5316.70±0.10	[e]	5316.88±0.25	3	[f]		1	5316.13±0.20
69	*5318*		3^-_9	[a]	$(3^-)^m$	5317.2±0.6	5317.74±0.06	$d_{5/2}$	5317.55±0.30	[i]	[f]		1	5317.80±2.00
70	5327		9^+_3	[12]	+	5326.6±0.2	5326.42±0.03	$j_{15/2}$	5327.25±0.90	1	13			[k]
71	5339		8^+_4	[12]	8^+	5339.46±0.06	5339.46±0.04	$j_{15/2}$	5339.49±0.06	4	10	< 20	2	5339.18±0.80
72	5347	t	3^-_{10}	[1]	3^-	5347.270±0.018	5347.25±0.10	$d_{5/2}$	5347.25±0.05	50	64	87	80	5347.20±0.40
	(5352)				+	5352 ±6								
	(5364)					5364 ±3								
73	**5374**		$\mathbf{7^+_4}$	[12]	$(6)^+$	5373.8±0.8	5373.53±0.03	$j_{15/2}$	5373.58±0.08	2	9		4	45374.00±0.30
74	**5380**		$\mathbf{5^-_{10}}$	[a]	−	5380.6±0.8	5381.00±0.10	$d_{5/2}$	5380.90±1.00	1	9		1	5381.70±0.40
75	**5383**		$\mathbf{4^+_3}$	[a]	3^+–5^+	5382.82±0.03	5383.05±0.10	[e]	5383.70±0.15	15	9		1	5383.05±0.20
76	5385		3^-_{11}	[1]	3^-	5384.59±0.03	5384.62±0.03	[e]	[i]		31	< 20	120	5384.65±0.18
	(5401)					5401 ±2								
77	*5419*		6^+_4	[12]	$(6)^+$	5418.6±0.5	5417.30±0.15	$j_{15/2}$	5417.81±0.14	1	7			[k]
78	**5473**		$\mathbf{7^+_5}$	[a]	+	5473 ±6	5472.95±0.15	[e]	[i]		[f]			[k]
79	5482	T	5^-_{11}	[1]	5^-	5481.87±0.03	5481.72±0.02	$d_{5/2}$	5481.96±0.08	70	75	367	10	5481.73±0.26
	(5489)					5490 ±2								
80	5490		6^-_7	[18]	$(4^-,6^-)$	5490.34±0.05	5490.10±0.03	$g_{9/2}$	5490.63±0.26	15	[i]		30	5490.48±0.20
81	5492		4^-_{10}	[18]	$(4^-,6^-)$	5491.53±0.03	5491.57±0.03	$d_{5/2}$	5491.50±0.40	[i]	31		[i]	5491.95±0.65
82	**5502**		$\mathbf{6^+_5}$	[a]		5502 ±3	5502.80±0.25	$j_{15/2}$	5502.42±0.45	1	[i]		3	5502.87±0.45

TABLE VI. (*Continued.*)

N^o	$\tilde{E}_x$	t,p p,t	Assignment I^π_M	Assignment Ref.	NDS2007 [1] I^π	NDS2007 [1] E_x	^{208}Pb(p,p') $E_p = 14$–18 (MeV) E_x [a]	^{208}Pb(p,p') Dominant IAR	^{208}Pb(d,d') $E_d = 22$ (MeV) E_x [a]	$d\sigma/d\Omega(\Theta^{avg})$ (d,d') [a]	$d\sigma/d\Omega(\Theta^{avg})$ (p,p') [34] $E_p = 22$ (MeV)	$d\sigma/d\Omega(\Theta^{avg})$ (α,α') [34] $E_\alpha = 40$ (MeV)	^{207}Pb(d,p) $E_d = 22$ (MeV) (d,p) [b]	^{207}Pb(d,p) E_x [a]
		[c]		[d]		(keV)	(keV)		(keV)	$[\frac{\mu b}{sr}]$	$[\frac{\mu b}{sr}]$	$[\frac{\mu b}{sr}]$	$[\frac{\mu b}{sr}]$	(keV)
83	5512	T,t	1^-_3	[1]	1^-	5511.78±0.14	5511.91±0.10	$d_{5/2}$	5512.20±0.08	80	63	624	130	5512.04±0.08
84	5517	T,t	3^-_{12}	[1]	3^-	5516.714±0.023	5516.63±0.06	$d_{5/2}$	5516.90±0.13	60	50		20	5516.92±0.45
	(5524)				+	5524 ±3								
	(5531)					5531 ±3								
85	5537		10^+_3	[12]	10^+	5536.58±0.19	5536.28±0.04	$j_{15/2}$	5536.28±0.14	2	14			[k]
86	5543		7^-_4	[1]	7^-	5543.01±0.14	5543.35±0.15	$g_{9/2}$	5542.94±0.28	20	27			[k]
87	5546		5^-_{12}	[1]	5^-	5545.46±0.04	5545.15±0.15	$d_{5/2}$	5545.58±0.20	[i]	[i]		50	5545.08±0.30
88	5548		2^-_4	[1]	2^-	5548.113±0.023	5547.76±0.15	$d_{5/2}$	5547.84±0.22	15	26		[i]	5548.39±0.50
	(5554)					5554 ±2								
	(5557)					5557.2±1.0								
89	5561	T,t	2^+_4	[1]	2^+	5561.31±0.05	5561.70±0.20	[e]	5561.89±1.20	35	50	235	150	5561.76±0.30
90	5564		3^-_{13}	[1]	3^-	5563.73±0.04	5563.50±0.02	$d_{5/2}$	5563.69±0.04	[i]	[i]		[i]	5563.88±0.45
	(5565)				(4^+)	5565.2±0.05								
	(5572)					5572.0±0.08								
	(5576)					5576.6±1.5								
	(5579)					5579.0±0.09								
91	5587		5^+_3	[12]		5587.7±0.5	5587.60±0.06	$j_{15/2}$	5587.53±0.08	2	2		2	5587.68±0.45
92	5599		0^-_2	[6]	0^-	5599.48±0.06	5599.32±0.06	$s_{1/2}$	5599.49±0.25	15	11		60	5599.31±0.23
93	5615	T,t	7^+_6	[12]	7^+	5615.4±0.4	5614.80±0.05	$j_{15/2}$	5614.87±0.03	3	3			[k]
	(5627)				+	5627 ±5								
94	5640		1^-_4	[18]	1^-	5639.55±0.09	5639.25±0.20	$s_{1/2}$	5639.52±0.11	15	5	27	15	5640.03±0.17
95	**5642**	T,t	$\mathbf{2^+_5}$	[a]	$1,2^+$	5641.98±0.20	5642.20±0.10		5642.25±0.18	[i]	[i]		15	5641.62±0.35
96	5643		2^-_5	[18]	2–7^-	5643 ±4	5642.62±0.04	$d_{5/2}$	5642.74±0.35	15	8		[i]	5642.55±0.60
97	5648		3^-_{14}	[18]	$3^-,4^-$	5649.01±0.06	5648.97±0.02	$d_{5/2}$	5648.42±0.08	3	1		3	5648.16±0.25
98	5649		9^+_4	[12]	6^+–9^+	5649.5±0.4	5649.30±0.05	$j_{15/2}$	5649.31±0.24	[i]	[i]			[k]
99	5659		5^-_{13}	[11]	5^-	5658.51±0.04	5658.46±0.13	$g_{9/2}$	5658.44±0.16	20	21	25	10	5658.91±0.16
100	5667		0^+_4	[20]		5665.7±1.1	5666.70±0.15	[e]	5667.00±1.30	1	2	34		[k]
101	5675		4^-_{11}	[18]	$2^-,3,4$	5675.366±0.023	5675.45±0.10	$d_{5/2}$	5675.34±0.13	4	9		20	5675.63±0.08
102	5686		6^-_8	[11]	6^-	5686.5±0.7	5686.13±0.04	$g_{9/2}$	5686.30±0.05	13	8		10	5685.80±0.25
103	5690		4^+_4	[1]	4^+	5690.117±0.023	5690.90±0.06	[e]	5690.01±0.05	65	32	114	5	5690.10±0.20
104	5694	T,t	7^-_5	[11]	7^-	5694.22±0.12	5694.84±0.05	$g_{9/2}$	5694.90±0.07	7	14		2	5694.44±0.60
105	**5705**		$\mathbf{5^-_{14}}$	[a]		[j]	5704.66±0.18	$d_{5/2}$	5705.11±0.35	1	[f]		2	5705.02±0.30
106	5715	T,t	2^+_6	[1]	2^+	5715.53±0.09	5715.23±0.07	[e]	5715.61±0.05	3	3		2	5715.85±0.65
107	**5721**		$\mathbf{6^+_6}$	[a]	7^-	5721.51±0.04	5721.42±0.13	$j_{15/2}$	5721.40±0.25	20	17	67	3	5721.72±0.23
	(5727)				+	5727 ±6								
	(5737)					5737.9±0.3								

TABLE VI. (*Continued.*)

N^o	$\tilde{E}_x$	t,p p,t [c]	Assignment I^π_M	Assignment Ref. [d]	NDS2007 [1] I^π	NDS2007 [1] E_x (keV)	^{208}Pb(p,p') E_p = 14–18 (MeV) E_x [a] (keV)	^{208}Pb(p,p') Dominant IAR	^{208}Pb(d,d') E_d = 22 (MeV) E_x [a] (keV)	$d\sigma/d\Omega(\Theta^{avg})$ (d,d') [a] $[\frac{\mu b}{sr}]$	$d\sigma/d\Omega(\Theta^{avg})$ (p,p') [34] E_p = 22 (MeV) $[\frac{\mu b}{sr}]$	$d\sigma/d\Omega(\Theta^{avg})$ (α,α') [34] E_α = 40 (MeV) $[\frac{\mu b}{sr}]$	$d\sigma/d\Omega(\Theta^{avg})$ (d,p) [b] $[\frac{\mu b}{sr}]$	^{207}Pb(d,p) E_d = 22 (MeV) E_x [a] (keV)
108	5741		8^+_5	[12]	6^+–9^+	5741.1±0.4	5741.60±0.02	$j_{15/2}$	5741.67±0.05	5	2		3	5741.45±0.18
109	**5750**		$\mathbf{12^+_1}$	[a]	(11^+)	5749.67±0.14	5749.38±0.30	[e]	5750.45±1.30	1	4			[k]
110	5765		6^+_7	[12]	6^+	5763.7±0.8	5765.18±0.02	$j_{15/2}$	5765.24±0.06	2	4			[k]
111	5778		2^-_6	[15]	$2^-,3^-$	5777.96±0.03	5777.85±0.02	$d_{5/2}$	5777.92±0.04	13	8		200	5778.27±0.22
	(5783)					5783.22±0.07								
112	**5789**		$\mathbf{3^+_3}$	[a]	2^+–4^+	5789.34±0.04	5780.25±0.35	[e]	5788.23±0.80	2	[f]		1	5788.35±0.70
113	**5799**		$\mathbf{5^+_4}$	[a]		5799.41±0.09	5799.31±0.25	[e]	5799.49±0.08	1	2		10	5800.10±0.20
114	**5805**		$\mathbf{1^-_5}$	[a]	1	5805.0±0.3	5804.12±0.25	[e]	5805.06±0.15	2	[f]		10	5805.73±0.22
115	5812		2^-_7	[15]	[j]		5812.68±0.03	$d_{5/2}$	5812.70±0.90	[i]	[i]		[i]	5812.98±0.10
116	5813		3^-_{15}	[15]	3^-	5813.27±0.04	5813.28±0.02	$d_{5/2}$	5813.17±0.12	45	88	306	150	5813.30±0.18
117	**5819**	T,t	$\mathbf{2^+_7}$	[a]	$1^+,2^+$	5819.49±0.20	5819.50±0.35	[e]	[i]		[f]			[k]
118	**5825**		$\mathbf{8^+_6}$	[47]		5825.3±0.5	5825.10±0.35	[n]	5824.56±0.12	3	[f]	35	20	5824.60±0.30
	(5835)					5835 ±2								
119	5836		8^-_2	[11]	8^-	5835.8±0.6	5836.19±0.03	$g_{9/2}$	5836.36±0.04	25	9		10	5836.36±0.23
120	5844		1^+_1	[1]	1^+	5844.49±0.20	5844.45±0.10	[e]	5844.68±0.50	10	14		7	5845.49±0.27
121	5864		11^+_2	[1]	11^+	5860 ±6	5862.93±0.35	[e]	5862.80±0.25	1	[f]			[k]
	(5867)					5867 ±4								
122	5874	T	3^-_{16}	[15]	3^-	5873.573±0.023	5873.54±0.01	$g_{7/2}$	5873.21±0.04	25	15	43	900	5873.75±0.15
123	5886		4^-_{12}	[15]	4^-	5885.55±0.04	5885.48±0.10	$d_{5/2}$	5885.37±0.30	15	19		120	5885.56±0.30
124	5901		9^+_5	[12]	9^+	5901 ±3	5899.76±0.05	$j_{15/2}$	5699.35±0.08	2	1	< 20		[k]
125	**5918**	T,t	$\mathbf{4^+_5}$	[a]	$3^-,4,5^-$	5918.28±0.04	5918.25±0.16	[e]	5918.68±0.12	2	6			[k]
126	5924		2^-_8	[1]	2^-	5923.67±0.03	5923.53±0.03	$d_{3/2}$	5923.31±0.45	12	3		1400	5923.51±0.10
127	5928		10^+_4	[1]	10^+	5928.0±0.3	5927.75±0.45	[e]	[i]		[i]			[k]
128	**5937**		$\mathbf{1^+_2}$	[a]	+	5944 ±5	5936.60±0.25	[n]	[i]		[f]			[k]
129	5947	T,t	1^-_6	[1]	1^-	5946.77±0.02	5946.77±0.01	$d_{3/2}$	5946.54±0.06	10	13		1200	5947.07±0.10
	(5954)				9^+	5954 ±6								
130	5957		$[8^+_7]$	[o]		5957.3±0.6	5958.80±0.13	[n]	5957.85±0.15	1	5		1	5956.96±0.27
	(5966)					5965.8±0.4								
	(5967)				≈ 9	5967.8±0.8								
131	5969		4^-_{13}	[1]	4^-	5968.55±0.06	5968.59±0.16	$g_{7/2}$	5968.38±0.20	30	32		2400	5968.90±0.30
132	5973		2^+_8	[1]	2^+	5973.0±0.4	5972.27±0.27	[e]	[i]		[i]	< 20		[k]
133	5981		$[7^+_7]$	[o]		5981 ±2	5982.15±0.22	[n]	[i]		1			[k]
134	5989	T,t	6^+_8	[12]		5989.1±1.2	5988.82±0.25	$j_{15/2}$	5988.73±0.40	10	12			[k]
135	**5993**		$\mathbf{5^-_{15}}$	[a]	6^+	5992.67±0.25	5994.51±0.16	$g_{7/2}$	5994.22±0.22	50	87	115	10	5994.36±0.25
	(5996)					5996 ±5								
136	6010		3^-_{17}	[15]	3^-	6009.75±0.04	6009.65±0.15	$d_{5/2}$	6009.13±0.50	90	79	308	80	6009.63±0.20
137	6012		4^-_{14}	[15]	4^-	6011.64±0.06	6011.40±0.05	$d_{5/2}$	6011.27±0.45	[i]	[i]		[i]	6011.31±0.13

TABLE VI. (*Continued.*)

N^o	$\tilde{E}_x$	t,p p,t [c]	Assignment I^π_M	Ref. [d]	NDS2007 [1] I^π	NDS2007 [1] E_x (keV)	^{208}Pb(p,p') $E_p=$ 14–18 (MeV) E_x [a] (keV)	Dominant IAR	^{208}Pb(d,d') $E_d=22$ (MeV) E_x [a] (keV)	$d\sigma/d\Omega(\Theta^{avg})$ (d,d') [a] $[\frac{\mu b}{sr}]$	(p,p') [34] $E_p=22$ (MeV) $[\frac{\mu b}{sr}]$	(α,α') [34] $E_\alpha=40$ (MeV) $[\frac{\mu b}{sr}]$	(d,p) [b] $[\frac{\mu b}{sr}]$	^{207}Pb(d,p) $E_d=22$ (MeV) E_x [a] (keV)
138	6023		$[7^+_8]$	[p]		6020.4±2.0	6023.62±0.40	[e]	6023.46±0.25	3	[f]		10	6023.87±0.12
139	6026		$[8^+_8]$	[p]		6025.8±0.6	6024.97±0.30	[e]	6024.75±0.50	1	[f]		[i]	6025.15±0.15
	(6033)					6033 ±2								
140	<u>**6037**</u>	T	$\mathbf{6^+_9}$	[a]	$(5^+,6^+)$	6037.5±1.2	6037.01±0.13	[e]	6037.30±0.24	3	6		10[q]	6037.90±0.60
141	6054		4^+_6	[1]	4^+	6053.7±0.6	6053.36±0.10	[n]	6053.37±0.26	4	6	<20		[k]
142	6068		$[5^+_5]$	[o]	$(5^+,6^+)$	6068.2±1.2	6067.57±0.18	[n]	[i]		1		10[q]	6067.34±0.10
	(6071)					6071 ±5								
143	<u>**6076**</u>	T	$\mathbf{1^-_7}$	[a]	$0^-,1^-$	6076.4±1.3	6075.75±0.10	$d_{3/2}$	6075.40±0.75	1	3		1	6076.03±0.30
144	6085		$[3^+_4]$	[o]		[j]	6085.90±0.10	[n]	6085.45±0.15	10	15		[i]	6085.07±0.12
145	6086		2^-_9	[1]	2^-	6086.56±0.04	6086.50±0.04	$s_{1/2}$	6086.62±0.15	[i]	[i]		200	6086.43±0.05
146	<u>**6089**</u>		$\mathbf{3^-_{18}}$	[19]		[j]	6088.64±0.20	[e]	[i]	[i]	[i]	32	[i]	6088.11±0.20
147	<u>**6099**</u>	T	$\mathbf{4^+_7}$	[a]		6099.8±0.4	6097.71±0.07	[n]	6098.05±0.60		[i]	2		[k]
148	6101		12^+_2	[1]	12^+	6100.69±0.14	6100.65±0.10	$g_{7/2}$	6100.55±0.50	2	[i]		5	6100.86±0.15
149	<u>*6102*</u>		5^+_6	[1]	(5^+)	6101.1±1.0	6101.90±0.45	[n]	6101.45±0.50	[i]	10		10[q]	6101.70±0.90
	(6103)					6103.5±0.5								
	(6147)					6147.8±0.8								
	(6179)					6179 ±5								
150	6191	T,t	3^-_{19}	[1]	3^-	6191.0±1.5	6191.23±0.16	[e]	6191.54±0.50	5	5	43	5	6190.67±0.40
151	6193	T,t	2^+_9	[1]	2^+	6193.1±0.4	6192.46±0.18	[n]	6192.28±0.20	[i]	12	[i]	[i]	6192.70±1.00

[a]This work.
[b]Values for states below 4100 keV are from Ref. [32], or else from Ref. [34]; values less than 10 μb/sr are mostly from this work.
[c]Observed in the ^{206}Pb(t,p), ^{209}Pb(p,t) reactions [36,37], denoted by T,t, respectively (Sec. V D 1 and Table XI).
[d]Assignment of spin and parity; determination of major particle-hole configurations.
[e]Mostly nonresonant (p,p').
[f]No data.
[g]Spins and particle-hole configuration mixing determined in 1973 [87].
[h]Spins and particle-hole configuration mixing determined in 1982 [88], updated in 2013 [89]; see also Ref. [87].
[i]Unresolved doublet (Sec. III F 2).
[j]Not listed in NDS2007.
[k]Not observed (Sec. III F 2).
[l]Section III G 3.
[m]"This leaves the 5317.7 level as the possible candidate for $I^\pi = 3^-$" [1].
[n]IARs with parents from members of the multiplet $g_{9/2} \otimes 3^-_1$ (Sec. V G).
[o]Tentative assignment (Sec. IV C 3).
[p]The eSM suggests spin 3^+, 7^+, or 8^+; selection and order are unknown (Sec. IV C 3).
[q]The analyzing power of ^{207}Pb(d,p) with polarized deuterons indicates $g_{9/2}p_{1/2} \otimes 3^-_1$ admixtures (Sec. V E).

available. Half of the observed γ rays are not placed and for the other half no data about the neutron excitation function is shown. Nevertheless, the careful study of Martin [1,107] yields an important primary step of the evaluation of all data existing in 2007.

The Nuclear Data sheets from 1971 [106] together with the ^{208}Pb(p,p') data obtained by experiments with semiconductor counters at the MPIK (Heidelberg) in 1968 [28] were used in the analysis of the lowest 20 negative-parity states [87]; the EXFOR database presents the fitted angular distributions [105].

Spins were determined by considering the orthogonality relations as described in Sec. III G 1 and in Ref. [29]. Some spin assignment turned out to be wrong; the main reason was the ignorance of the state with the dominant $h_{9/2}s_{1/2}$ strength. The data from the ^{209}Bi(d,^{3}He) reaction obtained in 1982 [40] allowed for an update [88]. It clearly showed the 3946 4^- state to contain nearly the full $h_{9/2}s_{1/2}$ strength. A minor improvement of the update is shown in Ref. [89]. Important ^{208}Pb(p,p') data performed with a proton beam of 35 MeV were added by Wagner *et al.* [58] in 1975.

With the Nuclear Data sheets from 1986 [107] another round of improvement took place. Data taken in the 1990s from ^{209}Bi(t,$\alpha\,\gamma$) [103], ^{207}Pb(d,$p\,\gamma$) [46,103], ^{208}Pb(p,$p'\,\gamma$) [46], and ^{208}Pb(α,α') experiments [33,34,42,44] and a ^{207}Pb(d,p) experiment with polarized deuterons [33,34] became available. The ^{209}Bi(t,$\alpha\,\gamma$) experiment [103] clarified much of the ^{209}Bi(d,^{3}He) data [40].

By good chance some original data are still available. Grabmayr kept four ^{209}Bi(d,^{3}He) spectra, two of them with good statistics [41]. In addition, four spectra for the reaction ^{208}Pb(d,^{3}He) show the single-hole states in ^{207}Tl with pure $s_{1/2}$, $d_{3/2}$, $h_{11/2}$, and $d_{5/2}$ configurations. The spectra were reanalyzed using the deconvolution code GASPAN [104] and recalibrated with the help of NDS2007. The four scattering angles are carefully chosen to show the relative enhancement of the cross section for the $L = 5$ transfer.

Atzrott kept the complete set of spectra of the ^{208}Pb(α,α') experiment taken with the Q3D magnetic spectrograph at MLL in 1991 [43]; the resolution was about 11 keV. The analysis of these data is complicated because five spectra have to be compared for each level [42].

Only part of the ^{208}Pb(p,p') data taken in 1968–1969 was analyzed by Glöckner [27,28]. All original data were reconstructed. The analysis finished in 1972 [27] is being refined by help of GASPAN [104]; the data taken across the $g_{7/2}$ and $d_{3/2}$ IARs [31] can be evaluated. A rough comparison to the work of Wharton *et al.* [25] was already presented [28].

C. Figures and tables

1. Description of Figs. 3–16

The level schemes for all spins with mSM configurations, 0^-, 1^-, 2^-, 3^-, 4^-, 5^-, 6^-, 7^-, 8^-, and 14^- and 0^+, 1^+, 2^+, 3^+, 4^+, 5^+, 6^+, 7^+, 8^+, 9^+, 10^+, 11^+, and 12^+, are shown in Figs. 3–16. No firm identifications exist for spins 9^-, 10^-, 11^-, 12^-, and 13^-; the yrast states are predicted above $E_x = 6.20$ MeV. In addition the level scheme for the two-particle–two-hole configurations with spin 0^+ is shown.

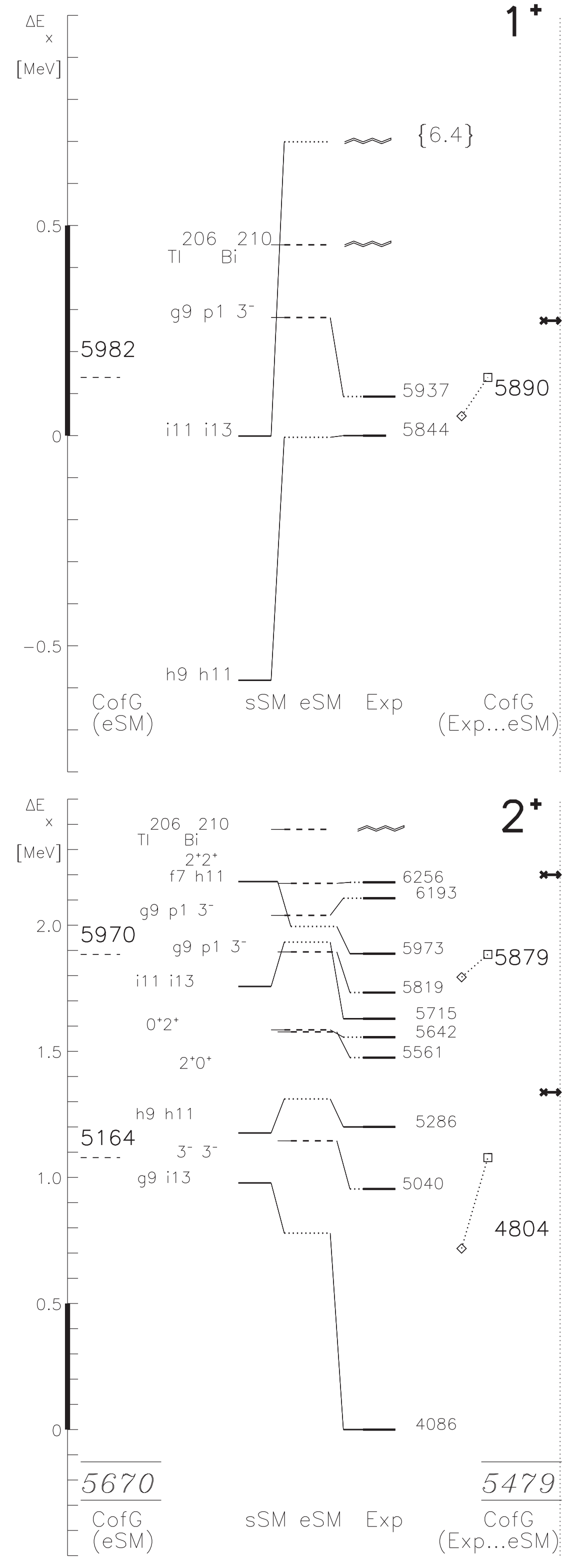

FIG. 3. Level schemes for states in ^{208}Pb with the spins of 1^+ and 2^+. For details, see Sec. III C 1.

Level schemes for states and configurations in ^{208}Pb are shown in Fig. 3 for spins 1^+ and 2^+ at $E_x < 7.4$ and 6.6 MeV, in Fig. 4 for spins 3^+ and 4^+ at $E_x < 6.4$ and 6.4 MeV, in

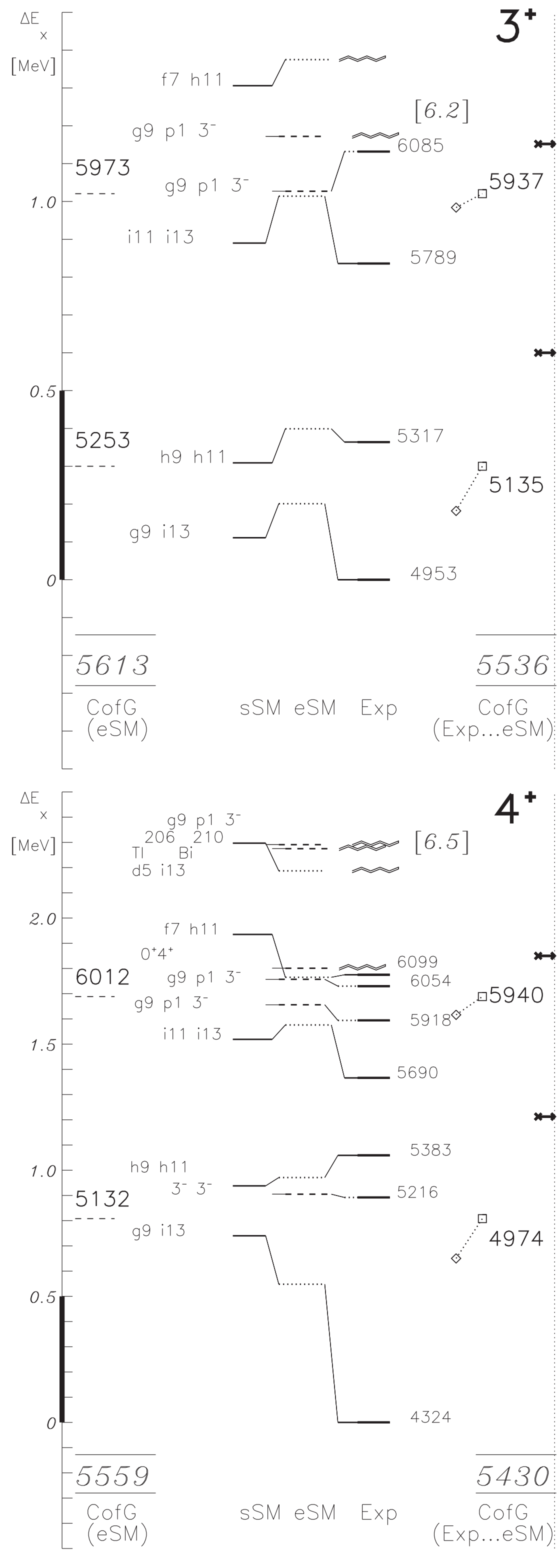

FIG. 4. Level schemes for states in ^{208}Pb with the spins of 3^+ and 4^+. For details, see Sec. III C 1.

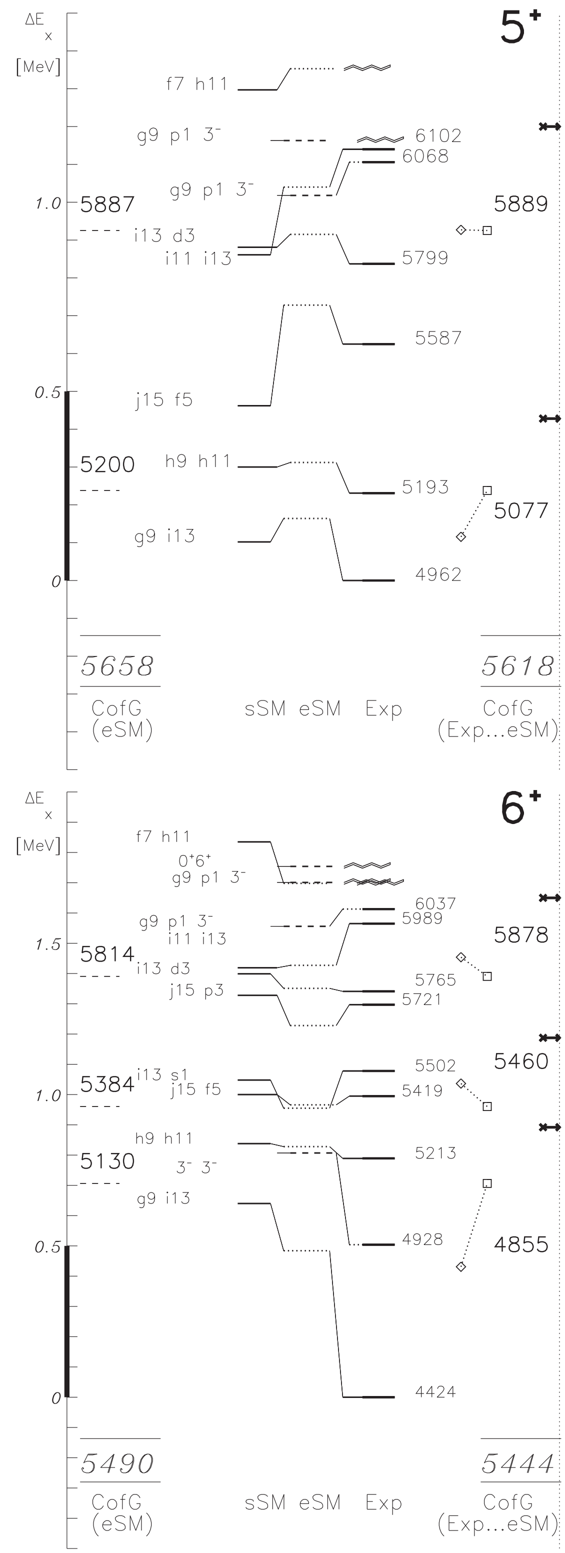

FIG. 5. Level schemes for states in ^{208}Pb with the spins of 5^+ and 6^+. For details, see Sec. III C 1.

Fig. 5 for spins 5^+ and 6^+ at $E_x < 6.4$ and 6.5 MeV, in Fig. 6 for spins 7^+ and 8^+ at $E_x < 6.4$ and 7.1 MeV, in Fig. 7 for spins 9^+ and 10^+ at $E_x < 6.5$ and 6.9 MeV, in Fig. 8 for spins 0^+ and 11^+ at $E_x < 6.3$ and 7.7 MeV, in Fig. 9 for spin 12^+ at $E_x < 8.7$ MeV, in Fig. 10 for spins 0^- and 1^- at $E_x < 7.8$ MeV and $E_x < 7.3$ MeV, in Fig. 11 for spin 2^- at $E_x < 7.2$ MeV, in Fig. 12 for spin 3^- at $E_x < 7.1$ MeV, in Fig. 13 for spin 4^- at $E_x < 7.0$ MeV, in Fig. 14 for spin

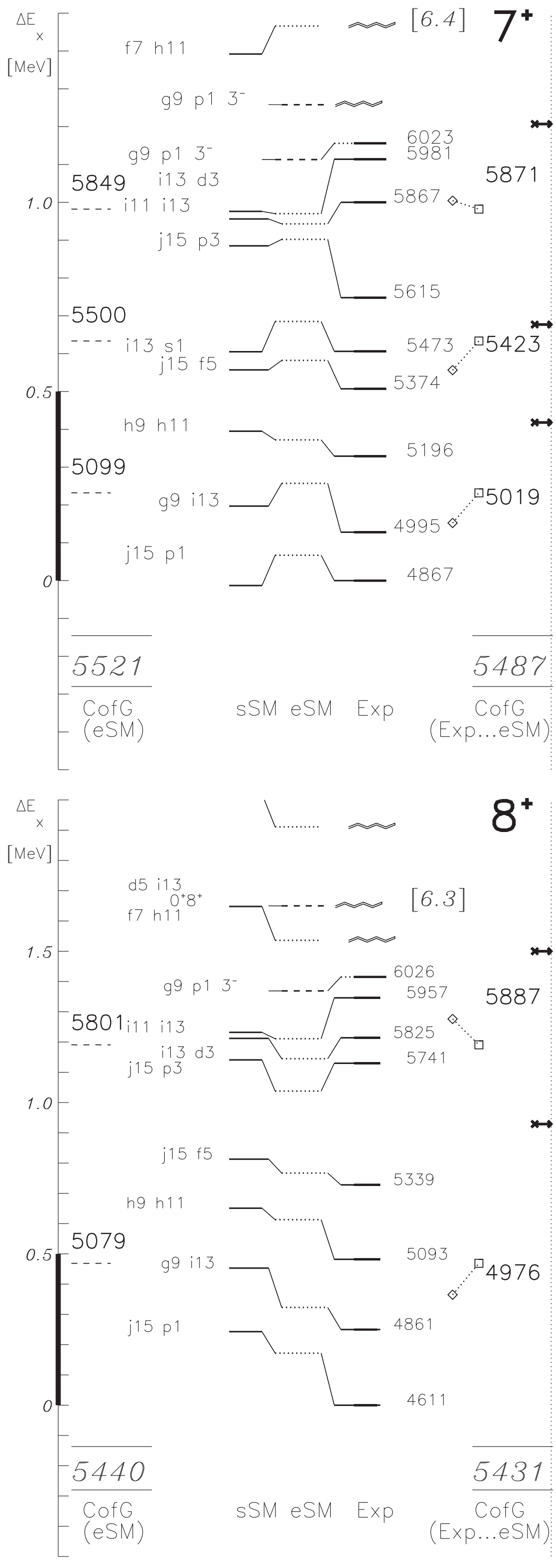

FIG. 6. Level schemes for states in ^{208}Pb with the spins of 7^+ and 8^+. For details, see Sec. III C 1.

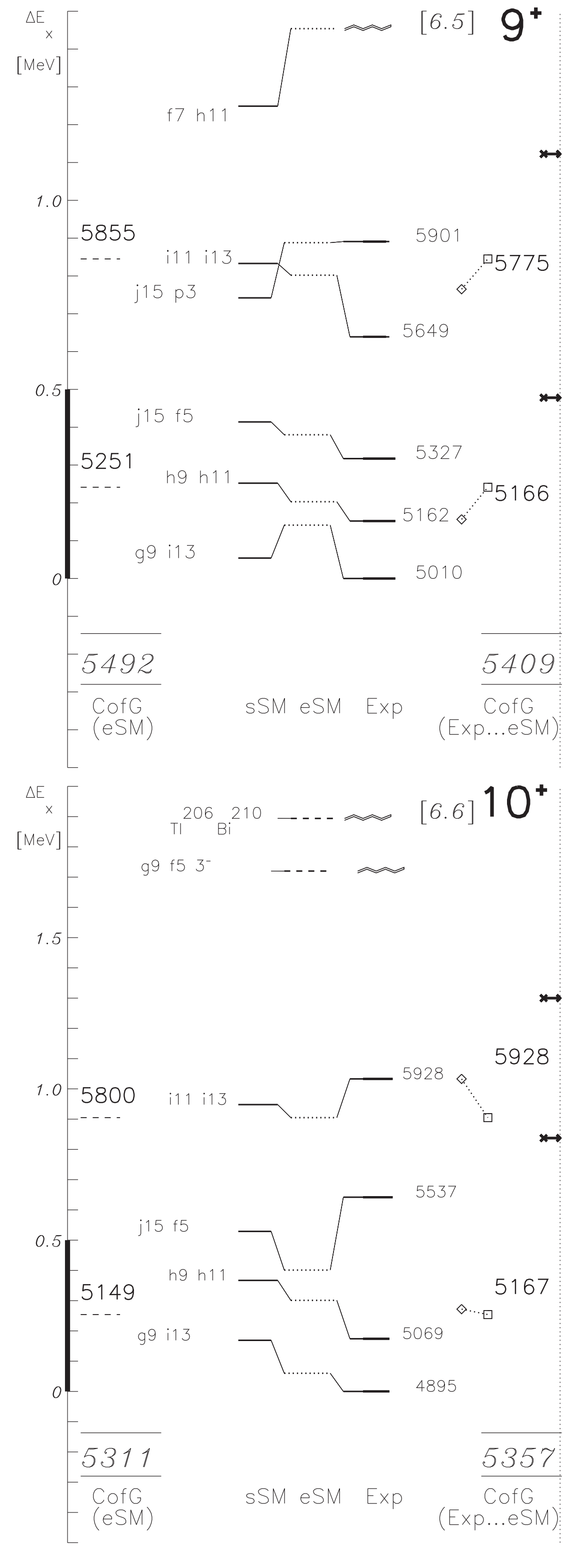

FIG. 7. Level schemes for states in ^{208}Pb with the spins of 9^+ and 10^+. For details, see Sec. III C 1.

5^- at $E_x < 6.7$ MeV, in Fig. 15 for spins 6^- and 7^- at $E_x < 6.9$ MeV and $E_x < 6.5$ MeV, and Fig. 16 for spins 8^- and 14^- at $E_x < 6.9$ MeV and $E_x < 7.8$ MeV, respectively.

In each figure, spin and parity are shown at the top. The relative energy scale starts with the excitation energy of the yrast state $E_x^{\rm exp}(I_1^\pi)$. The range of the lowest 0.5 MeV is

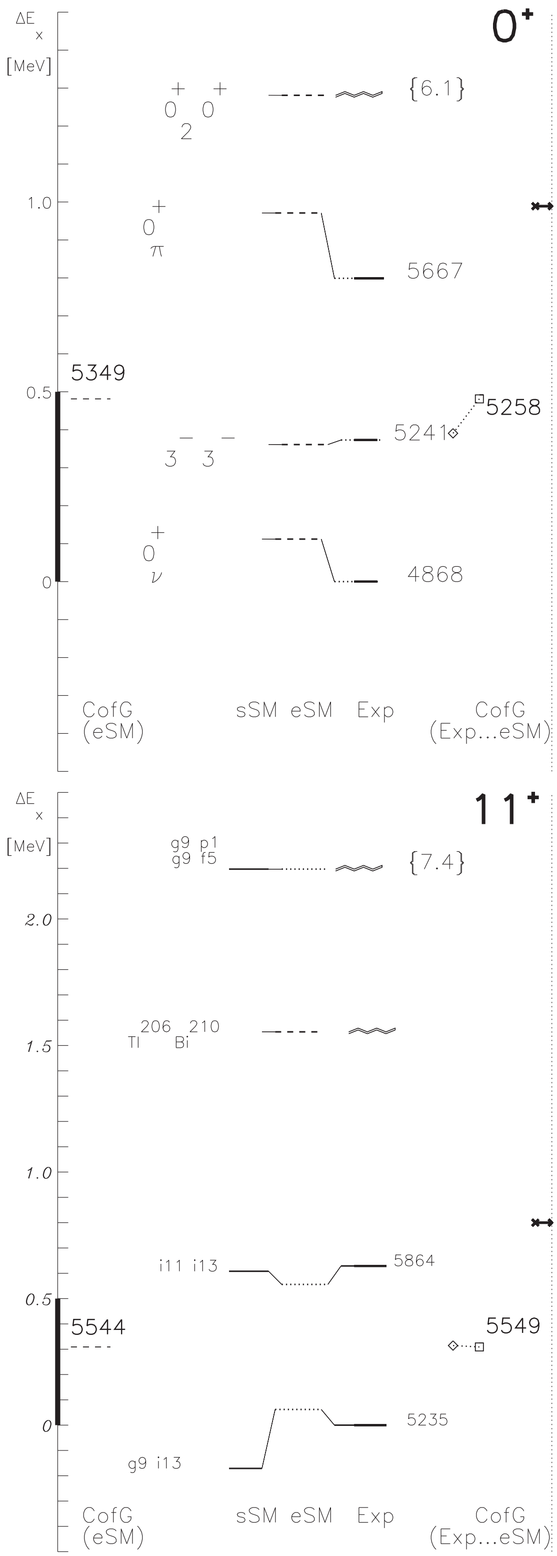

FIG. 8. Level schemes for states in ^{208}Pb with the spins of 0^+ and 11^+. For details, see Sec. III C 1.

marked because the shown ranges differ between 1.5 and 4.5 MeV for the various spins.

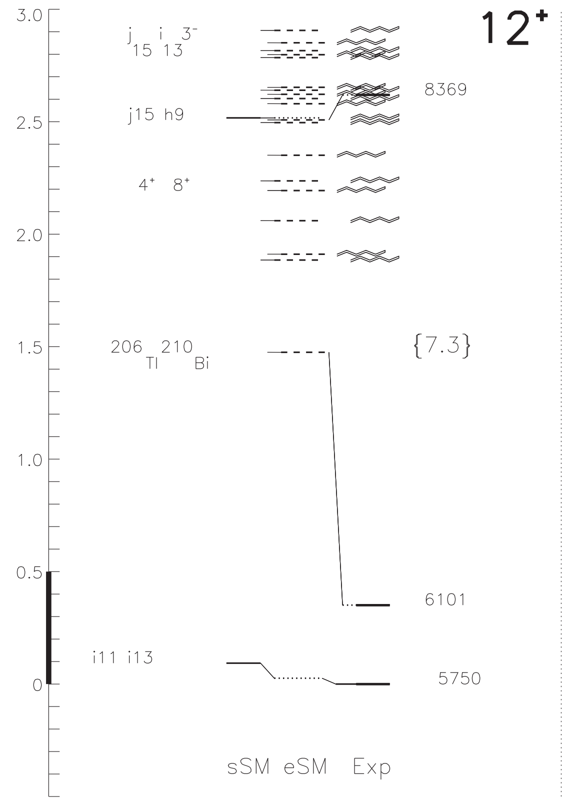

FIG. 9. Level scheme for states in ^{208}Pb with the spin of 12^+. The acronym of only five configurations is shown; Table IV shows all excitation energies and configurations. For more details, see Sec. III C 1. The 6101 state is discussed in Sec. IV B 3.

Each figure, from left to right, is as explained as follows.

(1) E_x^{cofg}(eSM) [Eq. (54)],

(2) $L_{2J}\, l_{2j}$ or name of eSM [Eqs.(15)–(31)],

(3) $E_x^{\mathrm{sSM}} - E_x^{\mathrm{exp}}$(yrast) [Eq. (3)],

(4) $E_x^{\mathrm{eSM}} - E_x^{\mathrm{exp}}$(yrast) [Eqs. (15)–(31)],

(5) $E_x^{\mathrm{exp}} - E_x^{\mathrm{exp}}$(yrast) [Eq. (10)],

(6) $\tilde{E}_x$ [Eq. (10)],

(7) E_x^{cofg}(exp) [Eq. (53)],

(8) E_x^{cofg}(eSM) [Eq. (54)].

(1) At left the centroid energy $\overline{E_x^{\mathrm{eSM}}}$ [Eq. (54)] calculated from the relevant eSM configurations is shown; at the bottom the global centroid energy for all considered eSM configurations is printed italic within a frame.
(2) The acronym of the sSM configuration (identical for mSM) is shown at left; $LJ\,lj$ is denoted by $L = s,p,d,f,g,h,i,j,\ \ l = s,p,d,f,g,h,i,\ \ 2J = 1,2,\ldots,$ and $2j = 1,2,\ldots$. The eSM configurations (Sec. II D) are described by the abbreviations in curly parentheses defined in Eqs. (15)–(31). For clarity, the acronym is omitted at higher energies for spins 2^-, 3^-, 4^-, and 6^- and for spin 12^+ in most cases.

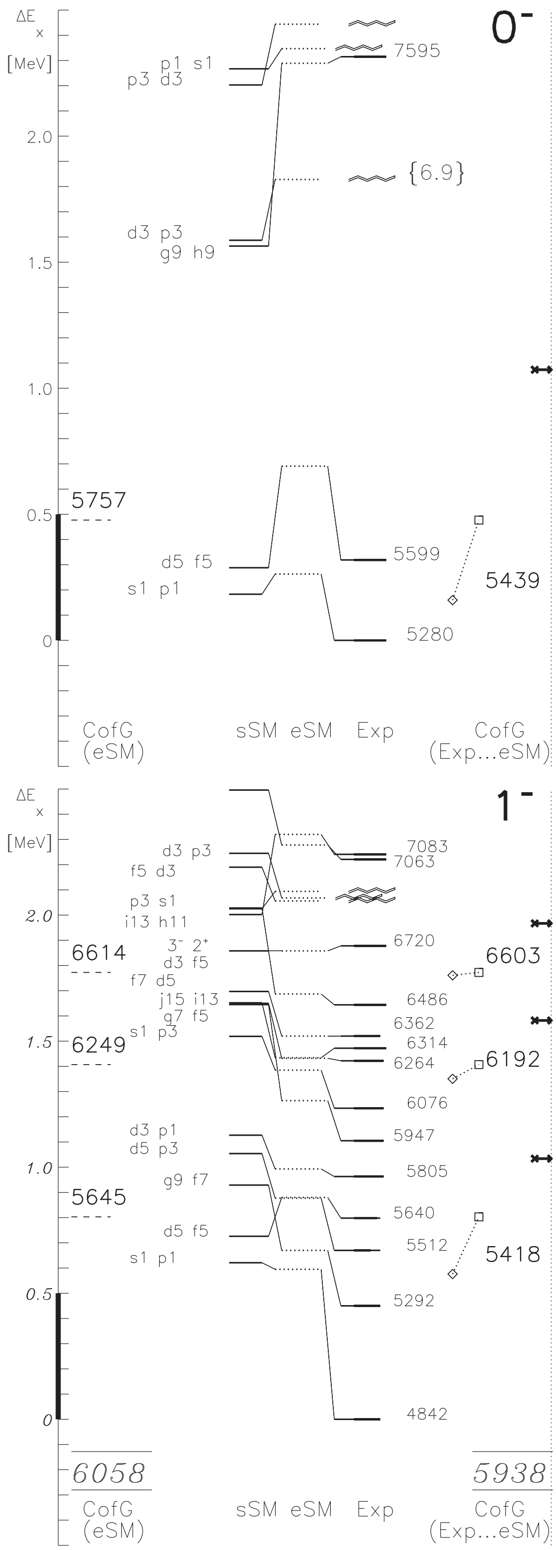

FIG. 10. Level schemes for states in ^{208}Pb with the spins of 0^- and 1^-. For details, see Sec. III C 1.

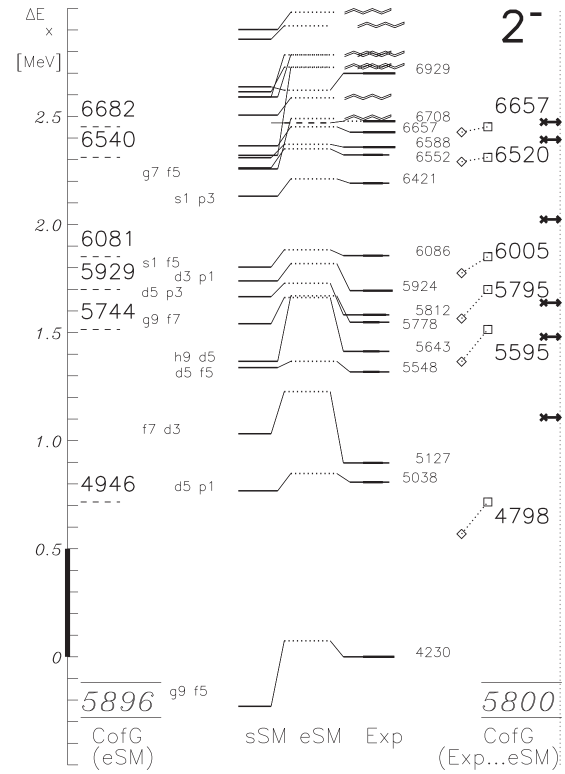

FIG. 11. Level scheme for states in ^{208}Pb with the spin of 2^-. For details, see Sec. III C 1.

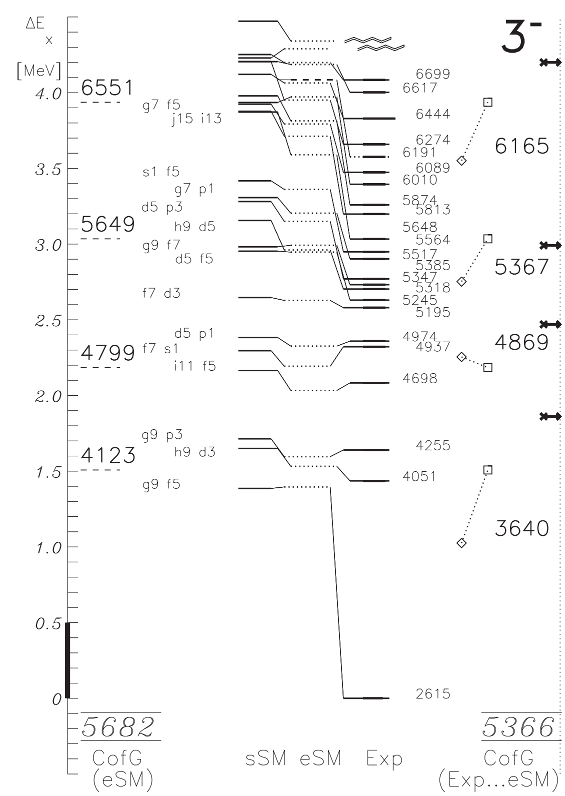

FIG. 12. Level scheme for states in ^{208}Pb with the spin of 3^-. For details, see Sec. III C 1.

(3) The energy $E_x^{\rm sSM}$ (Tables I and II) is drawn by a continuous line at left.

(4) The energy $E_x^{\rm mSM}$ [Eq. (6)] is shown in the middle by a dotted line; $E_x^{\rm eSM}$ calculated by Eqs. (6), (15)–(31) is

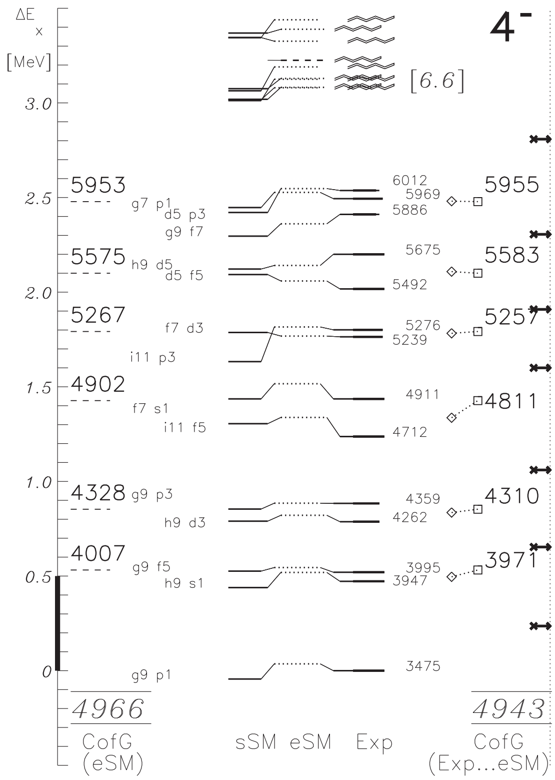

FIG. 13. Level scheme for states in ^{208}Pb with the spin of 4^-. For details, see Sec. III C 1.

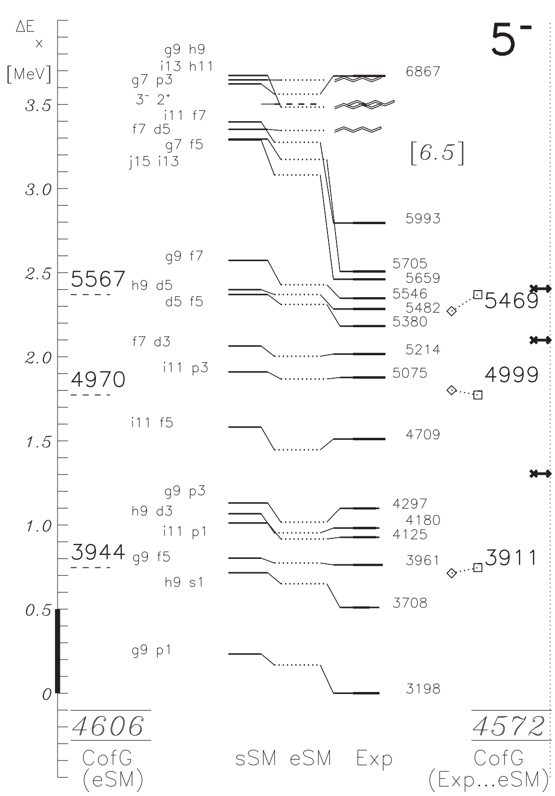

FIG. 14. Level scheme for states in ^{208}Pb with the spin of 5^-. For details, see Sec. III C 1.

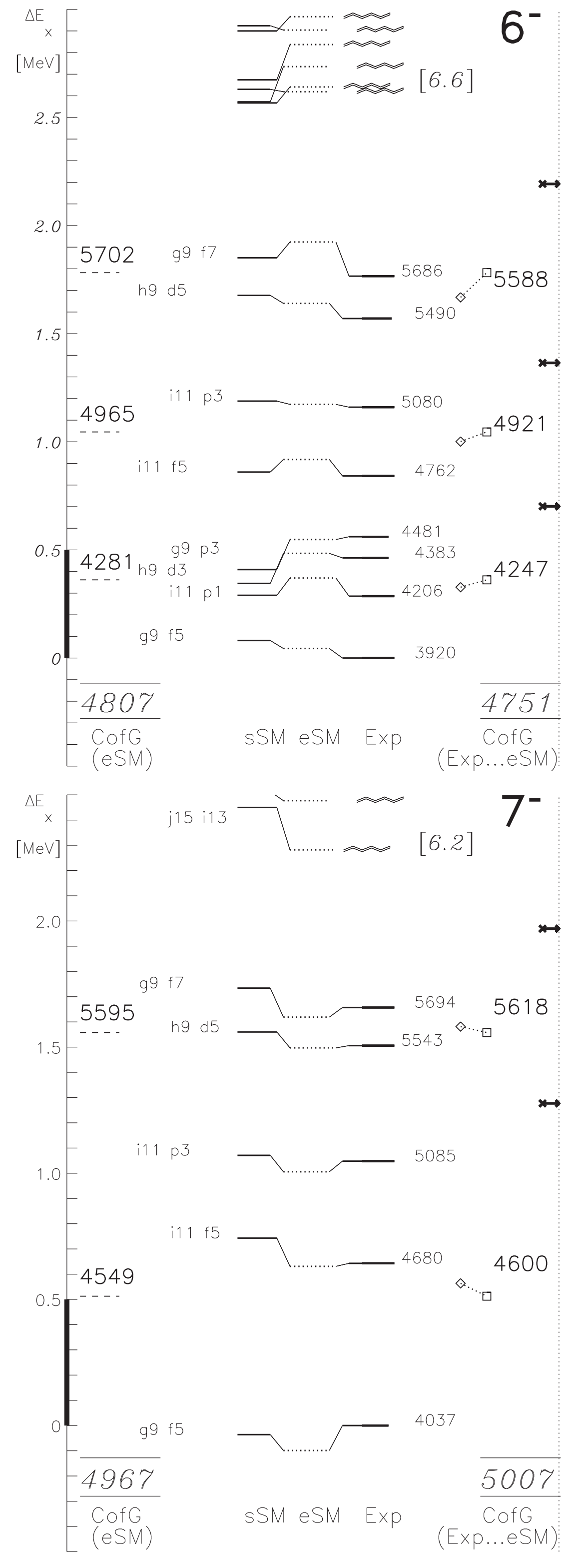

FIG. 15. Level schemes for states in ^{208}Pb with the spins of 6^- and 7^-. For details, see Sec. III C 1.

shown by a dashed line. The levels E_x^{mSM} are connected to E_x^{sSM} at left and E_x^{exp} at right. The two-particle–two-hole levels E_x^{eSM} are connected to E_x^{exp} at right. The

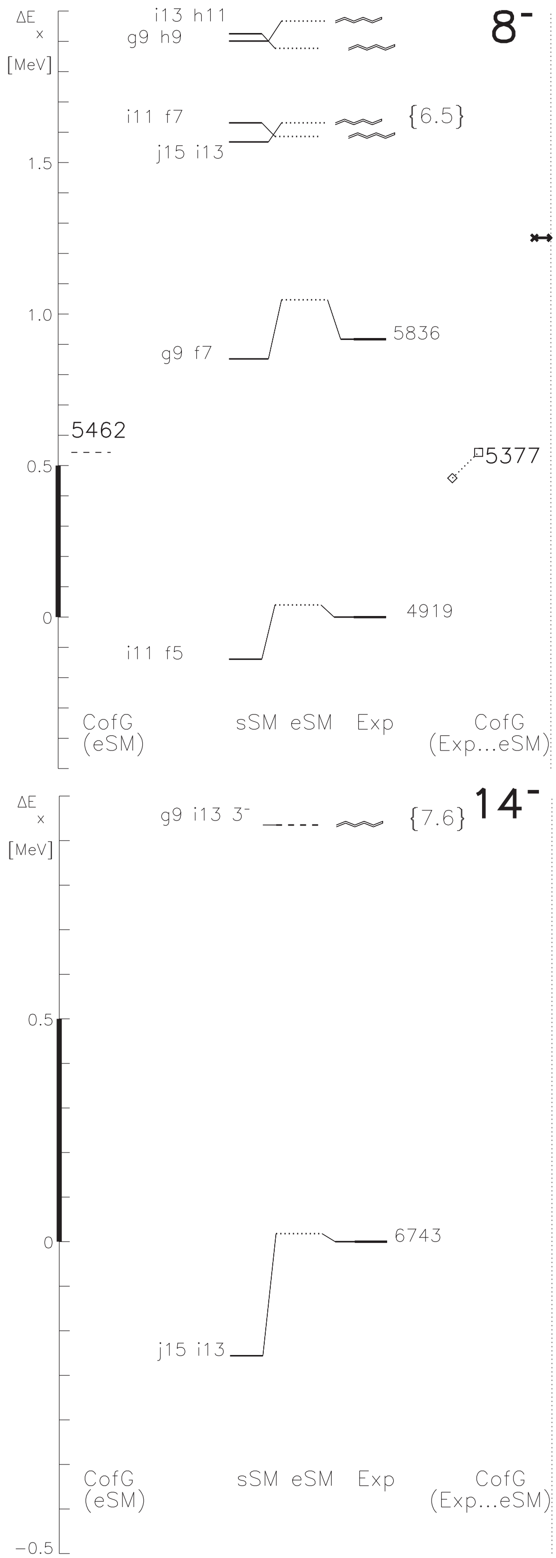

FIG. 16. Level schemes for states in ^{208}Pb with the spins of 8^- and 14^-. For details, see Sec. III C 1.

multiplet splitting is only shown for the configuration $g_{9/2}p_{1/2} \otimes 3_1^-$ [Eq. (27)].

(5) Energies E_x^{exp} are shown by a solid line at right. The staggering makes it possible to distinguish close-lying levels. States predicted within the shown range of excitation energies, but not yet identified are shown by a wavy line; for a few of them the expected excitation energy is given in units of MeV and curly parentheses.

(6) The energy label $\tilde{E}_x$ is shown at right.

(7) At right centroid energies are shown; they are listed in Table IX. Compartments for ensembles of states and corresponding configurations are denoted by short thick arrows at far right (Sec. V A). The centers of gravity $\overline{E_x^{\mathrm{exp}}}$ and $\overline{E_x^{\mathrm{eSM}}}$ [Eqs. (53) and (54)], marked by a diamond and a square, respectively, are connected by a dotted line; mostly the line is rising; see Eq. (57) and Sec. V B 1. The value $\overline{E_x^{\mathrm{eSM}}}$ is repeated at left and shown by a dashed line.

For clarity but rather arbitrarily, each configuration is connected to the state by assuming the order of the eSM configurations to be the same as the order of the states, M [Eq. (10)] = m [Eq. (36)]. Hence, the shown configuration does not have any meaning about its strength in the corresponding state.

The connection of the configurations to the state is sometimes contradicting because some states are known to contain more than 70% of another configuration as shown. Here we mention the following:

(i) the 5561 2_4^+ and 5819 2_7^+ states (these share the essential strengths of the two pairing vibration configurations $0^+2^+,2^+0^+$ [36,37] in Fig. 3 [see Eq. (20) and Sec. V D], but the eSM order numbers are 4 and 5);

(ii) the 5649 9_4^+ state with dominant $j_{15/2}p_{3/2}$ strength and the 5901 9_5^+ state with dominant $i_{11/2}i_{13/2}$ strength [12] in Fig. 7, but the eSM order numbers are 5 and 4;

(iii) the 5292 1_2^- state with dominant $s_{1/2}p_{1/2}$ strength [18,19,33,34], the 5512 1_3^- state with dominant $d_{5/2}f_{5/2}$ strength [18,19], the 5947 1_6^- state with dominant $d_{3/2}p_{1/2}$ strength [18,19,33,34], and the 6314 1_8^- state with dominant $s_{1/2}p_{3/2}$ strength [10,19] in Fig. 10, respectively. Yet the eSM order numbers are 1, 2, 5, and 7;

(iv) the 4051 3_2^- state with dominant $g_{9/2}f_{5/2}$ strength, the 4255 3_3^- state with dominant $h_{9/2}d_{3/2}$ strength, the 4698 3_4^- state with dominant $g_{9/2}p_{3/2}$ strength [87] in Fig. 12, the 5874 3_{16}^- state with dominant $g_{7/2}p_{1/2}$ strength [18,33,34], the 5648 3_{14}^- state with dominant $g_{9/2}f_{7/2}$ strength, and the 6010 3_{17}^- state with dominant $d_{5/2}p_{3/2}$ strength [18] in Fig. 12, respectively. Yet the eSM order numbers are 1, 2, 3, 13, 10, and 12;

(v) the 5239 4_8^- state with dominant $f_{7/2}d_{3/2}$ strength and the 5276 4_9^- state with dominant $i_{11/2}p_{3/2}$ strength [5] in Fig. 12, but the eSM order numbers are 9, 8;

(vi) the 3961 5_3^- state with dominant $h_{9/2}s_{1/2}$ strength [89] in Fig. 14, but the eSM order number is 2.

2. Description of Fig. 17

Figure 17 shows a spectrum for the ^{208}Pb(d,d') reaction at $3.1 < E_x < 4.0$ MeV on a logarithmic scale. Each peak has up to 23 resolved K and L satellites from the knockout of atomic electrons (Sec. III D). The combinations with the emission

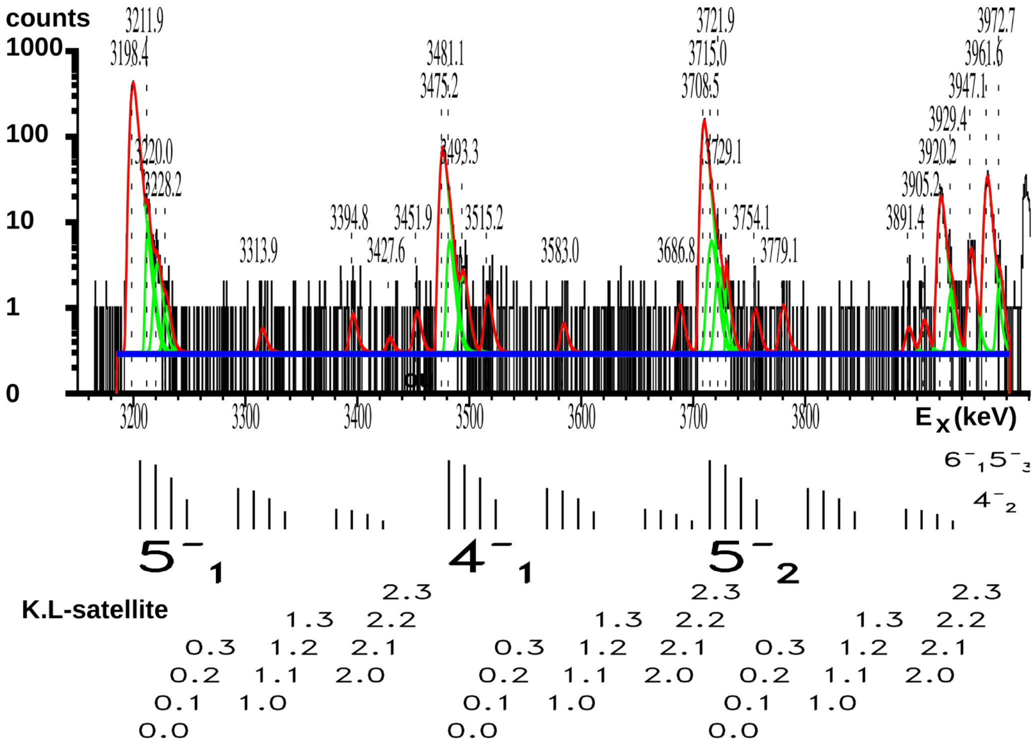

FIG. 17. Spectrum for the ^{208}Pb(d,d') reaction at $3.1 < E_x < 4.0$ MeV. For details, see Sec. III C 2.

of $K = 0,1,2$ electrons from the K shell and $L = 0,1,2,3$ electrons from the L shells are drawn in a schematic manner; they are denoted by $K.L = 0.0, \ldots, 2.3$. Several such satellites are recognized because of the high peak-to-valley ratio; the smooth background is fitted with 0.3 counts per channel.

Each peak is accompanied by the emission of up to 72 electrons from the M,N,O,P shells (Table VII); these satellites are not resolved but provide the finite resolution with a HWHM of 1.5 keV on the low-energy side.

TABLE VII. Binding energies of atomic electrons in lead; N_e is the number of electrons in the subshell.

Shell	Subshell	E_B (keV)	N_e
$\langle K\rangle$		88.005	⟨2⟩
L	I	13.066	2
L	II	15.200	2
L	III	15.861	4
$\langle L\rangle$		15.0	⟨8⟩
M	I	3.851	2
M	II	3.554	2
M	III	3.066	4
M	IV	2.586	4
M	V	2.484	6
$\langle M\rangle$		2.9	⟨18⟩
$\langle N\rangle$		0.5	⟨32⟩
$\langle O\rangle$		0.1	⟨18⟩
$\langle P\rangle$		0.1	⟨4⟩

3. Description of Figs. 18–20

Figures 18–20 show spectra on a linear scale for the ^{208}Pb(d,d') reaction at $3.90 < E_x < 6.20$ MeV. All states are identified; the excitation energy is shown by a vertical bar with the order number M above, spin I, parity π, and energy label $\tilde{E}_x$ below [Eq. (10)]. Each spectrum covers roughly 200 keV in excitation energy.

The spectra are chosen to avoid broad lines from contaminations of ^{12}C and other light nuclei. The scattering angles are $\Theta = 44°$, 44°, and 43° in Figs. 18(a)–18(c), 44°, 42°, and 43° in Figs. 19(a)–19(c), and 40°, 44°, 44°, and 38° in Figs. 20(a)–21(c), respectively. In Figs. 22(a) and 22(b) a broad contamination line is seen.

Satellites from the knockout of electrons are not fitted except for three L satellites near the 4086 2^- state: "4099.1", "4113.0", and "4141.1". However, they often are clearly recognized; see, e.g., near the 4324 4^+, 4424 6^+, 4974 3^-, 5038 2^-, and 5127 2^- states. In all evaluations they were fitted by GASPAN, tagged, and ignored in the subsequent analysis by NTNS (Sec. III E 1).

4. Description of Fig. 21

For the ^{208}Pb(p,p') reaction at $5920 < E_x < 6210$ keV taken near the $j_{15/2}$ IAR, Fig. 21 shows a spectrum on a logarithmic scale. Details are described in Sec. III E 2.

5. Identification of states in published spectra

Table V in Ref. [18] lists spectra with levels in ^{208}Pb in the energy range $2.4 < E_x < 6.5$ MeV published before 2014. Meanwhile, more spectra were shown in Refs. [19,20]. This

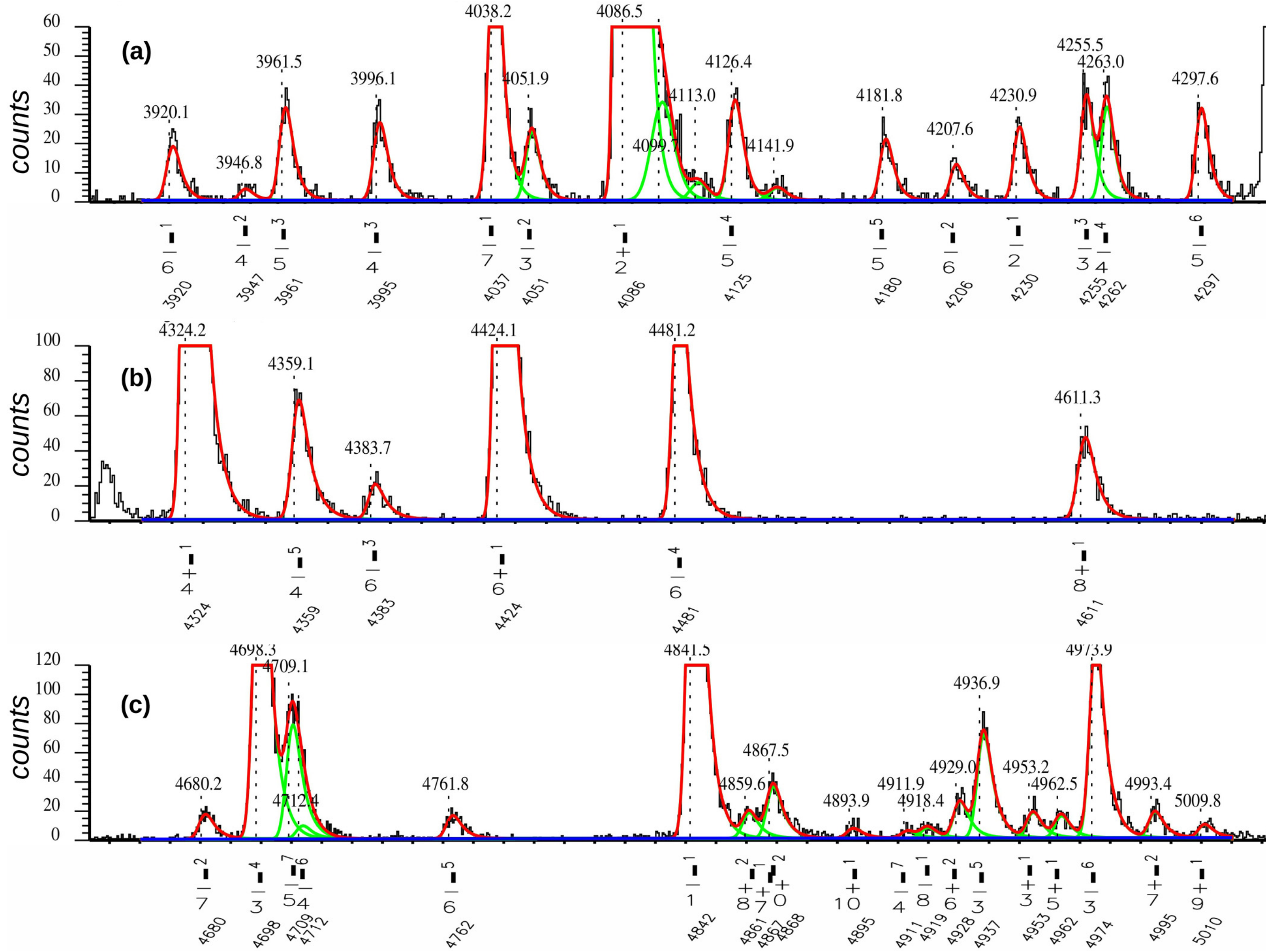

FIG. 18. Spectra for the ^{208}Pb(d,d') reaction at $3.9 < E_x < 5.0$ MeV. For details, see Sec. III C 4.

work identifies several states which were clearly observed in some earlier spectra fitted by GASPAN. In the following we mention some levels which were not yet identified in the relevant publications:

Figures 2 and 3 in Ref. [6] show ^{207}Pb(d,p) spectra. In Fig. 2 the 5239 4^-, 5245 3^-, 5779 4^-, 5280 0^-, 5286 2^+, 5291 1^-, 5327 9^+, 5339 8^+, and 5347 3^- states show up; the other levels are artifacts with L satellites. In Fig. 3 the 5548 2^-, 5564 3^-, 5587 5^+, 5599 0^-, 5715 7^+, 5640 1^-, and 5648 3^- states show up; the "5557.5", "5574.0", and "5578.3" levels are L satellites.
Figures 1–4 in Ref. [7] show ^{208}Pb(p,p') spectra taken on the $g_{9/2}$, $i_{11/2}$, $j_{15/2}$, $d_{5/2}$, $s_{1/2}$ IARs; they are also shown in Ref. [8]. Figure 1 shows the 5564 3^-, 5587 5^+, 5599 0^-, and 5715 7^+ states followed by the 5640 1^- state resolved from the two doublets with the unresolved 5642 2^+ and 5643 2^- states and the unresolved 5648 3^- and 5649 9^+ states. In Fig. 2 the 4709 5^- and 4712 4^- states are clearly resolved. Near most other IARs the 4698 3^- state is much more strongly excited and hence the two states are difficult to distinguish from L satellites of the 4698 state. Figure 3 shows three L satellites at 15, 30, and 45 keV distance to the 4481 6^- state. Figure 4 shows the 3947 4^- state clearly resolved despite the L satellite at 15 keV distance from the 3920 6^- state; the 3961 5^- state together with the first L satellite and the 3995 4^- state are shown, too.
Figures 1 and 2 in Ref. [10] show ^{208}Pb(p,p') spectra taken on the $s_{1/2}$ IAR. In addition to the marked 6086 2^- state, in Fig. 1 the 6068 5^+, 6075 1^-, and 6217 [1] states, the partially resolved doublets with the 6099 4^+, 6101 12^+, and 6102 5^+ states, and with the 6191 3^- and 6193 2^+ states show up. In Fig. 2 the unresolved doublet with the 6191 3^- and 6193 2^+ states shows up; the presented region $6.2 < E_x < 6.5$ MeV is of no interest to this paper.
Figures 2–4 in Ref. [11] show ^{208}Pb(p,p') spectra taken near the $g_{9/2}$, $j_{15/2}$, and $d_{5/2}$ IARs. In addition to the marked states, in Fig. 2 the unresolved doublets with the 5642 2^+ and 5643 2^- and the 5648 3^- and 5649 9^+ states and also the 5675 4^-, 5659 5^-, 5686 6^-, and 5695 7^- states show up; the proton beam energies cover the $i_{11/2}$, $d_{5/2}$, $s_{1/2}$ IARs and an off-resonance region. Figure 3 shows the same region as Fig. 2 but near the $g_{9/2}$ and

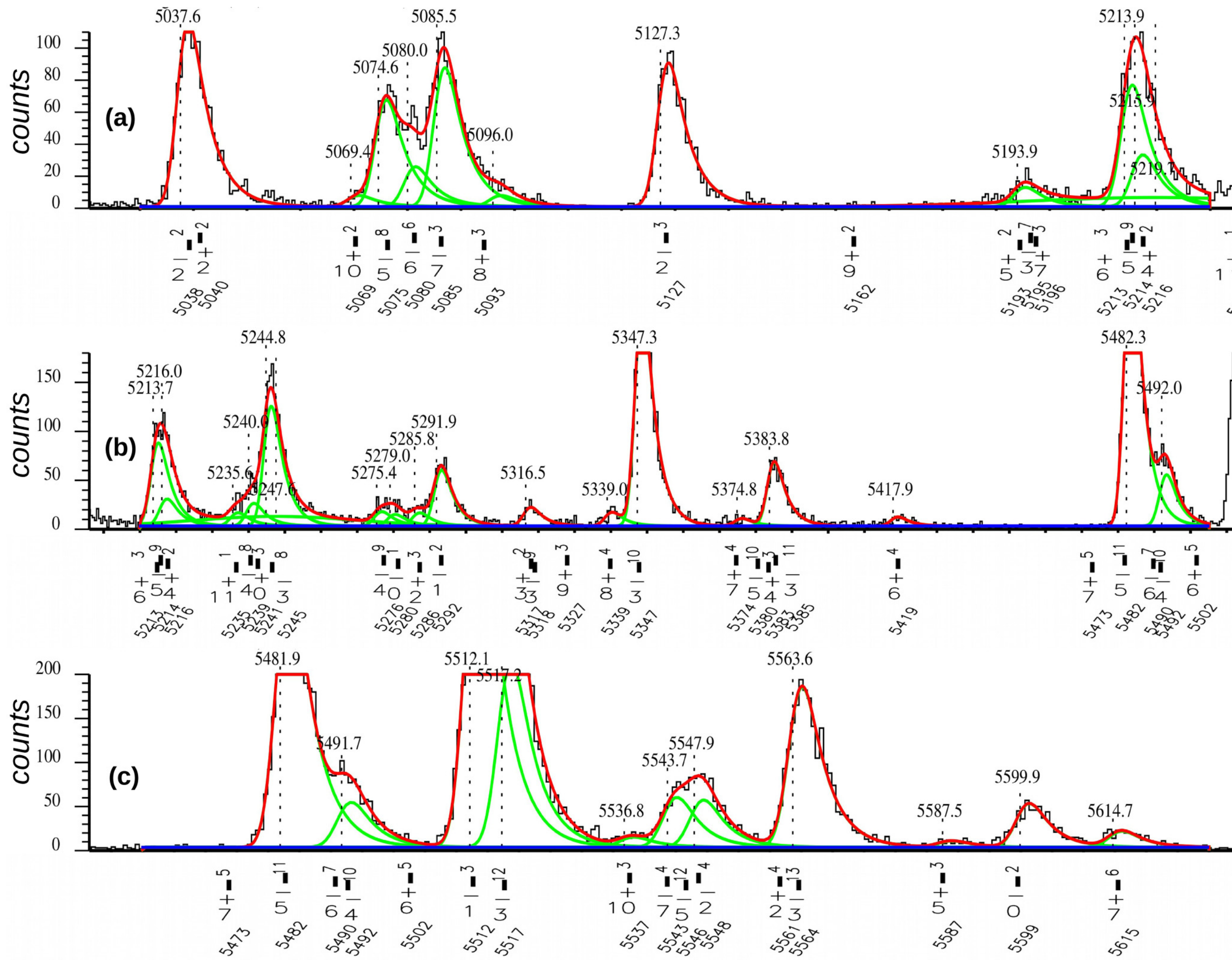

FIG. 19. Spectra for the ^{208}Pb(d,d') reaction at $5.0 < E_x < 5.6$ MeV. For details, see Sec. III C 4.

$i_{11/2}$ IARs. Near the $g_{9/2}$ IAR the 5640 1^- state appears in addition; the 5659 5^-, 5686 6^-, and 5695 7^- states with dominant $g_{9/2}f_{7/2}$ strength are much more strongly excited. In Fig. 4 the 5778 2^-, 5836 8^-, 5844 1^+, 5874 3^-, and 5886 4^- states and the unresolved 5812 2^-, 5813 3^- and 5819 2^+, 5825 8^+ doublets show up.

Figures 6–9 in Ref. [12] show ^{208}Pb(p,p') spectra taken near the $j_{15/2}$ and $d_{5/2}$ IARs; Fig. 12 in Ref. [12] shows a ^{207}Pb(d,p) spectrum. In addition to the marked states, in Fig. 6 the 4911 4^- and 4919 8^- states show up; in Fig. 7 the 4928 6^+, 5075 5^-, 5080 6^-, and 5085 7^- states show up; in Fig. 8 the 5640 1^- state next to the unresolved doublets with the 5642 2^+ and 5643 2^- states and with the 5648 3^- and 5649 9^+ states and also the 5675 4^-, 5675 6^-, and 5695 7^- states show up (the 5667 0^+ state is visible but not fitted); in Fig. 9 the 5874 3^-, 5886 4^-, 5924 2^-, 5938 1^+, 5947 1^-, 5957 6^+, 5969 4^-, and 5993 5^- states show up. In Fig. 12 the 5020 level belongs to the $\frac{5}{2}$ state at $E_x = 4388$ keV in ^{207}Pb produced by weak contaminations of ^{206}Pb in the target (Table V).

Figure 1 in Ref. [15] shows ^{208}Pb(p,p') spectra for the region $5.96 < E_x < 6.05$ MeV taken on the $d_{5/2}$ and $g_{7/2}$ IARs, demonstrating the capability of GASPAN to resolve 2-keV doublets. This work refines it (Fig. 21) and shows besides the L satellites the existence of the 5981 7^+, 5989 6^+, 5993 5^-, and 6023 7^+ states next to the strong peaks of the 5969 4^-, 6010 3^-, and 6012 4^- states. Figure 2 in Ref. [15] corresponds to Figs. 22 and 23.

Figures 3–10 in Ref. [18] show ^{208}Pb(p,p') spectra taken near all IARs. All states known at that time are marked. We mention only new states and changed spin assignments. In Fig. 3 the 5474 7^+ state cannot be discerned; it only shows up if the spectrum is displayed on a logarithmic scale and if the peak-to-valley ratio would be better. The 5502 6^+ state is newly recognized (Sec. IV C 2). In Fig. 9 the 5474 7^+, 5502 6^+, 5642 2^+, 5667 0^+, 5789 3^+, 5799 5^+, 5805 1^-, and 5825 8^+ states are newly recognized (Sec. IV C 2). The 5537 10^+, 5561 2^+, 5587 5^+, 5614 7^+, 5690 4^+, 5715 2^+, 5764 6^+, and 5844 1^+ states show up in addition to the marked states (which all have negative parity). In Fig. 10 the 5901 9^+, 5938 1^+, 5957 8^+, 5981 7^+, 5993 5^+, 6023 7^+, 6037 6^-, and 6068 5^+ states and the unresolved doublet with the 6191 3^- and 6193 2^+ states are newly recognized

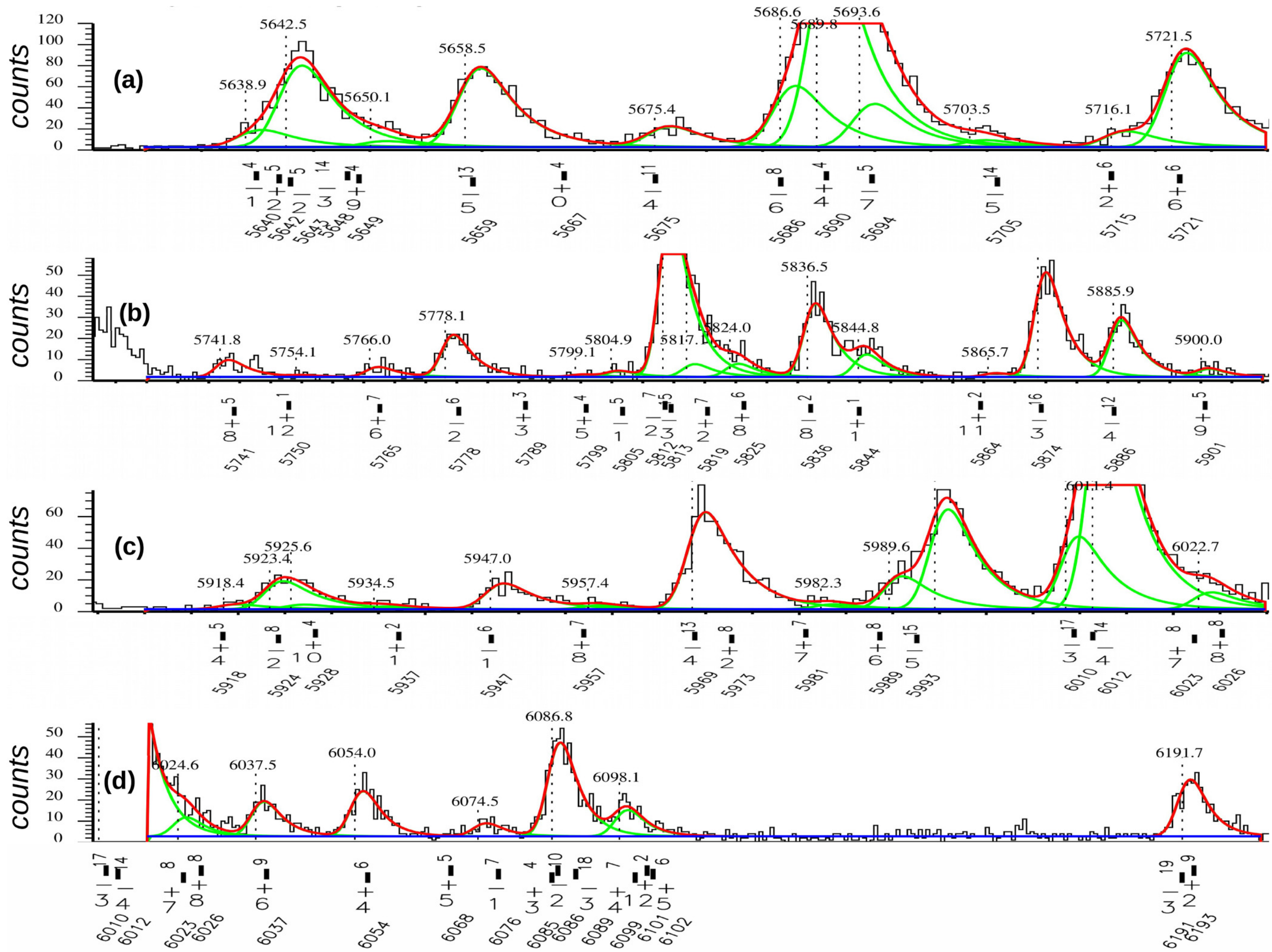

FIG. 20. Spectra for the ^{208}Pb(d,d') reaction at $5.60 < E_x < 6.20$ MeV. For details, see Sec. III C 4.

(Sec. IV C 2). The 5918 4^+, 5928 10^+, 5973 2^+, 6054 4^+, 5973 2^+, 5973 2^+, 6076 1^-, 6085 3^+, 6086 2^-, and 6089 3^- states cannot be discerned. The doublet with the 6191 3^- and 6193 2^+ states is unresolved. The "5907.3" level is not confirmed.

Figures 1–5 in Ref. [19] show ^{208}Pb(d,d') and ^{207}Pb(d,p) spectra and ^{208}Pb(p,p') spectra taken near the $g_{9/2}$, $i_{11/2}$, $j_{15/2}$, $d_{5/2}$, and $s_{1/2}$ IARs. In addition to the marked 1^- states, in Fig. 1 the 4860 8^+ and 4867 7^+ states unresolved from the 4868 0^+ and 4595 10^+ states show up. Figure 2 displays the clearly resolved 5935 11^+ and 5241 0^+ states next to the much stronger 5245 3^- state and the clearly resolved 5280 0^- and 5286 2^+ states next to the much stronger 5292 1^- state. Figure 3 displays the clearly resolved 5640 1^- state next to the unresolved doublets with the 5642 2^+ and 5643 2^- and with the 5648 3^- and 5649 9^+ states. (The "5664.8" level is a contamination line.) Figure 4 displays the resolved 6089 3^- state on the high-energy side of the 6086 2^- state. The partially resolved doublet with the 6099 4^+, 6101 12^+, and 6102 5^+ states and the weakly excited 6054 4^+, 6068 5^+, and 6076 1^- states are clearly recognized.

Figure 1 in Ref. [20] shows spectra summed up from several runs taken for ^{208}Pb(p,p') taken near the $g_{9/2}$, $i_{11/2}$, $j_{15/2}$, and $d_{5/2}$ IARs and for ^{208}Pb(d,d'). The 5640 1^- state next to the unresolved doublets with the 5642 2^+ and 5643 2^- states and with the 5648 3^- and 5649 9^+ states and also the 5675 4^-, 5686 6^-, 5690 4^+, and 5695 7^- states show up.

6. Description of Table VI

Table VI shows all levels reported by NDS2007 and all identified states at $E_x < 6.20$ MeV. The 151 identified states are enumerated in the first column. The next column show the energy label $\tilde{E}_x$ [Eq. (10)] followed by the footmarks "T" and "t" referring to the observation by the ^{206}Pb(t,p) and ^{210}Pb(p,t) reactions (Sec. V D 2). Vertical lines denote doublets (Sec. III A). Doublets with spacings of 2–6 keV are marked by single vertical lines and discussed in Sec. III F 3; doublets with a spacing of less than

2.5 keV are marked by double vertical lines and discussed in Sec. III F 4.

In the columns "Assignment" the spin I, parity π, and order number M are shown; the given reference shows the main source of the spin and parity assignment and/or the determination of the major particle-hole configurations (Sec. IV). The two following columns show the information from NDS2007 about spin assignments and excitation energy. The next two columns show the excitation energy determined by ^{208}Pb(p,p') and the IAR with a dominant configuration; because of the large difference in the single-particle widths for the holes [28], the indication of "dominance" has no strict meaning; it just gives a hint to the IAR where a large cross section was observed. States excited by the nonresonant reaction are marked. The two following columns show the excitation energy and the mean cross section for the ^{208}Pb(d,d') reaction determined by this work.

They are followed by the information about the mean cross section for the ^{208}Pb(p,p') and ^{208}Pb(α,α') reactions with $E_p = 22$ MeV and $E_\alpha = 40$ MeV [33,34]. The mean cross sections are taken at $\Theta^{\rm avg} \approx 43^\circ, 40^\circ, 27.5^\circ$, and 25° for the (d,d'), (p,p'), (α,α'), and (d,p) reactions, respectively. Only one entry for a doublet with natural parity states is shown. Values for ^{208}Pb(α,α') are shown for levels where data are known. [Note that (α,α') excites essentially only natural parity states.] In the last column the excitation energy for the ^{207}Pb(d,p) reaction is shown, $E_d = 22$ MeV [33,34]. The values for the ^{207}Pb(d,p) reaction are supplemented by results from this work (Table V).

New spin assignments discussed in this work are printed in boldface, confirmed spin assignments in italic, and tentative assignments in square parentheses. New spin assignments since the publication of NDS2007 are underlined. Energy labels $\tilde{E}_x$ in parentheses show levels considered to be spurious (Sec. VI).

D. Knockout of atomic electrons

The identification of nuclear states in ^{208}Pb by particle spectroscopy is hindered by the knockout of atomic electrons (Table VII). The reaction ^{208}Pb$(p,p'+ze^-)^{208}$Pb^{z+}, $z = 0,1,2,\ldots$, was already discussed [12] and more details were shown [7].

The emission of electrons from the outer shells M,N,O,P broadens the peak and produces a tail to each peak. The fit by the computer code GASPAN uses a Gaussian peak and an exponential tail modeled by the complementary Gaussian error function [12]. The M electrons with binding energies between 2.4 and 3.8 keV limit the resolution to 1.5 keV HWHM.

The K electrons from the innermost shell with a binding energy of $E_B = 88$ keV produce K satellites with a probability of about 1 per mill. About a dozen strong peaks are observed in spectra with peak-to-valley ratios from 1000:1 to 10 000:1.

The most annoying effect derives from the L satellites; here the binding energy is $E_B \approx 15$ keV (Table VII). Relative to the main peak, the cross section for the first L satellite at 15 keV distance is about 1%. For stronger peaks a series of satellites in multiples of 15 keV with decreasing probability is generated; in total there are eight L satellites (Fig. 17). During the fit of the spectra by GASPAN, peaks recognized as L satellites are tagged. In the later analysis by NTNS they are handled like background from contaminations by light nuclei (^{1}H, ^{2}H, ^{12}C, ^{14}N, ^{16}O, ^{40}Ar).

In a pragmatic fit procedure, the Gaussian peak of the L satellite is assumed to be slightly broader while the exponential tail is similar. The peak of a L satellite may have nearly the same position in the detector as the peak from a state about 15 keV higher in excitation energy but without a L satellite; GASPAN does fit both peaks at the same position in the detector. The fit sometimes is not affected by the order of the two peaks with different widths; in such cases the order is chosen by comparison of the excitation energy to data from NDS2007. A systematic uncertainty is thus introduced.

Figure 17 shows satellites observed for the 3198 5^-_1, 3475 4^-_1, and 3709 5^-_2 states in the ^{208}Pb(d,d') reaction; the peak-to-valley ratios are about 1500:1, 200:1, and 500:1, respectively. The expected energies for 12 satellites are indicated.

For each level without K and L satellites (the main peak which contains more than 90% of the total intensity) the first two L satellites without accompanying K electrons are clearly visible. The intensities of these L satellites are a few percent of the main peak. The two K satellites accompanied by L electrons are observed with an intensity of a few per mill of the main peak.

Because of the low probability $K+L$ satellites appear stochastically with often only one to three counts. Note that K satellites in contrast to $K+L$ and L satellites are not broader than peaks from physical states.

The relative intensity for the 3946 4^-_2 state is comparable or even less than the intensity of the first L satellite of the 3198 5^-_1 state. It is only a few times larger than estimated for satellites of the 3709 5^-_2 state with two K and four L electrons (denoted as K^2+L^4 or $K.L = 2.4$). Yet the peak is not broader than other main peaks and hence any contribution from satellites is low.

The 4086 2^+ level in Fig. 21 shows many of the 23 satellites from the expulsion of K and L electrons. Clearly observed are the first four L satellites (here the level 4125 5^- coincides with one satellite). About nine combinations of K and L satellites can be recognized; seven levels nearly coincide with levels from states in ^{208}Pb.

In Sec. III E 2 a realistic example is discussed where two L satellites mask five states (Fig. 18). Similar examples are found in the ^{206,207,208}Pb(d,p) reactions and also for the ^{208}Pb(p,p') reaction via IARs in ^{209}Bi, where $p_{1/2}$ and $p_{3/2}$ holes are coupled to $s_{1/2}$, $d_{3/2}$, $d_{5/2}$, $g_{7/2}$, and $g_{9/2}$ particles and thus produce huge cross sections, but more often other levels appear in between. More examples and detailed analyses of L satellites are discussed in Refs. [7,8]; see Sec. III C 5.

Each spectrum taken with the ^{208}Pb(p,p'), ^{208}Pb(d,d'), and ^{207}Pb(d,p) reactions covers up to 200 levels. For each level possible satellites from the K and L shells are considered with the restriction that the peak-to-valley ratio suggests the appearance. For L satellites a ratio larger than 100:1 in a distance of around 15–45 keV is needed; for $K+L$ satellites a ratio larger than 1000:1 in 100 and 200 keV distance.

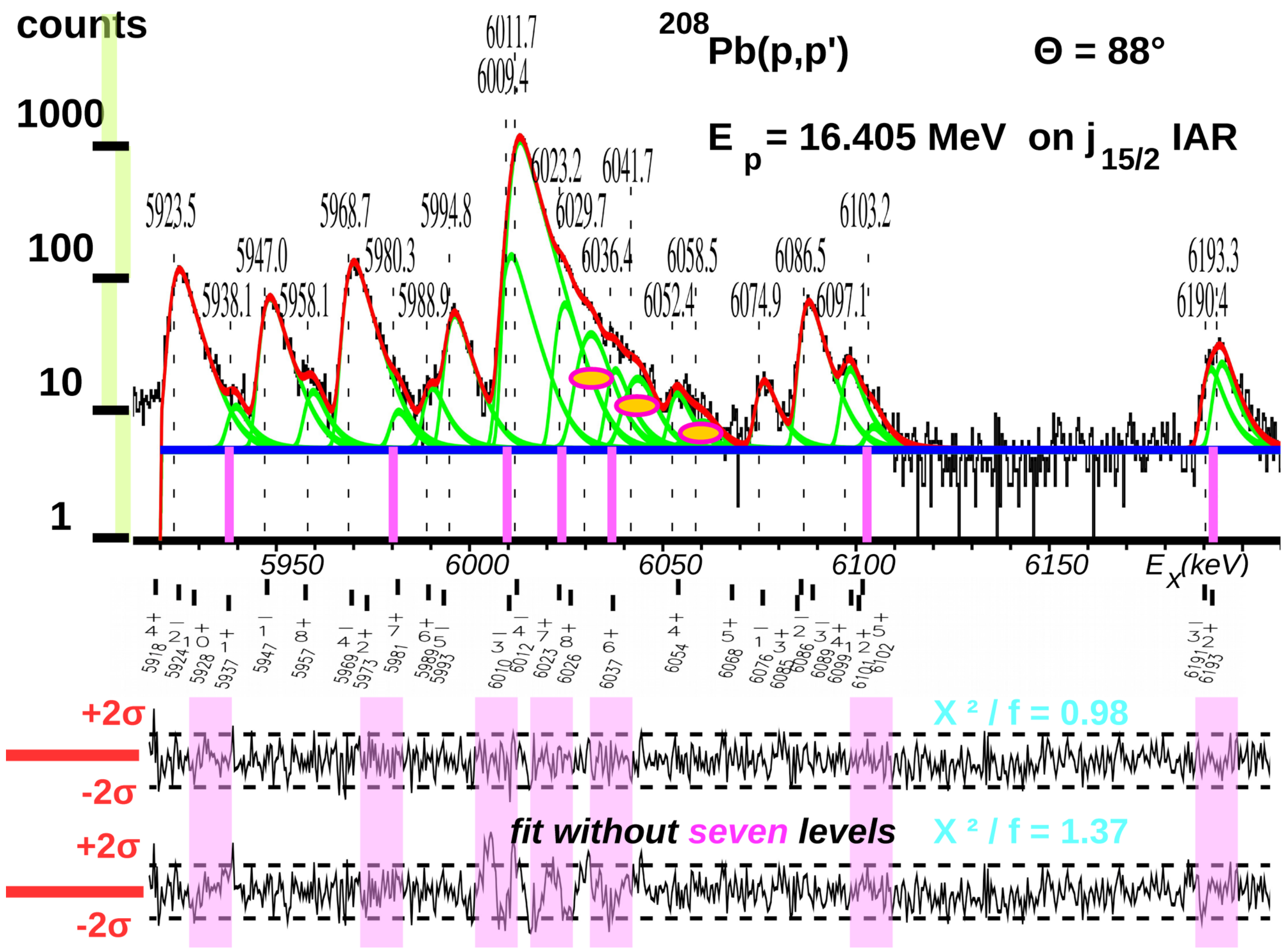

FIG. 21. Example for the fit of doublets with GASPAN. The lower residuum spectrum belongs to a fit without the seven levels marked magenta; the ovals mark L satellites. For details, see Sec. III E 2.

In cases of doubt, a state is identified to be existent if the excitation energy does not vary by more than about 0.5 keV in different runs and if it shows up in at least three different out of the ten reactions studied. The gap at $6.11 < E_x < 6.19$ MeV is thus established; within 2 keV no level shows up in more than three different spectra and for more than two reactions. The region is void in agreement with the predictions by the mSM (Figs. 2 and 18; see also published figures mentioned in Sec. III C 5).

E. Dissolving doublets

1. *Fitting doublets with GASPAN*

The fit by GASPAN is described by Eqs. (A1)–(A6) in Ref. [12]. For the fit by GASPAN the spectra are divided up into at least three regions covering less than 400 keV for ^{208}Pb(p,p') in excitation energy [700 keV for ^{208}Pb(d,d') and ^{207}Pb(d,p)]; it is dictated by the pragmatic limitation to have at most 27 peaks in one region; otherwise, the computing time increases too much.

Each peak is essentially fitted by two parameters, the width A_G of the Gaussian and A_T of the complementary Gaussian error function describing the tail [12]. In the spectra (Figs. 17–21) the position of the Gaussian is shown by the vertical, dashed line.

In preliminary studies the dependence of the width A_G on the position in the detector is determined; a precision of 30% is sufficient. Similarly, the dependence of the width A_T of the tail is determined with a precision of 50%; normally, there is only the tail towards increasing excitation energies. Only some ^{207}Pb(d,p) spectra need both tails; a possible reason might be that the dehysteresis procedure of the Q3D magnets during the relevant experiment was not perfectly handled.

To speed up the fitting, after first trials the widths A_G are no longer varied; they must be numerically different, however. During the sequence of fitting trials, the position of physical peaks [states in ^{208}Pb for (p,p')] and the correlated position of L satellites (in rare cases also $K + L$ satellites; see Fig. 17) is determined; the width A_G of the L satellites is assumed to be larger (Table VII) and the levels are tagged by using the last digit of A_G with units in eV. Tagged levels are ignored in the subsequent analysis by NTNS.

By inspection of the residuum spectrum doublets are determined. (An automatic search may determine peaks until the residuum spectrum drops below the 2σ level everywhere; it is sometimes used but takes much compute time.) Each spectrum is fitted in up to 100 trials by modeling the number of levels to be fitted and the insertion of L satellites (rarely also K satellites; see Fig. 17).

2. A realistic example

Figure 21 shows a realistic example for the region $5.92 < E_x < 6.21$ MeV taken near the $j_{15/2}$ IAR. The spectrum is shown in the upper frame; two residua spectra are shown in the lower frames. The upper residuum spectrum belongs to the shown spectrum where 22 levels are fitted with $\chi^2/f = 0.98$. The lower residuum spectrum belongs to a fit where seven levels marked by magenta lines were omitted. Consequently, the fit is worse with $\chi^2/f = 1.37$. The residua at the omitted levels clearly deviate from the two limits $\pm 2\sigma$ per channel indicated by the dashed lines.

Because of the large peak-to-valley ratio of 500, two L satellites for the $E_x = 6.01$ MeV doublet are present; the fit yields the values "6029.7", "6041.7", and "6058.5"; they are marked in orange in Fig. 21. The Gaussian width A_G for the L satellites (Eqs. (A1)–(A6) in Ref. [12]) is chosen larger in accordance with Table VII. The residuum spectra show that between the L satellites levels from physical states in ^{208}Pb show up. In this example the 6023 ("6023.2") and 6037 ("6036.4") states are clearly discerned; the 6054 ("6058.5") state is taken into account because it is clearly identified by the ^{208}Pb(d,d') spectra.

GASPAN resolved the doublets at $E_x = 6.01$, 6.10, and 6.19 MeV with the 6010 ("6009.4") and 6012 ("6011.7"), 6099 ("6097.1"), and 6101 + 6102 ("6103.2"), 6191 ("6190.4"), and 6193 ("6193.3") states.

It also resolved the weak level of the 5937 ("5938.1") state left from the much stronger 5947 ("5947.0") state and of the 5981 ("5980.3") state right from the 5969 ("5968.7") state. Yet in this spectrum GASPAN failed to resolve the 5928 10^+, 5973 2^+, 6047 0^+, 6068 5^+, 6085 3^+, 6089 3^-, and 6101 12^+ states; the peak near the 6068 state has too-low statistics. Often it is a matter of endurance to resolve all levels until the residuum spectrum appears smooth everywhere; but mostly the statistics set a limit to find all levels.

Many dozen fit iterations were done for all spectra (more than 500 in total; see Table V). With good statistics levels separated by less than 1.0 keV are often resolved in case the weaker level has a lower excitation energy; otherwise, because of the asymmetric peak shape the separation must be larger.

3. Determining excitation energies by NTNS

The resolution. The instrumental resolution of the Q3D magnetic spectrograph is about $\Delta E/E = 2.5 \times 10^{-4}$, already achieved in 1973 with a semiconductor detector of 50 mm length for the first realized Q3D magnetic spectrograph (MPIK Heidelberg [108]). The binding energy of the M electrons in lead (together with the less bounded N, O, P electrons) limits the resolution to 2.9 keV (Table VII).

At $4.8 < E_x < 6.2$ MeV, about 150, 40, and 40 spectra were taken for the ^{208}Pb(p,p'), ^{207}Pb(d,p), and ^{208}Pb(d,d') reactions, respectively (Table V). The highest precision of the excitation energies derives from the ^{208}Pb(p,p') reaction (Table VI). With bombarding energies from 14.8 to 18.2 MeV, the energies of the outgoing protons are the lowest, from 9 to 13 MeV; for ^{207}Pb(d,p) the energies of the detected protons are from 11 to 14 MeV and from 16 to 19 MeV for ^{208}Pb(d,d').

The excitation energies are determined by two fitting routines, GASPAN followed by another computer code (NTNS). GASPAN uses values for levels tabulated by ND2007 and clearly recognized as single states for calibration. It assumes a quadratic dependence of the excitation energy on the position in the detector. The deviation of the fit function from a parabola of second order should have a characteristic shape representing the magneto-optic nonlinearities of the Q3D magnetic spectrograph.

The results from GASPAN are fitted by NTNS using another quadratic function [12] in two steps. In the first step, values for levels tabulated by ND2007 known to be no doublets within 4 keV are used for calibration. In the second step, all identified levels are used. In effect, the excitation energies are fitted by a polynomial of fourth degree. Corrections for the relativistic kinematics are not needed; they are less than a few keV for the heavy nuclei anyhow.

Resolving close doublets. The computer code GASPAN offers several methods to disentangle doublets in a spectrum [12].

(i) One method is used while performing the fit with GASPAN. One of the first steps during the fit is the determination of the Gaussian width A_G and the exponential tail A_T in dependence of the position of the detector [12]; see Sec. III G 3. The significant broadening of a level yields a hint to a doublet. In an iterative manner new levels are introduced until the residuum spectrum does not change anymore significantly. A big problem derives from the knockout of atomic electrons (Sec. III D).

(ii) Another method uses fixed energies for one member of the doublet and a series of neighboring states; only the energy of the second doublet member is fitted.

(iii) A special case is discussed in Sec. III G 3.

(iv) In a doublet with two states the cross section may change with the proton energy in the ^{208}Pb(p,p') reaction differently. It introduces a systematic shift of the centroid energy. One example is given by the dissolution of the 5648 3^-, 5648 9^+ doublet where the 3^- state is excited near the $g_{9/2}$ and $d_{5/2}$ IARs, while the 9^+ near is excited solely near the $j_{15/2}$ IAR [12]. Another example is the 5490 6^-, 5492 4^- doublet selectively excited near the $g_{9/2}$ and $d_{5/2}$ IARs, respectively [18].

(v) The change of the cross section with scattering angle introduces a correlated shift of the excitation energy. Hence, in a doublet with two states having different angular distributions the spread of the excitation energies is larger than for a single state. An example is given by the disentanglement of the 5812 2^-, 5813 3^- doublet [15]. Both states have dominant $d_{5/2}p_{3/2}$ components, but the angular distribution for spin 3^- has the pronounced maximum near $\Theta = 90^\circ$ [typically for $I = J + j - 1$)], while for 2^- it is flat.

The first method is used extensively in the beginning of the analysis. The second method is used only casually; it takes much computer time. The two latter methods are much used for this paper.

Determining excitation energies and their uncertainties. Doublets with spacings down to about 0.5 keV are often recognized by GASPAN if the cross sections are similar and the statistics high enough. However, close doublets with spacings less than 0.5 keV are resolved only for a fraction of the runs. Therefore, for one run only one energy is determined by GASPAN, whereas for another run two values are obtained. In determining the excitation energies of both members of the doublet the single value is used twice. The uncertainties of excitation energies determined by GASPAN are δE_x.

Individual values of excitation energies obtained from one run are clustered within $\delta E_x \approx 50$ eV for well-isolated states with high statistics and still 500 eV for states with low statistics (states with cross sections of less than 10 μb/sr). The extension of the cluster increases in case an unresolved doublet is present. Because many states are members of incompletely resolved doublets, the centroid energy of each state is determined in several steps; in addition many iterations of the complete evaluation cycle were done.

It starts with the recognition of the doublet by other means, mostly relying on NDS2007, but an iteration does work also. Systematic variations with either of the ten reactions may help to suspect a doublet, too.

(i) For a chosen member of the doublet with energy $E_x^{\rm req}$ the differences $E_x(i,g) - E_x^{\rm req}$ are determined for a group g defined by a range of beam energies and a range of scattering angles; between three and six groups are defined. For the ^{208}Pb(p,p'), ^{207}Pb(d,p), and ^{208}Pb(d,d') reactions, the mean value for N runs ($i = 1,\ldots,N$) within each group g is then determined as

$$\overline{E_x(g) - E_x^{\rm req}} = \frac{1}{N}\sum_{i=1}^{N}\left[E_x(i,g) - E_x^{\rm req}\right]$$

and its uncertainty as

$$\delta E_x(g) = \sqrt{\frac{\sum_{i=1}^{N}\left[\delta E_x(i,g) - \overline{E_x(g) - E_x^{\rm req}}\right]^2}{N(N-1)}}$$

with values $|E_x(g) - E_x^{\rm req}| \leqslant \Delta E_x^{\rm req}$, $0.1 \lesssim \Delta E_x^{\rm req} \lesssim 0.5$ keV. (39)

(ii) The extension of the values $\overline{E_x(g) - E_x^{\rm req}}$ is generally restricted to a range $\pm\Delta E_x^{\rm req}$ covering the cluster δE_x within more than 80%; all data are evaluated with two or three different limits of the restrictions.

(iii) For doublets the restrictions $\Delta E_x^{\rm req}$ are defined in an asymmetric manner; for close doublets (with distances less than about 1.0 keV) the energy of the centroid with the neighbor augmented by a small amount is taken as a border. Yet the limit $\Delta E_x^{\rm req}$ near the centroid of the doublet should cover more than 50% of the cluster by slightly extending the border; see Figs. 22 for an example.

(iv) From the values $\overline{E_x(g) - E_x^{\rm req}}$ thus determined the mean value of the requested member of the doublet is derived as a mean determined in a certain choice of groups $g = 1,\ldots,G$,

$$\overline{E_x} = \frac{1}{G}\sum_{g=1}^{G}\left[\overline{E_x(g) - E_x^{\rm req}} + E_x^{\rm req}\right]$$

and its uncertainty as

$$\overline{\delta E_x} = \sqrt{\frac{\sum_{g=1}^{G}\left[\overline{E_x(g) - E_x^{\rm req}} + E_x^{\rm req} - \delta E_x(g)\right]^2}{G(G-1)}}. \quad (40)$$

Here values $\overline{E_x(g)}$ are ignored where the uncertainty $\delta E_x(g)$ is too large. The reason is often that in such groups too few values $E_x(i,g)$ are given, the cross sections are out of range, or the peak-to-valley ratios are low.

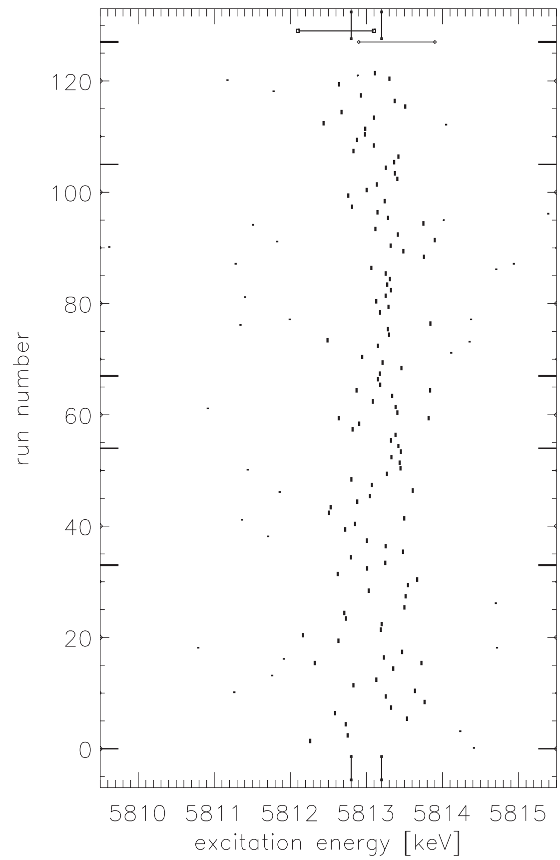

FIG. 22. Example for resolving a doublet. Here, for the 0.5-keV doublet of the 5812 2^- and 5813 3^- states, the distribution of the values E_x obtained by GASPAN is shown without the uncertainties; in Fig. 20 they are shown with the uncertainties. The abscissa shows the excitation energies for $5810 < E_x < 5815$ keV, the ordinate the run number. The two requested values $E^{\rm req} = 5812.8$ and 5813.2 keV are marked at top and bottom. The 120 runs are divided up into five groups marked by short horizontal lines at left and right. The chosen limits are shown at top with $\Delta E_x^{\rm req} = 0.60$ and 0.30; the asymmetric limits distribute the values E_x over two parts.

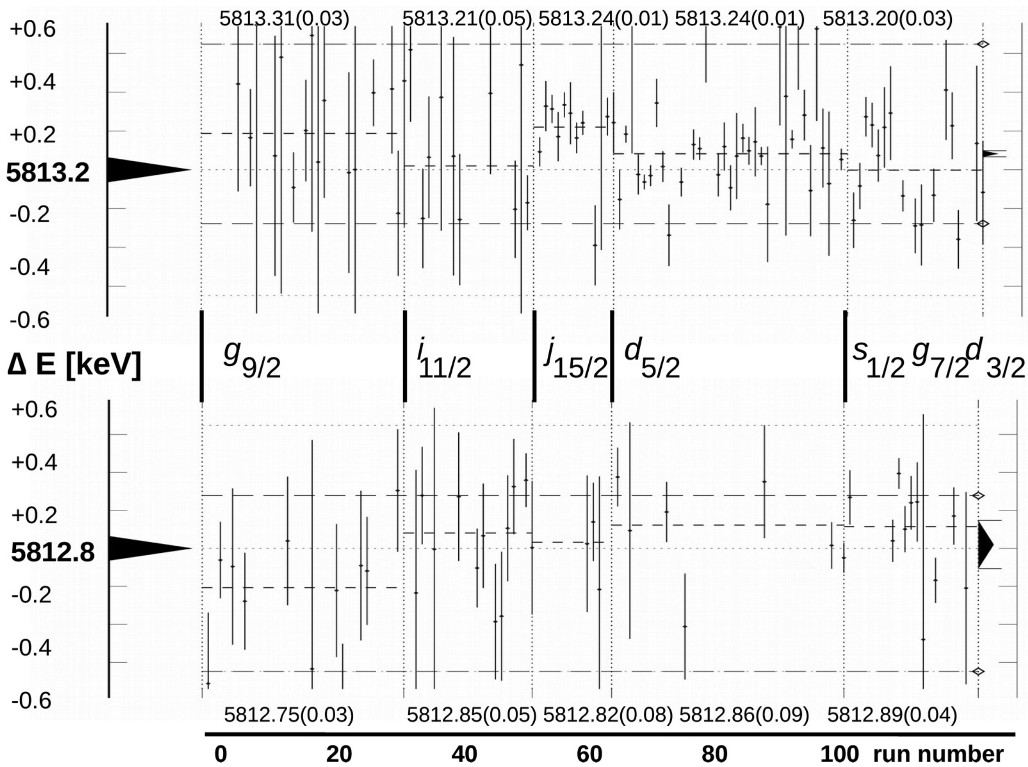

FIG. 23. Another display of the data shown in Fig. 19. The two figures show the distribution for the deviations from the requested values $E^{\rm req} = 5812.8$ and 5813.2 keV (long arrows at left) for 120 runs. Long-dashed lines ending in open diamonds at right denote the chosen limits $\Delta E_x^{\rm req}$. For each of the five groups (marked by vertical dotted lines) the mean values $\overline{E_x(g) - E_x^{\rm req}}$ [Eq. (39)] are shown by a short dashed line; the value and its uncertainty is shown at top and bottom, respectively. The global mean values $\overline{E}_x = 5812.75 \pm 0.02$ and 5813.24 ± 0.02 keV [Eq. (40)] are shown at far right by short arrows; the black arrow at left shows the value $E_x^{\rm req}$. Near the $j_{15/2}$ and $d_{5/2}$ IARs (third and fourth group) the 5813 3^- state is more strongly excited than the 5812 2^- state at most chosen scattering angles; the scattering angles $20^\circ \leqslant \Theta \leqslant 138^\circ$ increase from left to right.

(v) The values $\overline{E_x}$ should agree within the uncertainty $\overline{\delta E_x}$ for different choices of the restricting limits chosen in (i)–(iii).

The spread of the uncertainties. Figures 22 and 23 provide an example for the 0.5-keV doublet consisting of the 5812 2^- and 5813 3^- states [15]. Using Eqs. (39) and (40) the excitation energies are determined as $\overline{E}_x = 5812.75 \pm 0.02$ and 5813.24 ± 0.02 keV. Differing values in Table VI arise from averaging over several such trials.

Excitation energies are determined by GASPAN with an uncertainty of typically 0.1–0.5 keV and systematic uncertainties up to 1 keV because of the magneto-optic nonlinearities. The corrections by NTNS eliminate the systematic uncertainties and thus reduce the uncertainties. The statistical factors $N(N-1)$ in Eq. (39) and $G(G-1)$ in Eq. (40) reduce the individual uncertainties by typically a factor 5–10. The median uncertainty in excitation energies is 70 eV for ^{208}Pb(p,p'), 150 eV for ^{208}Pb(d,d'), and 250 eV for ^{207}Pb(d,p); the logarithmic distribution of the uncertainties starts with about 20, 40, and 100 eV, respectively.

In most cases, the uncertainties of the excitation energies derived from the ^{208}Pb(p,p'), ^{207}Pb(d,p) and ^{208}Pb(d,d') data compare to those shown by NDS2007 within about two standard deviations. Exceptions are discussed elsewhere in the paper (Secs. IV and VI B).

F. Resolving doublets

In this section each state is denoted by the energy label $\tilde{E}_x$, spin I, and parity π [Eq. (10)]. Yet note that the identification of the state and the spin assignment is discussed only later (Sec. IV).

1. *Uncertainty of cross sections*

In this paper we discuss cross sections only as far as needed. The main purpose is the identification of states; spin, parity, and structure are discussed to find out the identity. In the majority of cases we rely on published data.

Excitation energies of states can be determined in doublets with spacings larger than about 0.4 keV, but cross sections only if the spacings are larger than the resolution (about 3 keV). Namely, the excitation energy is determined by the centroid energy as discussed in Sec. III E 3, but the cross section is given by the covered area which is dictated by the full resolution. For this reason Table VI gives the cross section for close doublets without discriminating the distribution across the involved states, whereas the excitation energies are determined for all members (with very few exceptions).

2. Disentangling doublets

Because of the high level density in ^{208}Pb, γ spectroscopy often cannot decide about the existence of a state because a γ ray may be placed two or three times. Previous particle-transfer experiments yielded an uncertainty of excitation energies of typically 1–2 keV because of the lower resolution [23,28,40,42,47,58] except for the Q3D data taken with the older detector [33,34]; here the uncertainties were lower but the nonlinearity of the detector introduced systematic uncertainties.

Twenty-three doublets with distances between the states of less than 2.5 keV (Sec. III F 4) and 22 6-keV multiplets (Sec. III F 3) were resolved, as were nearly two dozen weakly excited states close to strong levels (Secs. III F 5 and III G 3); see also Sec. III C 5 for published spectra.

3. Resolution of 2–6-keV doublets

Doublets of states with similar cross sections are well resolved if the spacing is larger than 2 keV. In case the state at higher excitation energy is more weakly excited, the spacing must be larger because of the asymmetric peak shape. For a very high difference in the two cross sections, see Secs. III F 5 and III G.

In Table VI, doublets of states within less than 6 keV are marked by vertical lines. Doublets with a spacing less than 2.5 keV are marked by double vertical lines and discussed in Sec. III F 4.

The 4255 3^- *and 4262* 4^- *states.* The 4255 3^- and 4262 4^- states are selectively excited on the $g_{9/2}$ IAR; the 4255 3^- state is also excited on the $d_{5/2}$ IAR reaction. The ^{208}Pb(d,d') reaction excites both states similarly (Fig. 18). The ^{207}Pb(d,p) reaction excites the 4255 3^- state stronger than the 4262 4^- state [5].

The 5069 10^+*, 5075* 5^-*, 5080* 6^-*, 5085* 7^-*, and 5093* 8^+ *states.* The 5075 5^-, 5080 6^-, and 5085 7^- states are selectively excited on the $i_{11/2}$ IAR; the 5069 10^+ and 5093 8^+ states are selectively excited on the $j_{15/2}$ IAR. The ^{208}Pb(d,d') reaction excites all states in the ensemble (Fig. 19), but the 5075 5^- and 5085 7^- states stronger. The ^{207}Pb(d,p) reaction excites all four states and interestingly also the 5069 10^+ state (Sec. V E).

The 5276 4^-*, 5280* 0^-*, 5286* 2^+*, and 5292* 1^- *states.* The 5276 4^- state is selectively excited on the $i_{11/2}$ IAR [5]. The 5280 0^-, 5292 1^- states are excited on the $d_{5/2}$ and $s_{1/2}$ IARs. The 5286 2^+ state is excited in a nonresonant manner. In the ^{207}Pb(d,p) reaction, the strong excitation of the 5280 0^- and 5292 1^- states [33,34] hinders to clearly resolve the 5286 state. The ^{208}Pb(d,d') reaction excites all four states with similar cross sections (Fig. 19).

The 5512 1^- *and 5517* 3^- *states.* The 5512 1^- and 5517 3^- states are strongly excited on the $d_{5/2}$ IAR; the 5512 1^- is excited on other IARs, too. The ^{207}Pb(d,p) reaction excites the 5512 1^- state more strongly than the 5517 3^- state; the ^{208}Pb(d,d') reaction excites both states similarly strongly (Fig. 19).

The 5686 6^-*, 5690* 4^+*, and 5694* 7^- *states.* The 5686 6^- and 5694 7^- states are selectively excited on the $g_{9/2}$ IAR [11]; the 5690 4^+ state is visible near all other IARs and off-resonance. The ^{208}Pb(d,d') reaction excites all three states, but the 5690 4^+ state more strongly (Fig. 19). Interestingly, the ^{207}Pb(d,p) reaction excites the 5690 4^+ state (Sec. V E).

The 5715 2^+ *and 5721* 6^+ *states.* The 5715 2^+ state is weakly excited in a nonresonant manner; the 5721 6^+ state is selectively excited near the $j_{15/2}$ IAR. The ^{208}Pb(d,d') reaction excites both states but the 5721 6^+ state stronger (Fig. 20). Interestingly, the ^{207}Pb(d,p) reaction excites both states (Sec. V E).

The 5799 5^+ *and 5805* 1^- *states.* The 5799 5^+ and 5805 1^- states are both excited in the ^{208}Pb(p,p') and ^{207}Pb(d,p) reactions with similar cross sections. The doublet with the 5812 2^- and 5813 3^- states strongly excited is well separated from them. The ^{208}Pb(d,d') reaction excites both states weakly; the doublet is strongly excited but well separated.

The 5989 6^+ *and 5993* 5^- *states.* The 5989 6^+ state is selectively excited on the $j_{15/2}$ IAR, while the 5993 state is more strongly excited on the $d_{5/2}$ IAR. Both states are similarly excited by the ^{208}Pb(d,d') and ^{207}Pb(d,p) reactions.

4. Disentanglement of 2.5-keV doublets

The 4709 5^- *and 4712* 4^- *states.* The 4709 5^-, 4712 4^- states are selectively excited on the $i_{11/2}$ IAR [5]. The 4712 4^- state is weakly excited also on the $g_{7/2}$ IAR; the 4709 5^- state is weakly excited on other IARs, too. The ^{207}Pb(d,p) reaction weakly excites both states. In the ^{208}Pb(d,d') reaction the 4712 4^- state cannot be distinguished from L satellites of the 4698 3^- state because of the lower resolution. The first L satellites from the 4698 3^- state often present a difficulty to resolve the 4709 5^-, 4712 4^- doublet from the 4698 3^- state.

The 4861 8^+*, 4867* 7^+*, and 4868* 0^+ *states.* In the ^{208}Pb(p,p') reaction, the 4861 8^+ and 4867 7^+ states are strongly excited near the $j_{15/2}$ IAR, the 4868 0^+ state off resonance. The distance between the 4867 7^+ and 4868 0^+ states is determined as 0.50 ± 0.15 keV for (p,p') and 0.40 ± 0.25 keV for (d,d'); it agrees with the value 0.44 ± 0.10 keV from NDS2007. The ^{207}Pb(d,p) reaction excites only the 4867 7^+ state.

The 5193 5^+*, 5195* 3^-*, and 5196* 7^+ *states.* The 5193 5^+ and 5196 7^+ states are only weakly excited while the 5195 3^- state shows a resonant excitation on the $d_{5/2}$ IAR. The ^{207}Pb(d,p) reaction excites only the 5195 3^- state.

The 5213 6^+*, 5214* 5^-*, and 5216* 4^+ *states.* The 5213 6^+ and 5216 4^+ states are only weakly excited in the ^{208}Pb(p,p') reaction, while the 5214 5^- state is selectively excited on the $g_{9/2}$ IAR rather strongly. The ^{207}Pb(d,p) reaction excites only the 5214 5^- state.

The 5235 11^+*, 5239* 4^-*, 5241* 0^+*, and 5245* 3^- *states.* The 5245 3^- state is selectively excited on the $d_{5/2}$ IAR, but rather strongly also on other IARs; the 5239 4^- is selectively excited on the $i_{11/2}$ IAR at forward-scattering angles [5]; the 5235 11^+ is selectively excited on the $j_{15/2}$ IAR with a cross section of about 1 μb/sr. The 5239 4^- and 5245 3^- states are observed in the ^{207}Pb(d,p) reaction; all four states are observed in the ^{208}Pb(d,d') reaction, although not clearly resolved. The distance between the 5239 4^- and the 5241 0^+ states is determined as 1.45 ± 0.15 keV for (p,p') and 1.25 ± 0.25 keV for (d,d'), in congruence with 1.8 ± 0.5 keV from NDS2007.

The 5380 5^-, *5383* 4^+, *and 5385* 3^- *states.* The 5385 3^- state is strongly excited by the ^{208}Pb(p,p') and ^{207}Pb(d,p) reactions. The two other states in the 5.38-MeV doublet have lower excitation energies; hence, with the HWHM of 1.5 keV they are resolved in many ^{208}Pb(p,p') spectra but not by ^{208}Pb(d,d'). The distance between the 5383 4^+ and the 5385 3^- states is 1.55 ± 0.15 keV in congruence with 1.77 ± 0.04 keV by NDS2007. Most spectra in the ^{208}Pb(d,d') reaction are affected by the broad contamination line from ^{12}C(d,d') in the region.

The 5490 6^- *and 5492* 4^- *states.* The 5490 6^- and 5492 4^- states are disentangled by the selective excitation on the $g_{9/2}$ and $d_{5/2}$ IARs [18].

The 5537 10^+, *5543* 7^-, *5546* 5^-, *and 5548* 2^- *states.* The 5537 10^+ state is selectively excited on the $j_{15/2}$ IAR. It is hardly seen in spectra taken outside the $j_{15/2}$ IAR; the cross section does not exceed 1 μb/sr. In the ^{208}Pb(p,p') reaction, the 5546 5^- state next to the 5543 3^- state is resolved at few proton energies and scattering angles because it is mostly more weakly excited and the asymmetry of the peak shape [12] hinders the resolution. The ensemble of three states near $E_x = 5.55$ MeV—the 5543 7^-, 5546 5^-, and 5548 2^- states—is resolved by the different excitation at proton energies $14.8 < E_p < 18.2$ MeV and scattering angles $20^\circ \leqslant \Theta \leqslant 138^\circ$. Among the three states, essentially only the 5548 2^- state is excited by the ^{207}Pb(d,p) reaction.

The 5561 2^+ *and 5564* 3^- *states.* In the ^{208}Pb(p,p') reaction, the 5561 2^+ state is sitting on the leading edge of the peak from the strongly excited 5564 3^- state; hence, it may be resolved despite the low cross section.

The 5648 3^- *and 5649* 9^+ *states.* The 5648 3^- state is excited with similar angular distributions both on the $g_{9/2}$ IAR and on the $d_{5/2}$ IAR, the 5649 9^+ state selectively on the $j_{15/2}$ IAR [12]. The distance between the 5648 3^- and 5649 9^+ states is 0.35 ± 0.06 keV for (p,p') and 0.9 ± 0.3 keV for (d,d'). Only the 5648 3^- is excited by the ^{207}Pb(d,p) reaction.

The 6085 3^+, *6086* 2^-, *and 6089* 3^- *states.* While the 6086 2^- state is excited on the $s_{1/2}$ IAR mainly, the 6089 3^- state is excited near all IARs and up to $E_p \approx 18$ MeV [19]. The 6085 3^+ state is recognized near the $g_{9/2}$ and $d_{5/2}$ IARs with a clearly lower excitation energy; it is newly identified. The ^{207}Pb(d,p) reaction strongly excites the 6086 2^- state. For the ^{208}Pb(d,d') reaction there are too few data; the doublet is not well resolved. The distances between the three states are determined as about 1.0 and 2.0 keV.

The 6191 3^- *and 6193* 2^+ *states.* The 6191 3^- and 6193 2^+ states are resolved in the ^{208}Pb(p,p'), ^{208}Pb(d,d'), and ^{207}Pb(d,p) reactions. The distance is determined as 1.3 ± 0.2 keV for (p,p') and 0.8 ± 0.6 keV for (d,d') in congruence with 2.1 ± 0.4 keV by NDS2007.

5. *Weak levels close to strong peaks*

Weak levels close to strong peaks are difficult to analyze. In the following several such levels are discussed. In Sec. III G more complicated situations are discussed.

With the exemption of three 0.5-keV doublets, all states in the region $5.57 < E_x < 6.08$ MeV are readily discerned by the ^{208}Pb(d,d') reaction (Fig. 20). Most states are identified by the ^{208}Pb(p,p') reaction; only few states are almost never resolved. Many states are selectively excited on a single IAR [12,18].

The 5038 2^- *and 5040* 2^+ *states.* The 5056 level was introduced [5] because the peak for the 5040 level does not have the same shape as for the neighboring 4974 and 5127 levels. The 5056 level is certainly a L satellite, while the 5.04-MeV level is a doublet (Secs. III F 5, III G 3, and IV C). Since the time when the data presented in Ref. [5] were analyzed, more data have become available and the methods of the analysis were refined; see also Sec. III C 5. In Sec. III G the disentanglement of the 5.04-MeV doublet is discussed. The excitation energy of the 5038 2^- state is determined as 5037.45 ± 0.04 keV, in agreement with 5037.538 ± 0.018 keV reported by NDS2007, and for the newly identified 5040 2^+ state as 5039.4 ± 0.3 keV for (p,p') and 5039.0 ± 0.3 keV for (d,d') (Table VI).

The 5317 3^+ *and 5318* 3^- *states.* The 5317 3^+ and 5318 3^- states are shown by NDS2007 to have a distance of 0.2 ± 0.6 keV. By the method described in Sec. III E 3 the existence of two close–lying states is proven; a distance of 1.05 ± 0.15 keV for (p,p'), 0.7 ± 0.4 keV for (d,d'), and 1.6 ± 2.0 keV for (d,p) is determined (Table VI), slightly wider than determined by NDS2007. In the ^{208}Pb(p,p') and ^{207}Pb(d,p) reactions the L satellites from the 5292 1^- state render a difficulty to resolve the doublet.

The 5474 7^+ *and 5482* 5^- *states.* The 5474 state is weakly excited by the ^{208}Pb(p,p') reaction. The asymmetry of the peak shape and the large gap between the 5416 6^+ and 5482 5^- states with its voidness in all spectra favor the detection of the weak 5474 level. At excitation energies below the 5482 5^- state, peak-to-valley ratios up to 1000:1 are observed. Therefore, a dozen spectra indicate the presence of a state at 5474 keV with a maximum cross section of 0.6 μb/sr and a weak enhancement near the $j_{15/2}$ resonance ($E^{\rm res} = 16.38$ MeV [12]). The ^{209}Bi$(d,^3$He$)$ reaction indicates a weak admixture of $h_{9/2}h_{11/2}$ [40,41].

The 5502 6^+ *and 5512* 1^- *states.* The 5502 6^+ state lies between the strongly excited ensemble of the 5482 5^-, 5490 4^-, and 5492 6^- states [11] and the 5512 1^- and 5517 3^- states. It is difficult to distinguish the 5502 level from L-electron satellites of the 5.49-MeV doublet; yet the determination of the excitation energy clearly demonstrates the existence.

The 5640 1^-, *5642* 2^+, *and 5643* 2^- *states.* The 5640 1^- state is selectively excited on the $g_{9/2}$ IAR, the 5643 2^- state is strongly excited on the $d_{5/2}$ IAR [11,15,18,19]. The excitation energy of the 5643 2^- state is determined as 5642.62 ± 0.04 keV. A weak excitation of the 5642 2^+ state in about 0.5 keV distance could be marginally confirmed (Table VI). Near the $g_{9/2}$ and $i_{11/2}$ IAR the 5643 2^- state is weakly excited and the statistics are low; near the $d_{5/2}$ and higher IARs the cross section of the 5643 2^- state is large. For ^{208}Pb(d,d') the resolution and statistics are insufficient. The excitation of level 48 [37] by ^{206}Pb(t,p) and ^{210}Pb(p,t) yielding $E_x^{\rm calib} = 5640.4$ keV [Eq. (65)] is identified with both the 5640 1^- and the 5642 2^+ states (Table XI).

The ensemble at $5.79 < E_x < 5.85$ MeV. Eight states are identified in the region $5.78 < E_x < 5.85$ MeV, the 5799 5^+

and 5805 1^- states preceding the unresolved doublet of the 5812 2^- and 5813 3^- states followed by the 5819 2^+, 5825 8^+, 5836 8^-, and 5844 1^+ states. Figure 20(b) shows the ensemble for ^{208}Pb(d,d'). The 5812 2^-, 5813 3^- doublet is seldom resolved, but the centroid energy exhibits a correlation with the scattering angle and the proton energy in the ^{208}Pb(p,p') reaction, which makes it possible to determine the individual excitation energies [14,15]; see Sec. III E 3. The cross section of the 5.81-MeV level is one of the largest observed for ^{208}Pb(p,p') [25]. The cross section for ^{207}Pb(d,p) is also rather high. The 5799 5^+ and 5805 1^- states are resolved because their distance from the 5.81-MeV doublet is much larger than the HWHM of 1.5 keV. The 5819 2^+, 5825 8^- states are resolved near the $g_{9/2}$, $i_{11/2}$, $g_{7/2}$, and $d_{3/2}$ IARs where the 5.81-MeV doublet is weak. The ^{208}Pb(d,d') reaction excites the 5812 2^- and 5813 3^- states not much more strongly than the next two states (Fig. 20).

The 5864 11^+ *state.* The 5874 3^- state is strongly excited by both ^{208}Pb(p,p') and ^{207}Pb(d,p). The 5864 11^+ is often resolved because the asymmetric peak shape favors the detection of a weak state at the low-energy side of a strong peak. The ^{208}Pb(d,d') reaction resolves all states (Fig. 20).

The 5901 9^+ *and 5918* 4^+ *states.* The 5886 4^- state is excited by both ^{208}Pb(p,p') and ^{207}Pb(d,p). The 5901 9^+ is selectively excited by the $j_{15/2}$ IAR [12]). The ^{208}Pb(d,d') reaction resolves both states (Fig. 20).

The 5928 10^+*, 5937* 1^+*, and 5957* 8^+ *states.* The 5928 10^+ state is rarely discerned in ^{208}Pb(p,p') or ^{207}Pb(d,p) spectra because of the large cross section of the 5924 2^- state and the following L satellites, see Fig. 21. Similarly, the 5973 2^+ state cannot be discriminated from the 5969 4^- state strongly excited in both the ^{208}Pb(p,p') and the ^{207}Pb(d,p) reactions. The 5937 1^+ state is well resolved in several ^{208}Pb(p,p') spectra, see Fig. 21. The ^{208}Pb(d,d') reaction resolves all states (Fig. 20).

The 5973 2^+ *and 5981* 7^+ *states.* Near the 5969 4^- state with a large cross section, the 5973 2^+ state is not discerned in ^{208}Pb(p,p') or ^{207}Pb(d,p) spectra; the 5981 7^+ state is discerned in a few spectra, see Fig. 21. The ^{208}Pb(d,d') resolves both states in some spectra; the 5973 2^+ state is not fitted in Fig. 20, but the 5981 7^+ state.

The 6010 3^- *and 6012* 4^- *states.* The 6010 3^- and 6012 4^- states are selectively excited on the $d_{5/2}$ IAR [15], see Fig. 21; the 6010 3^- state is more strongly excited on other IARs, too [23]. The ^{207}Pb(d,p) reaction excites the 6010 3^- state more strongly; the ^{208}Pb(d,d') reaction excites both states about equally. The 6.10-MeV doublet is often resolved by GASPAN for all reactions because of the good statistics (Sec. III C 5).

The 6023 7^+*, 6026* 8^+*, 6037* 6^+*, 6054* 4^+*, and 6068* 5^+ *states.* Five states are identified in the region $6.02 < E_x < 6.06$ MeV. In both the ^{208}Pb(p,p') and the ^{207}Pb(d,p) reactions, the weakly excited states can be distinguished only with difficulty from L satellites of the 6010 3^- and 6012 4^- states because of their huge cross sections (Figs. 20 and 21).

The 6099 4^+*, 6101* 12^+*, and 6102* 5^+ *states.* The 6099 4^+, 6101 12^+, and 6102 5^+ states are resolved in the ^{208}Pb(p,p') reaction, see Fig. 21. The 6101 12^+ and 6102 5^+ states are excited by ^{207}Pb(d,p); 6099 4^+ apparently is not excited.

G. Digression: Resolution of the 5.04-MeV doublet

1. The 5038 2^- state

Spin and structure of the 5038 state. The 5038 state is assigned the spin of 2^- [10]. It contains 60% of the $d_{5/2}p_{1/2}$ strength; the remainder (30%) is essentially located in the 5127 2^- state [33,34]. The 5038 and 5127 2^- states do not contain large other fragments of particle-hole configurations; especially the proton configuration $h_{9/2}d_{5/2}$ contributes less than 2% [40,41]. The complementary configuration is $f_{7/2}d_{5/2}$, which is unobservable [18]. Hence, the two 2^- states may be considered as a rather complete two-level system.

Completeness and deviation matrices. The amplitudes describing the two states by Eq. (10) are

$$c_{2i} \equiv c_{2,i}^{2_2^-}, \quad i = 1,2,\ldots \quad \text{for the 5038 } 2_2^- \text{ state,}$$
$$c_{3i} \equiv c_{3,i}^{2_3^-}, \quad i = 1,2,\ldots \quad \text{for the 5127 } 2_3^- \text{ state.} \quad (41)$$

They obey four relations which yield the deviation functions for the orthogonality with

$$d^{0,0} = \sum_i c_{2i}c_{3i}, \quad (42)$$

for the sum rules of each configuration with

$$d^{1,i} = 1 - c_{2i}^2 + c_{3i}^2, \quad (43)$$

and for the normality of the states with

$$d^{2,0} = 1 - \sum_i c_{2i}^2, \quad d^{3,0} = 1 - \sum_i c_{3i}^2. \quad (44)$$

The deviation functions are expected to nearly vanish,

$$d^{k,l} \approx 0 \quad \text{for } k = 0,1,2,3, \text{ and } l = 0,1,\ldots. \quad (45)$$

Determination of amplitudes from angular distributions. The angular distributions of the two 2^- states near the $d_{5/2}$ IAR are not isotropic; admixtures of the configurations $d_{5/2}f_{5/2}$ and $d_{5/2}p_{3/2}$ to the dominant $d_{5/2}p_{1/2}$ strength are present. In the resonant ^{208}Pb(p,p') reaction via IAR the angular distribution is described by a series of Legendre polynomials P_K [15,29],

$$d\sigma/d\Omega(\Theta) = \sum_K a_K P_K[\cos(\Theta)]. \quad (46)$$

As shown in the analysis of the ^{140}Ce(p,p') reaction [29], the relative amplitudes of three configurations can be determined from the anisotropy coefficients a_K including the relative sign [Eqs. (4a)–(4e) in Ref. [29]], namely $c_{d_{5/2}p_{1/2}}^{2_M^-}$, $c_{d_{5/2}f_{5/2}}^{2_M^-}$, $c_{d_{5/2}p_{3/2}}^{2_M^-}$, where M is the order number. The size of the third amplitude [Eq. (41)] is determined by the relation

$$c_{k1} = +\sqrt{1 - c_{k2}^2 - c_{k3}^2}, \quad (47)$$

the coefficient a_0 [Eq. (46)], and the single-particle widths [28].

Similar to Fig. 3 in Ref. [29], Fig. 24 shows the dependence of the amplitudes from the anisotropy coefficients for the two 2^- states. The orthogonality relations yield the shown solution for the 5038 2_2^- and the 5127 2_3^- states, $c_{k1}, c_{k2} = -0.4, +0.1$ and $-0.3, +0.5$, respectively. The $d_{5/2}p_{1/2}$ strengths derived

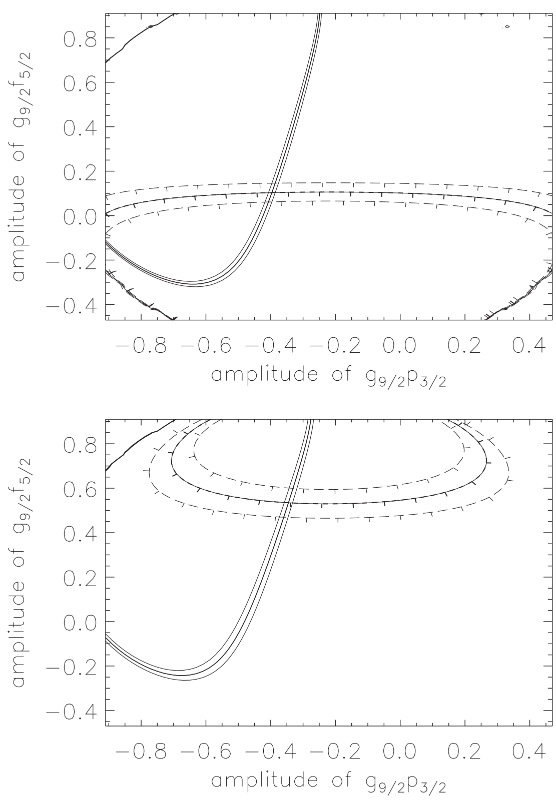

FIG. 24. Dependence of the amplitudes $c^{I^\pi_M}_{LJ,lj}$ [Eq. (10)] from the anisotropy coefficients A_K/A_0 [Eq. (46)] for the (top) 5038 2^-_2 and (bottom) 5127 2^-_3 states. The drawn lines show A_2/A_0 with the uncertainty $\pm 1\sigma$, the dashed lines show A_4/A_0 with the uncertainty [28]. The amplitudes near (top) $c^{2^-_2}_{g_{9/2}p_{3/2}} = -0.4$, $c^{2^-_2}_{g_{9/2}f_{5/2}} = +0.1$ and (bottom) $c^{2^-_3}_{g_{9/2}p_{3/2}} = -0.3$, $c^{2^-_3}_{g_{9/2}f_{5/2}} = +0.5$ fit the angular distributions (Sec. III G 1).

from ^{208}Pb(p,p') (Table VIII) agree with the spectroscopic factors determined from the ^{207}Pb(d,p) data [33,34].

The relative amplitudes determined from Fig. 24 together with the single-particle widths [28] and the spectroscopic factors derived from ^{207}Pb(d,p) [33,34] and ^{209}Bi$(d,{}^3$He) [40,41] are used. By minimizing the deviation relations [Eqs. (42)–(44)], seven amplitudes are determined for each 2^- state from experiment; they are shown in Table VIII. The sum rules show that only few percent of the strength for the first three configurations is missing, namely less than 5% of $g_{9/2}f_{5/2}$, less than 3% of $d_{5/2}p_{1/2}$ [which is also observed by ^{207}Pb(d,p)], and less than 20% of the unobservable configuration $f_{7/2}d_{3/2}$. They are located in higher 2^- states [10].

TABLE VIII. Amplitudes of the first three 2^- states in ^{208}Pb multiplied by a factor of hundred. The relative sign is determined for the configurations with a particle $LJ = g_{9/2}$ or $d_{5/2}$.

$\tilde{E}_x$	I^π_M		Amplitude $c^{I^\pi_M}_{LJ\,lj}$ [Eq. (10)]						
		LJ	$g_{9/2}$	$g_{9/2}$	$d_{5/2}$	$d_{5/2}$	$d_{5/2}$	$h_{9/2}$	$f_{7/2}$
		lj	$f_{5/2}$	$f_{7/2}$	$p_{1/2}$	$f_{5/2}$	$p_{3/2}$	$d_{5/2}$ [a]	$d_{3/2}$ [b]
4230 [c]	2^-_1		+98	+21	−21	+3	−5	+5	+5
		±	1	3	3	6	1	5	5
5038	2^-_2		+15	+15	+78	+10	−30	−10	−54
		±	5	5	2	5	3	5	5
5127	2^-_3		+10	−15	+57	+30	−15	+15	+75
		±	5	5	4	3	5	5	4

[a]From Refs. [40,41].
[b]Assuming vanishing deviation elements [Eqs. (42)–(44)].
[c]From Ref. [87].

2. *Presence of two states at $E_x = 5.04$ MeV*

The ^{208}Pb(α,α') reaction essentially excites only natural parity states [20]. The evaluation of ^{208}Pb(α,α') data [33,34] exhibits a rather strong excitation at $E_x = 5.04$ MeV. The still available spectra [31,43] clearly reveal the isolated peak amidst the 4974 3^- and 5195 3^- states (Sec. III G 3).

Hence, a natural parity state [Eq. (7)] at $E_x = 5.04$ MeV is present. Yet with the assignment of spin 2^- to the 5038 state (Sec. III G 1) the presence of another state with unnatural parity [Eq. (7)] is proven. Therefore, the 5.04-MeV level is a doublet beyond any doubt.

3. *The newly identified 5040 2^+ state*

The 5040 2^+ state in the ^{208}Pb(α,α') reaction. The 5040 2^+ state is excited by the ^{208}Pb(α,α') reaction [33,34,42,43]. By chance, the resolution of 11 keV in the experiment done in 1991 [42] is sufficient to distinguish the 5040 2^+ state clearly from the neighboring 4974 3^-, 5193 5^+, 5195 3^-, 5196 7^+, 5213 6^+, 5214 5^-, and 5216 4^+ levels. The existence of a natural parity state at $E_x = 5.04$ MeV is thus verified.

The excitation energies of the 5.04 MeV level were determined by ([a]) Atzrott [42] and ([b]) Valnion *et al.* [33,34],

E_x(keV)

^{208}Pb(α,α')	^{207}Pb(d,p)	^{208}Pb(p,p')	
5038.6 ± 0.1[a]			(48)
5038.1 ± 0.8[b]	5037.4 ± 0.4[b]	5037.2 ± 0.6[b]	

The excitation energies of the 5038 2^- state from ^{208}Pb(p,p') and ^{207}Pb(d,p) agree with the value from NDS2007 (Table VI); they also agree with the values from Eq. (48). The shown ^{208}Pb(α,α') values, however, are larger. Hence, the natural parity state is certainly above the 5038 2^- state; the distance is suggested as about 1 keV.

Resolving the 5040 2^+ state in the ^{208}Pb(p,p') reaction. The parity of the 5040 doublet state is positive because all negative-parity states predicted by the sSM below $E_x^{\rm sSM} = 6361$ keV were identified [17,18]. The spin of 0^+ is excluded by the low excitation energy [20]; we assign the spin of 2^+ (Sec. IV C 2). The 2^+ member of the 5.04-MeV doublet is much more weakly excited by all particle-transfer reactions than the 5038 2^- state.

The strength of the configuration $d_{5/2}p_{1/2}$ is determined to be about 60% (Sec. III G 1). Hence, the cross section of the 5038 2^- state for the ^{207}Pb(d,p) reaction is about 1500 μb/sr [33,34] and for ^{208}Pb(p,p') near the $d_{5/2}$ IAR about 300 μb/sr [25,28]. A weak doublet state with a suggested relative intensity of less than 1% can be only hardly discerned near the $d_{5/2}$ IAR or in the ^{207}Pb(d,p) reaction.

The cross section for the ^{208}Pb(p,p') reaction near the $s_{1/2}$ IAR the cross section is still large (50 μb/sr) because of the Lorentzian tail from the $d_{5/2}$ IAR; near the $g_{7/2}$ and $d_{3/2}$ IARs it has dropped to 10–20 μb/sr, but here only few spectra are available (Table V). Because of the asymmetric excitation function [25], the cross section near the $g_{9/2}$ and $i_{11/2}$ IARs is less than 10 μb/sr. Among the few spectra taken near these IARs, the fit by GASPAN gives some hint to the doublet state.

One hundred times more statistics are available for the ^{208}Pb(p,p') reaction near the $d_{5/2}$ IAR and at higher proton energies. Yet there is no chance to resolve the weak level on the high-energy side. Namely, the peak shape is asymmetric [12]; on the low-energy side a HFHM of 1.5 keV is achieved, but on the high-energy side only 2–5 keV is achieved.

The 4974 3^-, 5038 2^-, and 5127 2^- states often have rather similar cross sections, especially about 300 μb/sr near the $j_{15/2}$, $d_{5/2}$ [25,28], and $s_{1/2}$ IARs, where most spectra for ^{208}Pb(p,p') were taken (Table V). The width of the peak depends on the position in the detector: A linear function reproduces the trend; the steepness increases by a factor of about two from one end to the other end.

The similarity of the cross sections and the high statistics (often one million counts) make it possible to compare the shape of the peaks in much detail. Remarkably, near the $d_{5/2}$ IAR, the width of the 5.04-MeV level is 5%–10% smaller than calculated by the linear function of the width in dependence on the position in the detector.

Modeling the 5.04-MeV doublet with GASPAN . The fitting procedure of GASPAN works as follows. The Gaussian width A_G increases by a factor of two across the 100-cm-long detector; the numeric value of A_G should be different at least in the last digit presenting units of eV. (Normally, to speed up the fit, the width is set negative, $A_G < 0$; GASPAN then uses the absolute value and does not fit it.) Usually, the width A_T of the tail is varied according to a linear function in dependence on the position in the detector. The sum of the two widths A_G and A_T fits the shape of the peak. Except for forward-scattering angles ($\Theta \lesssim 20^\circ$), the shape is highly asymmetric.

Naively, an unresolved doublet should have a larger width A_G. This is true if the relative intensities of the two constituents are similar or the weaker level is on the low-energy side. Yet if the doublet member on the high-energy side is much weaker than the main peak, then the tail just raises somewhat in a small region of channels. If the Gaussian width is varied in the fit by GASPAN (i.e., $A_G > 0$), in effect the tail may become larger and the Gaussian width smaller. Namely, the sum of the width A_G and the exponential tail A_T is nearly constant.

A study of spectra modeling the 5.04-MeV doublet was done. A strong peak on a low background taken from a real spectrum was used as a template. In a distance of 0.5–3.0 keV on the high-energy side, a second peak with a much lower intensity was inserted into the model spectrum. The fit by GASPAN consistently yielded the following results.

(i) If the relative intensity of the doublet member or the distance between the two members exceeded some limit, the Gaussian width A_G became larger, as naively expected.

(ii) At low distances the Gaussian width A_G diminished systematically with the relative intensity of the doublet member.

(iii) Relative intensities of 0.1%–5% yielded Gaussian widths A_G less than that of the main peak. A minimum reduction by 10% was observed for distances between the two doublet members of about 1–4 keV.

The peculiar shape of the 5.04-MeV level was already noted in the first evaluation [5]; see Sec. VI B 6. The excitation energies are determined from ^{208}Pb(p,p'), ^{208}Pb(d,d'), and ^{207}Pb(d,p) reactions (Table VI) as

$$\begin{aligned} E_x(5038\ 2_2^-) &= 5037.45 \pm 0.04 \text{ keV for } (p,p'), \\ &= 5037.28 \pm 0.04 \text{ keV for } (d,d'), \\ E_x(5040\ 2_2^+) &= 5039.40 \pm 0.30 \text{ keV for } (p,p'), \\ &= 5039.01 \pm 0.30 \text{ keV for } (d,d'), \end{aligned} \tag{49}$$

in consistency with the values determined by Atzrott [42] and Valnion *et al.* [33,34]; see Eq. (48).

Other positive-parity states with spins 2^+ at $E_x > 5.0$ MeV have cross section $d\sigma/d\Omega \lesssim 5\ \mu$b/sr (Table VI). Hence, a similarly small cross section and a nonresonant (p,p') excitation is consistent with the assignment of spin 2^+ to the 5040 state.

H. Isotopic contaminations

1. ^{207}Pb *targets*

The enrichment of the ^{207}Pb targets was between 80% and 99.96% (Table V). Strong excitations of several states in the isotopes ^{207,209}Pb show up in (d,p) spectra even if the ^{206,208}Pb isotopes are present with 0.04% only.

A difficulty presents the near coincidence of the proton energies for the reactions ^{206,207,208}Pb(d,p) in the region $5.8 < E_x < 6.0$ MeV. In this region states with extremely large cross sections show up; they contain the essential fragments of the configurations $g_{9/2}p_{1/2}$ and $d_{3/2}p_{1/2}$. Hence, weak levels in this region are discerned with difficulty.

States in ^{208}Pb observed by the ^{207}Pb(d,p) reaction observed for less than four runs are mostly ignored. In the (d,p) reaction on lead targets, the energies of the emitted protons for some states in ^{208}Pb are close to those for states in other isotopes,

$$\begin{aligned} E_x^{\text{contam}}(^{206}\text{Pb}) &= E_x(^{207}\text{Pb}) + Q[^{206}\text{Pb}(d,p)], \\ E_x^{\text{contam}}(^{208}\text{Pb}) &= E_x(^{209}\text{Pb}) + Q[^{208}\text{Pb}(d,p)]. \end{aligned} \tag{50}$$

The Q values are shown in Table V. Corrections for the relativistic kinematics are up to 20 keV.

As we have used targets of four different isotopic mixtures (Table V), especially one target with 80% ^{207}Pb, we are sure about the correct identification of states in ^{208}Pb. However, in the ^{207}Pb(d,p) reaction, the proton energies are contaminated by lines from the ^{206}Pb(d,p) or ^{208}Pb(d,p) reactions within less than 2 keV for the following states in ^{208}Pb: 4051, 4206, 4255, 4262, 4359, 4974, 5374, 5517, 5705, 5825, 5924, and 5993.

Consequently, there is an additional systematic uncertainty for these excitation energies. The shell model is simply a good description of states with similar constituents in different isotopes; therefore, the energies of the outgoing particles from the (d,p) reaction with different isotopes are similar.

2. ^{208}Pb *targets*

In the ^{208}Pb(p,p') and ^{208}Pb(d,d') reactions, the enrichment of the ^{208}Pb targets was 99.98% (Table V). Among the states in ^{208}Pb with $3.90 < E_x < 6.20$ MeV no state in ^{206,207}Pb has a sufficiently large cross section which makes it possible to show up if the relevant isotope is present with 0.02%. Three spectra for ^{207}Pb(d,d') were taken to confirm the statement.

IV. IDENTIFICATION OF STATES IN ^{208}Pb AND SPIN ASSIGNMENTS

In this section each state is mostly denoted by the energy label $\tilde{E}_x$, spin I, and parity π [Eq. (10)]. Table VI shows data for states at $E_x < 6.20$ MeV in ^{208}Pb, the detailed description of the entries is given in Sec. III C 6. Figures 3–16 compare the excitation energies of states at $E_x \lesssim 6.2$ MeV in ^{208}Pb with predictions by the sSM, mSM, and eSM (Tables I–III); the detailed description is given in Secs. III C 1–III C 3.

All negative-parity states predicted by sSM below $E_x^{\rm sSM} = 6361$ keV were recently identified [17,18], as were many positive-parity states [12].

The multiplet splitting of the states consisting essentially of one configuration is often well explained by the diagonal part of the SDI [16]. The configuration mixing within pairs of states consisting of essentially only two configurations is large if the excitation energies of the two configurations approach each other (Sec. V C). Natural parity configurations tend to mix more strongly than unnatural parity configurations.

A. Structure information and spin assignments

The determination of the structure and the assignment of spin and parity to particle-hole states are intimately correlated. In this paper we use structure information only as far as needed, namely to determine the spin and parity of the states.

For ^{208}Pb, amplitudes $c^{I^\pi}_{M,i}$ [Eq. (10)] can be derived by the analysis of the reactions ^{208}Pb(p,p') via IAR, ^{207}Pb(d,p), and ^{209}Bi$(d,^3$He$)$. A big advantage of the resonant ^{208}Pb(p,p') reaction is the possibility to determine relative signs of the amplitudes. Often it helps to exclude certain spin assignments [29,30].

The method for the determination of amplitudes from the analysis of the reactions ^{208}Pb(p,p') via IAR is sketched in Sec. III G. Here the spin of the 5038 2^- state is confirmed by demonstrating the amplitudes of seven configurations in the lowest three 2^- states to be described by a nearly orthogonal matrix. The method has been used to determine the spins and configuration mixing in the lowest twenty negative-parity states. The unique angular distributions of the 4037 and 4230 states on the $g_{9/2}$ IAR [28] clearly assigned the dominant configuration $g_{9/2}f_{5/2}$ and the spin of 7^- and 2^- [87], respectively.

In the first essay [87] the 3947 state was not yet identified, although it showed up in the very first high-resolution spectra of ^{208}Pb(p,p') [21]; the resolution was about 9 keV. Instead, another state was wrongly suggested within an unresolved doublet [32,107]. Therefore, some spin assignments were wrong. After the identification of the 3947 state to contain the major fraction of the proton configuration $h_{9/2}s_{1/2}$ with the spin of 4^- [38–40], all spins and the orthogonal matrices $||c^{I^\pi_M}_{LJ,lj}||$ [Eq. (10)] of the lowest 20 negative-parity states were derived [88] and later slightly improved [89]. In Table VI the relevant states are marked by footnotes.

From the wave functions determined by experiment [87–89] some matrix elements of the residual interaction where determined by use of Eq. (12). Further preliminary studies show that the distribution of the matrix elements is logarithmic. A median value $\langle v\rangle \approx 100$ keV is estimated; for natural parity it is about twice as large than for unnatural parity.

B. Confirmed and accepted spin assignments to positive-parity states

1. Confirmed assignments with low spins

The 4868 0^+ *state.* The 4868 0^+ state lies only 0.5 keV above the 4867 7^+ state (Sec. III F 4). While the 4867 7^+ state is excited selectively on the $j_{15/2}$ IAR, the 4868 0^+ state is excited only nonresonantly. The excitation energy of the unresolved 4.68-MeV level near the $j_{15/2}$ IAR is significantly smaller than elsewhere (Sec. III F 4).

The 4953 3^+*, 5193* 5^+*, 5317* 3^+*, 5587* 5^+*, and 5844* 1^+ *states.* Several states with spins from $1^+, 3^+$, and 5^+ are weakly excited in the ^{208}Pb(p,p'), ^{208}Pb(d,d'), and ^{207}Pb(d,p) reactions but rather well known from other experiments [1,12]. The 5844 1^+ (Sec. IV B 4), 5317 3^+, and 5193 5^+ states contain the major fraction of the configuration $h_{9/2}h_{11/2}$ [40]. The 4953 3^+ and 5587 5^+ states are identified to contain the major fraction of the configurations $g_{9/2}i_{13/2}$ and $j_{15/2}f_{5/2}$ [12].

The 5241 0^+ *state.* The existence of the 5241 0^+ state is verified by spectra where neither the 5239 4^- nor the 5245 3^- state is strongly excited; the corresponding proton energies for the ^{208}Pb(p,p') reaction are $E_p < 15.7$ MeV, $16.7 \lesssim E_p \lesssim 17.2$ MeV, and $E_p > 17.8$ MeV. While the 5239 4^- state is excited selectively on the $i_{11/2}$ [5] and $g_{7/2}$ IARs, the 5241 0^+ state is excited only nonresonantly. The distance between the 5239 4^- 5241 0^+ states reported as 1.8 ± 0.6 keV [1] is determined as 1.4 ± 0.2 keV. In the ^{207}Pb(d,p) reaction the 5241 0^+ state is not observed (Table VI).

The 5561 2^+ *and 5819* 2^+ *states.* The recalibrated excitation energy from the ^{206}Pb(t,p) and ^{210}Pb(p,t) reactions (Table XI) agrees with the adopted value for the 5561 2^+ state; the assignment of spin 2^+ is confirmed by the ^{208}Pb$(n,n'\gamma)$ study.

In the ^{208}Pb(p,p') reaction, while the 5564 3^- state shows a resonant excitation on the $d_{5/2}$ IAR, the 5561 2^+ state shows a smooth excitation function with low a cross section.

The 5819 2^+ is only rarely observed because of the close-lying strongly excited 5.81-MeV doublet (Sec. III F 5). The recalibrated excitation energy from the ^{206}Pb(t,p) and ^{210}Pb(p,t) reactions indicates an excitation of the 5813 3^- state. Yet the ^{208}Pb$(n,n'\gamma)$ study clearly assigns the spin of 2^+; namely, the spin of 1^+ can be ruled out because the next 1^+ state must have a higher excitation energy than 5844 keV.

The 5667 0^+ *state.* The 5667 0^+ state is identified as the rather pure proton pairing vibration state [20].

2. Confirmed assignments with high spins

Several states with spins 8^+, 11^+, 12^+, and 14^- are weakly excited in particle spectroscopy but rather well known from other experiments [1].

The 5235 11^+ *state.* The assignment of spin 11^+ to the 5235 state [70,71] is confirmed by the resonant excitation on the $j_{15/2}$ IAR (Sec. III F 4). An admixture of 1% $j_{15/2}f_{7/2}$ in the 5235 11^+ state is deduced. The 5235 11^+ state is clearly recognized in the ^{208}Pb(d,d') reaction (Fig. 22; Fig. 2 in Ref. [19]); in the ^{207}Pb(d,p) reaction it is not observed. In the spectrum for the ^{208}Pb(p,p') reaction taken at $E_p = 85$ MeV and $\Theta = 64^\circ$ by Fujita *et al.* [64] the 5235 11^+ and 5750 12^+ states are most strongly excited besides the four 10^+ states.

The 5750 12^+ *state.* The 5750 12^+ state is observed by the ^{208}Pb(p,p') reaction at $E_p > 17$ MeV; in the ^{207}Pb(d,p) reaction it is not observed. The observed γ transitions connecting the 5750 state to the 6101 12^+, 5069 10^+, and 4895 10^+ states [70,71] are weak. NDS2007 suggests a spin 11^+. Yet already two 11^+ states with the 5235 (Sec. IV B 2) and 5864 states (see below) are known. Hence, the spin of 12^+ is assigned to the 5750 state.

The 5864 11^+ *state.* The 5864 11^+ state clearly shows up in spectra taken for both the ^{208}Pb(p,p') and the ^{208}Pb(d,d') reactions (Fig. 23). It is identified with $E_x = 5862.93 \pm 0.35$ keV and $E_x = 5862.80 \pm 0.25$ keV, respectively (Table VI). In the ^{207}Pb(d,p) reaction it is not observed. NDS2007 assigns spin 11^+ based on the analysis of the ^{208}Pb(e,e') experiment [48,49]. We accept the assignment.

In the ^{208}Pb(p,p') spectra taken with proton energy 135 MeV [59,60] the peaks from the two 11^+ states exhibit an interference effect similar as described in Secs. V C and V D 3.

The 6743 14^- *state.* The 6743 14^- state is shown in Fig. 16 for completeness; its spin assignment from the study of the ^{208}Pb(e,e') reaction is beyond any doubt [48–52]. The excitation energy predicted by the mSM agrees with the observed value within 18 keV [16]. In the ^{208}Pb(p,p') spectra taken with proton energies 80–135 MeV [59–61,63,64] the peak with the 6743 14^- state is prominent. The eSM predicts the next configuration 1.2 MeV higher; hence, the $j_{15/2}i_{13/2}$ strength in the 6743 14^- state certainly exceeds 98%.

3. The puzzling 6101 state

The 6101 state is strongly excited by deep inelastic reactions [70,71]. The γ cascade starts with a state at $E_x = 13.7$ MeV and proceeds through the 6744 and 6449 states with suggested spins 14^- and 13^-; it ends in the 4895 10^+_1 0.5-μs isomer. In the ^{208}Pb(p,p') spectrum taken with $E_p = 85$ MeV at $\Theta = 64^\circ$ by Fujita *et al.* [64] the 6101 state exhibits the largest cross section in the range of $4.8 < E_x < 8.5$ MeV. In the ^{208}Pb(p,p') spectra taken with proton energy 135 MeV [59,60] the peak from the 6101 12^+ state is also prominent; the 12^+ yrast state is clearly visible.

The 6101 state is assigned the spin of 12^+ [1] based on the analysis of the ^{208}Pb(e,e') experiment [49,50,52] and the ^{208}Pb(p,p') experiments with bombarding energies $E_p = 80$–318 MeV [59–64]. We accept the assignment of the spin 12^+ to the 6101 state by NDS2007.

The mSM cannot explain the assignment as already stated [16]; the eSM does not provide an immediate explanation either. Figure 9 illustrates the situation. Table III shows that after the yrast state identified with the 5750 state (Sec. IV C 2) the next configurations ^{210}Bi$(I_1^-) \otimes ^{206}$Tl(I_2^-) are predicted above 7.3 MeV only. The 8369 state observed by Fujita *et al.* [64] may correspond to one member of the configurations shown in Fig. 9.

Among all 151 states identified at $E_x < 6.20$ MeV and the schematic one-to-one correspondence of configurations shown in Figs. 3–16, the cluster of 20 configurations within 1 MeV for the 12^+ configurations is the densest one. The large downshifts of the 2^+, 4^+, 6^+, 1^-, and 3^- yrast states similar to the 1-MeV downshift of the 12^+ yrare state are not well reproduced by calculations [83].

4. Accepted spin assignments

The 5317 3^+ *and 5318* 3^- *states.* We confirm the spin of 3^+ for the 5317 state [103]; we accept the spin of 3^- suggested by NDS2007 for the 5318 3^- state. The ^{209}Bi$(t,\alpha\,\gamma)$ reaction excites only the 5317 state; the ^{207}Pb(d,p) reaction excites only the 5318 state. The angular distribution of ^{209}Bi$(d,^3$He) for the level at $E_x = 5314(3)$ shows a $L = 5$ transition with a spectroscopic factor of 0.42, but clearly there is a considerable $L = 2$ admixture with an estimated spectroscopic factor of 0.08 (Fig. 4 in [40]). [We note that the level at $E_x = 5335(4)$ shows a $L = 5$ transition with a significant admixture of $L = 2$, too. The level is identified with the 5327 9^+, 5339 8^+, and 5347 3^- states.]

The 5715 2^+ *state.* Close to the 5686 6^-, 5690 4^+, and 5694 7^- states there is the 5715 2^+ state. The vanishing cross section in the ^{208}Pb(p,p') reaction confirms the spin 2^+ assigned by NDS2007. The observed ^{207}Pb(d,p) cross section is explained by an admixture of the eSM configuration $g_{9/2}p_{1/2} \otimes 3_1^-$ (Sec. V E).

The 5844 1^+ *state.* The 5844 1^+ state does not contain the full $h_{9/2}h_{11/2}$ strength [39,40]. The mSM predicts the excitation energy of the 1^+ members of the $h_{9/2}h_{11/2}$ and $i_{11/2}i_{13/2}$ multiplets at 5840 and 6543 keV (Table I, Fig. 3). Yet two-particle–two-hole configurations are also present; because of the unnatural parity only the lower one is relevant, namely $g_{9/2}p_{1/2} \otimes 3_1^-$ (Table III). The mixing among the two lowest 1^+ configurations explains the incomplete $h_{9/2}h_{11/2}$ strength in the 1^+ yrast state; Grabmayr *et al.* [40] report a $h_{9/2}h_{11/2}$ strength of 55%. Indeed, the next 1^+ state is identified with the 5944(6) level reported by Grabmayr *et al.* (Sec. IV C 2).

The 5928 10^+ *state.* The 5928 10^+ state is not observed in the ^{208}Pb(p,p') and ^{208}Pb(d,d') reactions because of the strongly excited 5924 2^- neighbor but clearly by ^{209}Bi$(t,\alpha\,\gamma)$. The structure of the four lowest 10^+ states is well understood [103]. In the ^{208}Pb(p,p') spectra taken with proton energies 135 MeV [59,60] and 80 MeV [64] the peaks for all four 10^+ states are prominent; they are rather similar to each other.

The 5973 2^+*, 6054* 4^+*, and 6102* 5^+ *states.* The assignments by NDS2007 are accepted.

C. New spin assignments

Because of the high resolution of the Q3D magnetic spectrograph at the MLL, several new states are identified. In addition, levels with large uncertainties in the excitation energy are verified and the uncertainty is reduced to a low multiple of 10 eV.

In the following the spin assignments are shown in order of increasing excitation energies. However, they depend on each other and should be thought to be done in another order: first of all the assignments of the spin of 2^-, 3^-, 5^-, and 8^-, then 2^+, 5^+, 6^+, and 7^+, and finally 1^+ and 1^-.

Historically, however, the identification and the spin assignments were done more like a grand puzzle, where the solution of one corner implies another unexpected solution. The range of spin and parity assignments suggested by NDS2007 is taken as the basis of the analysis.

1. New spin assignments to negative-parity states

The major strength of the particle-hole configurations with negative parity predicted at $E_x^{\rm sSM} = 6361$ keV is located in 72 states at $E_x = 6.4$ keV [18]. The additional appearance of the 1^- and 3^- yrast states has been already noted.

In this section, seven more negative-parity states consisting mainly of configurations other than one-particle–one-hole configurations are identified.

Since the publication of NDS2007 new spin and parity assignments together with the main particle-hole configuration were determined for about 30 states; here two dozen more states are discussed. Table VI gives the references. The identification of several states are already discussed in Secs. III F 3 and III F 4. A few spin assignments are confirmed (Sec. IV B). The analysis of the configuration composition for some states is refined in Sec. V, but, as noted, this paper is devoted to the identification of states mainly.

The 5380 5^- state. The 5380 5^- state belongs to an ensemble of four states within 10 keV, including the 5374 7^+, 5383 4^+, and 5385 3^- states [Fig. 22(b)]. NDS2007 wonders about the 2766 and 2768 γ rays. In the ^{209}Bi($t,\alpha\,\gamma$) reaction, the transition with $E_\gamma = 2766.1 \pm 0.8$ keV to the 2615 3^- state is consistent with the difference derived from the values for the 5380 level (Table VI). In the ^{208}Pb($n,n'\,\gamma$) reaction, the transition with $E_\gamma = 2768.31 \pm 0.05$ keV and $I_\gamma = 0.315 \pm 0.015$ to the 2615 3^- state is consistent with the difference derived from the values for the 5383 level (Table VI). NDS2007 proposes the 5383 state to have spin 3^+ or 4^+ or 5^+; the spin of 4^+ is assigned in Sec. IV C 2. There is a printing error in Table 1 of Ref. [40] which misled Rejmund *et al.* [103] to doubt the assignments of the L values for the 5378(3) and 5388(5) levels. Indeed, both are $L = 2$. The angular distribution of the unresolved level at $E_x = 5388(5)$ [40] clearly shows a $L = 2$ transition. Hence, two states within the 5378(3) and 5388(5) levels have negative parity. (We note that the given spectroscopic factor of 0.21 with $L = 5$ for the level at $E_x = 5097(3)$ is another printing error; Fig. 4 in Ref. [40] clearly shows a $L = 2$ transition with some $L = 5$ admixture.)

The 5385 state has the spin of 3^-; it is strongly excited by ^{207}Pb(d,p). While it is observed in ^{209}Bi($d,^3$He) as the 5388(5) level [40], Rejmund *et al.* report only the excitation by ^{207}Pb(d,p). The ^{209}Bi($d,^3$He) spectra [41] clearly show a doublet level with both the 5380 and the 5384 states. The unobserved excitation of the 5380 state in the ^{208}Pb($n,n'\,\gamma$) reaction is explained by a high spin $I \geqslant 5$. We assign the spin of 5^- to the 5380 state. Namely, all negative states predicted below $E_x^{\rm sSM} = 6361$ keV are identified [18]. Natural parity configurations tend to mix more strongly than unnatural parity configurations. Spin 7^- is excluded because the spacing among the mSM configurations is always large; higher odd spins with negative parity are excluded because they are expected at much higher excitation energies. The spectroscopic factor of 0.240 with $L = 2$ in the ^{209}Bi($d,^3$He) reaction for the 5380 state [103] supports the assignment of the spin of 5^-.

The newly identified 5705 5^- state. The 5705 state is newly identified between the two groups with the 5686 6^-, 5690 4^+, and 5695 7^- states and the 5715 2^+ and 5721 6^+ states. The cross sections of all states do not differ very much; hence, the 5705 state is clearly identified on all IARs and by the ^{208}Pb(d,d') and ^{207}Pb(d,p) reactions. A possible isotopic contamination in ^{207}Pb(d,p) (Sec. III H 1) is ruled out. It is assigned the spin of 5^-. Namely, the excitation function for the ^{208}Pb(p,p') reaction shows an enhancement near the $g_{9/2}$ and $d_{5/2}$ IARs. The angular distribution near the $g_{9/2}$ IAR is similar to the 5659 5^- state (which contains about 50% $g_{9/2}f_{5/2}$ strength [11]) with a maximum near $\Theta = 90^\circ$; the $g_{9/2}f_{5/2}$ strength is estimated as 20%. The angular distribution near the $d_{5/2}$ IAR has a minimum at $\Theta = 90^\circ$ characteristic for a $d_{5/2}f_{5/2}$ component. The weak excitation by the ^{207}Pb(d,p) reaction is explained by small $g_{9/2}p_{1/2}$ and $i_{11/2}p_{1/2}$ components.

The 5705 5^- state is barely visible in the ^{209}Bi($d,^3$He) spectra [41]. The weak cross sections explain the absence of the detection by ^{209}Bi($t,\alpha\,\gamma$) and ^{207}Pb($d,p\,\gamma$) reactions [46,103]; the high spin explains the absence of the detection by ^{208}Pb($n,n'\,\gamma$) [1]. More than 70% of the total strength is not explained by particle-hole configurations predicted at $E_x^{\rm sSM} = 6361$ keV. The ^{208}Pb(α,α') reaction did resolve the ensemble consisting of five natural parity states only partially, it contains the 5690 4^+, 5694 7^-, 5705 5^-, 5715 2^+, and 5721 6^+ states (Table VI); excitation energies were determined as $E_x = 5694.2(12)$ and 5722.1(4) keV [42] and $E_x = 5690.8(8)$ and 5718.4(8) keV [33].

The 5805 1^- state. The γ transition to the ground state observed by Radermacher *et al.* [46] may be doubted. Namely, the difference of 511.1 keV between the reported energies $E_\gamma = 5802.9$ keV and $E_\gamma = 6313.8$ keV exactly matches the production energy of an electron-positron pair; yet only part of the 5802.9-keV transition belongs to the single escape peak of the 6314 1^- state; the observation on the $s_{1/2}$ IAR is in agreement with the dominant $s_{1/2}p_{3/2}$ strength in the 6314 1^- state [10]. The energies reported by Schramm *et al.* [47] are $E_\gamma = 5805.9$ keV and $E_\gamma = 6313.7$ keV. They differ from the values reported by Radermacher *et al.* [46] considerably. Because of the limited neutron energy, the 6314 1^- state was not observed in the ^{208}Pb($n,n'\,\gamma$) reaction [1]; the reported energy $E_\gamma = 5804.9$ keV agrees with the value observed by ^{207}Pb($d,p\,\gamma$). A spin of 1^+ is ruled out because the third 1^+ state is expected at 6.5 MeV only (Sec. III F 5). A spin of 2^+ is ruled out because of the rather strong excitation by ^{207}Pb(d,p) (Table VI). By this agreement the spin of 1^- for the 5805 state is established.

The 5993 5^- *state.* The 5989 state had been shown to have the spin of 6^+ and the 5993 state to have negative parity [12]. We assign the spin of 5^- to the 5993 state. The spin of 3^- is ruled out because the distance of only 19 keV to the next state (6010 3^-_{17}) is far less than the minimum distance between any two states with the same spin and the same parity at $E_x < 6.20$ MeV; the minimum distance of 30 keV is observed between the 5317 3^-_9 and the 5347 3^-_{10} states. All 12 5^- states predicted by the sSM below $E_x^{\mathrm{sSM}} = 6361$ keV are identified [18]. Among the next eight 5^- states expected at $6.4 < E_x < 6.9$ MeV, three 5^- configurations (two mSM, one eSM) are predicted with almost the same excitation energy (Fig. 14). Similar to the pushing down of the 5^- yrast state out of the ensemble of the first six states, the strong residual interaction among the natural parity particle-hole configurations explains the downshift of the 5659, 5705, and and 5993 states (Sec. II D, Fig. 14).

The 6076 1^- *state.* The 6076 1^- state is not excited on the $s_{1/2}$ but near the $d_{3/2}$ IAR. It rules out the interpretation [1] by a purely $L = 0$ transfer [19]. It is weakly excited by the ^{207}Pb(d,p) reaction; the angular distribution shows a vanishing analyzing power of the polarized deuterons [33,34]. However, there are only four data points for $25^\circ \leqslant \Theta \leqslant 35^\circ$ with low statistics. A dominant $L = 2$ transfer with a weak admixture of a $L = 0$ transfer could explain the vanishing analyzing power. The spin of 0^- is ruled out because the mSM predicts the next state at $E_x > 6.6$ MeV (Fig. 10). The spin of 2^- is ruled out because the distance of only 10 keV to the next state (6086 2^-_9) is far less than the minimum distance of 30 keV between any two states with the same spin and the same parity at $E_x < 6.20$ MeV. The structure of the 1^- 6076 state is explained by a dominant $d_{3/2}p_{1/2}$ component with a weak $s_{1/2}p_{1/2}$ admixture.

The newly identified 6089 3^- *state.* The 6086 2^- state contains much $s_{1/2}f_{5/2}$ strength with admixtures of $s_{1/2}p_{3/2}$ and $d_{3/2}p_{1/2}$ [10]. The neighboring 6089 state is more weakly excited by the ^{207}Pb(d,p) reaction and more strongly excited on several IARs (Sec. III F 4). The excitation by the ^{208}Pb(α,α') reaction implies a doublet with a natural parity state. The excitation on the $s_{1/2}$ IAR assigns the spin of 3^- and a considerable $s_{1/2}f_{5/2}$ strength [19]. NDS2007 reported a γ transition $E_\gamma = 1113.57 \pm 0.03$ keV with $I_\gamma = 0.31 \pm 0.04$ as starting from the 6086 2^- state and remarked that the placement is uncertain. Indeed, the newly identified 6089 state explains the transition as populating the 4974 3^- state by the particle exchange $d_{3/2} \to d_{5/2}$ with the $p_{1/2}$ hole as the spectator. The excitation energy is determined as $E_x = 6087.20 \pm 0.20$ keV, in approximate agreement with the values shown in Table VI. The placement from the suggested 5075 level is thus ruled out.

2. New spin assignments to positive-parity states

The 4928 6^+ *and 4962* 5^+ *states.* The 4962 state is not observed by ^{207}Pb(d,p), but in the ^{208}Pb(d,d') and ^{208}Pb(p,p') reactions. The extremely weak ^{208}Pb(p,p') cross section (less than 0.5 μb/sr at $14.8 < E_p < 18.2$ MeV) excludes negative parity. It is assigned the spin of 5^+, as suggested by NDS2007. The weak excitation in the $j_{15/2}$ IAR indicates the 4962 5^+ state to contain little $j_{15/2}f_{5/2}$ admixture. The sSM predicts only three 5^+ states at $E_x < 5.8$ MeV. The 5193 and 5587 states contain the major $h_{9/2}h_{11/2}$ [40] and $j_{15/2}f_{5/2}$ [12] fractions; hence, the 4962 5^+ state consists almost entirely of the lowest sSM configuration $g_{9/2}i_{13/2}$.

The 4928 state is resonantly excited on the $j_{15/2}$ IAR [12]; it is assigned the spin of 6^+ in contrast to the previous assignment of 5^+ [12]. The reanalysis of the 4928 level does not show a doublet with another state.

The 5040 2^+ *state.* The 5038 2^- state consists mainly of the $d_{5/2}p_{1/2}$ configuration [10], but has an admixture of 30% ± 5% of the unobservable configuration $f_{7/2}s_{1/2}$ (Table VIII). The rather strong excitation by the ^{208}Pb(α,α') reaction implies a doublet with natural parity. As discussed in Sec. III G 3, the 5038 2^- state has a neighbor at an about 2-keV-higher excitation energy [Eq. (49)]. Spin 0^+ is excluded because the proton pairing vibration state is identified with the 5667 state [20] and higher 0^+ states are expected at higher excitation energies (Fig. 8). Higher spins with natural parity are also not expected (Figs. 3–8). Hence, the spin of 2^+ is assigned to the 5040 state.

The 5286 2^+ *state.* The 5286 2^+ state is observed by ^{208}Pb(p,p') and ^{208}Pb(d,d'), but not by ^{207}Pb(d,p). The spin of 3^- is excluded because the ^{208}Pb(p,p') reaction does not show any resonant behavior; the cross section is low.

The 5383 4^+ *state.* The 5383 state is observed by the ^{208}Pb(d,d'), ^{208}Pb(p,p'), and ^{207}Pb(d,p) reactions; the cross sections for ^{208}Pb(p,p') and ^{207}Pb(d,p) are low. NDS2007 suggests spin 3^+, 4^+, or 5^+. Spin 5^+ is excluded because the sSM predicts the next 5^+ state with order number $m > 3$; namely the 5587 5^+_3 state is known [12]. Spin 3^+ is excluded because the next 3^+ state with order number $M > 2$ is only expected at $E_x \approx 5.8$ MeV (Table I). The spin of 4^+ is thus assigned.

The 5474 7^+ *and 5502* 6^+ *states.* The sSM predicts the $i_{13/2}s_{1/2}$ configuration with spins 6^+ and 7^+ at $E_x^{\mathrm{sSM}} =$ 5522 keV (Table I). We suggest the 5474 state to contain almost the complete 7^+ strength of the unobservable configuration $i_{13/2}s_{1/2}$. All other known 7^+ states are rather pure and admixtures of other configurations are generally less than a few percent [12]. The sensitive measurement of the ^{207}Pb(d,p) reaction reveals an admixture of $j_{15/2}p_{1/2}$ to the 5474 state to be less than 0.1%. Despite the low resolution, the ^{209}Bi(d,^{3}He) data indicate a weak $h_{9/2}h_{11/2}$ component in the 5474 state [41].

The corresponding 6^+ $i_{13/2}s_{1/2}$ strength is mainly located in the 5502 state. Because of the natural parity, all nine identified 6^+ states are strongly mixed (Fig. 5).

The 5642 2^+ *state.* In the ^{208}Pb(p,$p'\gamma$) study, Cramer *et al.* [45] report a ground-state transition with $E_\gamma = 5.63$ keV on the $d_{5/2}$ IAR; no anisotropy of the angular distribution is reported because the uncertainty is 50%. Radermacher *et al.* [46] report a γ ray with $E_\gamma = 5641.4 \pm 0.5$ keV; it is observed with nearly equal intensity on the $d_{5/2}$ and $s_{1/2}$ IARs. In the ^{208}Pb(n,$n'\gamma$) reaction, two γ rays with $E_\gamma = 5639.7 \pm 0.2$ and 5641.9 ± 0.2 keV with nearly equal intensities are reported [1]. With the ^{206}Pb(t,p) and ^{210}Pb(p,t)

reactions, the recalibrated energy of their level 48 yields $E_x^{\text{calib}} = 5640.4$ keV (Table XI); the uncertainty is estimated as 1.5 keV.

The 5640 state is assigned the spin of 1^- [11]; it is resonantly excited on the $g_{9/2}$ and $s_{1/2}$ IARs and weakly by ^{207}Pb(d,p). For the 5642 state spin 4^+ is excluded because seven 4^+ states at $E_x < 6.20$ MeV are known and hence another 4^+ state is expected at higher energies only (Fig. 4). Similarly, other higher spins with positive parity are excluded. Therefore, the spin of 2^+ is assigned and the 5642 state is assumed to have considerable admixtures of two-particle–two-hole configurations.

The 5721 state. The 5721 state is assigned the spin of 6^+. It is excited by the ^{208}Pb(α,α') reaction; hence, it has natural parity. The suggested spin of 7^- [1] is excluded because five states with spin 7^- are known in agreement with the prediction by the mSM; the next 7^- state is expected at $E_x = 6.5$ MeV (Fig. 15). The spin of 8^+ is excluded because no resonance for the ^{208}Pb(p,p') reaction near the $j_{15/2}$ IAR [12] is observed. The observed ^{207}Pb(d,p) cross section is explained by an admixture of the eSM configuration $g_{9/2}p_{1/2} \otimes 3_1^-$ (Table III).

The 5789 3^+ state. NDS2007 suggests spins of 2^+ or 3^+ or 4^+ for the 5789 state. The number of identified 2^+ and 4^+ states agrees with the predicted number of states (Figs. 3 and 4). Hence, the spin of 3^+ is assigned to the 5789 state.

The 5799 5^+ state. The 5799 state is weakly excited in the ^{208}Pb(p,p') reaction at $14.8 < E_p < 18.2$ MeV and by the ^{208}Pb(d,d') and ^{207}Pb(d,p) reactions. The excitation by ^{207}Pb(d,p) is explained in Sec. V E. Both the ^{208}Pb($n,n'\gamma$) and the ^{207}Pb($d,p\gamma$) reactions yield a transition to the 3475 4_1^- state. The spin of 5^+ is assigned to the 5799 state. The configuration $i_{13/2}d_{3/2}$ is assumed as the major configuration (Fig. 5).

The 5819 2^+ state. The assignment is based on the large cross section observed in both the ^{206}Pb(t,p) and the ^{210}Pb(p,t) reactions. The observed considerable $h_{9/2}h_{11/2}$ strength at $E_x = 5821 \pm 3$ keV [40] may be partially located in the 5825 8^+ state (see the following paragraph).

The 5825 8^+ state. Schramm *et al.* [47] suggest the 5825 state to have spin 8^+. It is more strongly excited near the $j_{15/2}$ IAR and in the ^{207}Pb(d,p) reaction with a considerable cross section; hence, the spin is either 7^+ or 8^+. The unnatural parity spin 7^+ is excluded because only the yrast 7^+ state contains a detectable $j_{15/2}p_{1/2}$ strength. The γ transition to the 4611 8^+ state with a large $g_{9/2}i_{13/2}$ fraction [103] suggests a considerable $i_{11/2}i_{13/2}$ admixture.

The 5918 4^+ state. NDS2007 suggests spin 3^-, 4, or 5^- for the 5918 state. All negative-parity states predicted by sSM below $E_x^{\text{sSM}} = 6361$ keV were recently identified [17,18]. The 5993 state is newly assigned the spin of 5^- (see Sec. IV C 1); the spin of 4^+ is assigned to the 5918 state.

The 5937 1^+ state. Grabmayr *et al.* report a $h_{9/2}h_{11/2}$ strength [39,40] at $E_x = 5944 \pm 5$ keV; it meets exactly the missing complement to the spectroscopic factor of unity for the spin of 1^+. The inspection of the four spectra [41] verifies the presence of the state, although marginally resolved from the 5928 10^+ state. The excitation energy is determined by the ^{208}Pb(p,p') reaction as $E_x = 5936.60 \pm 0.25$ keV (Table VI). In some ^{208}Pb(d,d') spectra it is also observed. The uncertainty of the excitation energy is large, however; therefore, no ^{208}Pb(d,d') value is shown in Table VI.

The 6037 6^+ and 6068 5^+ states. NDS2007 assigns either spin 5^+ or 6^+ to both the 6037 and the 6068 states. For the 6037 state, the large cross section observed in both the ^{206}Pb(t,p) and the ^{210}Pb(p,t) reactions (Table XI) excludes the spin of 5^+, hence leaving the assignment of 6^+ and natural parity. The 6068 state is tentatively assigned the spin of 5^+. The level at $E_x = 6071(5)$ keV with $L = 5$ reported by Grabmayr *et al.* [40] may correspond to the 6068 5^+ level.

The 6099 4^+ state. The 6099 state is identified with the level number 67 observed by Igo *et al.* [37], yielding a recalibrated energy of 6103.6 ± 2.0 keV (Table XI). The neighboring 6101 12^+ and 6102 5^+ states are not expected to be strongly excited by the ^{206}Pb(t,p) and ^{210}Pb(p,t) reactions. The pairing force may explain the large cross section for the 6099 state only with a spin of 4^+.

3. Tentative spin assignments to positive-parity states

The 5957 8^+ state. NDS2007 suggests a level near 5954 with spin 9^+ based on the study of ^{208}Pb(e,e'). The high spin is matched by the tentative assignment of spin 8^+ to the 5957 state. The excitation by the ^{207}Pb(d,p) reaction suggests a weak admixture of $j_{15/2}p_{1/2}$; no data for ^{208}Pb(p,p') on the $j_{15/2}$ IAR are available to prove such an admixture (Table V).

The 5981 7^+ state. The 5981 7^+ state was already observed by Valnion *et al.* [33]. Tentatively, the spin of 7^+ is assigned.

The 6023 7^+ and 6026 8^+ states. Among the states with the dominant configuration $i_{11/2}i_{13/2}$, the states with spin 9^+, 10^+, 11^+, and 12^+ are identified (Sec. IV B 2); the 1^+ and 6^+ members are identified with the 5937 and 6037 states (Sec. IV C 2). The 2^+ member is identified within the sequence of nine states, in agreement with the number of predicted configurations (Fig. 3). The 7^+ and 8^+ members are tentatively assigned to the 6023 and 6026 states, but neither the order is determined nor an assignment of one state with the spin 0^+ is excluded (Table III).

The 6068 5^+ state. The 6068 5^+ state is tentatively assigned in Sec. IV C 2.

The newly identified 6085 3^+ state. The 6085 state is recognized near the $g_{9/2}$ and $d_{5/2}$ IARs as neighbor of the 6086 2^- state (Sec. III F 4). NDS2007 reported a γ transition $E_\gamma = 1387.37 \pm 0.03$ keV with $I_\gamma = 0.24 \pm 0.02$ as starting from the 5363 2^- state and remarked that the placement is uncertain. Indeed, the newly identified 6085 state explains the transition as populating the 4698 3^- state; the excitation energy is determined as $E_x = 6085.69 \pm 0.05$ keV, in agreement with the values shown in Table VI. The 6085 state is tentatively assigned the spin of 3^+.

V. COMPLETENESS AND STRUCTURE INFORMATION

The number of states at $E_x < 6.20$ MeV is compared to the predictions by the eSM in Sec. V A; centroid energies are discussed in Sec. V B; a sketch of peculiar structure information for some states is done in sections Secs. V C, V D, and V E.

A. Completeness of states at $E_x < 6.2$ MeV

1. Comparing the number of states with predictions

Table VI enumerates the identified states at $E_x < 6.20$ MeV. The number of identified states is

$$N^{\text{ident}}(1) = 77 \text{ at } E_x < 5.45 \text{ MeV}, \quad (51)$$

$$N^{\text{ident}}(2) = 151 \text{ at } E_x < 6.20 \text{ MeV}. \quad (52)$$

(Already at the INPC in 2007 the number of identified states was given with approximately 150 [8].)

The number of identified states almost agrees with the number of predicted configurations $N^{\text{predict}}(1,2) = 72{,}146$ [Eqs. (37) and (38)]. Figure 2(b) shows deep minima near the two gaps ($E_x \approx 5.4$ and 6.2 MeV); before the minima the number of states is larger than predicted. This fact is explained by the global pushing down of all states by around 50 keV [Eq. (57)].

By mere chance the total number $N^{\text{predict}}(2) = 146 \pm 3$ of predicted configurations is similar to the number $N^{\text{ident}}(2)$ of identified states (Fig. 2). However, the coincidence has to be interpreted. There are more negative-parity states than predicted at $E_x < 6.20$ MeV. Namely, two 1^-, five 3^-, and three 5^- states with configurations predicted at $E_x < 6.20$ MeV are identified (Figs. 10, 12, and 14). Furthermore, some spin assignments are tentative (Sec. IV C 3).

There could also be positive-parity states unidentified at $E_x < 6.20$ because weak states are discerned only with difficulty. Some predicted excitation energies of the configurations are uncertain by about 100 keV; especially for proton configurations the Coulomb energy [Eq. (5)] is uncertain.

Figure 2 compares the number of predicted configurations, identified states, and levels listed in NDS2007 [1] in dependence of the excitation energy. In the top frame, the number of configurations predicted by the mSM (dotted curve) and eSM (drawn curve) is shown. Two large gaps at $E_x \approx 4.5$ and $E_x \approx 6.1$ MeV are common for all spins and both parities, with a minor gap for negative parity at $E_x \approx 5.4$ MeV; they are denoted by vertical dashed lines.

Figure 2(b) shows the difference between the number of predicted configurations and the identified states. At $E_x < 6.20$ MeV 151 states are observed, while 146 configurations are expected. As shown in Fig. 2(c), the number of identified states diverges from the number of levels listed in NDS2007 up to $E_x = 6.20$ MeV by more than 40 entries. In addition, five new states have been identified since 2007.

2. States with configurations predicted at $E_x > 6.20$ MeV

The 5813 3^-, 5874 3^-, 6010 3^-, 6089 3^-, and 6191 3^- states. The 5813 3^-, 5874 3^-, 6010 3^-, 6089 3^-, and 6191 3^- states are pushed down from energies $E_x^{\text{sSM}} > 6.5$ MeV. Even the mSM energies start only at $E_x^{\text{mSM}} = 6205$ MeV with the configuration $j_{15/2}i_{13/2}$; see Fig. 12. The numbers of configurations for the spin of 2^- and 3^-, 3^- and 4^-, 9 and 11 configurations, respectively, are the same at $E_x^{\text{eSM}} < 6.20$ MeV and there are less than three additional configurations for either spin (Sec. V A 3). The residual interaction for natural parity is larger than for unnatural parity. For this reason, the 3^- yrast state is pushed down dramatically, while the 2^- and 4^- states are mostly grouped into pairs; see Figs. 12, 11, and 13, respectively.

The 5947 1^- and 6076 1^- states. Figure 10 shows the level scheme of the 1^- states. The order number of the 5947 1^-_6 and 6076 1^-_7 states suggest dominantly mSM configurations with $E_x^{\text{mSM}} > 6.20$ MeV. The 5292 1^-_2 state is known to contain almost the full $s_{1/2}p_{1/2}$ strength, the 5512 1^-_3 state 10% of the $d_{3/2}p_{1/2}$ strength, and the 5947 1^-_6 state 90% of the $d_{3/2}p_{1/2}$ strength [33,34]. The other 1^- states at $E_x < 6.20$ MeV are weakly excited by all particle-transfer reactions. We note that admixtures of the configuration $g_{9/2}f_{7/2}$ are deduced with difficulty; namely, the single-particle width is weak [28] and the angular distribution on the $g_{9/2}$ IAR is steep [11].

Some 1^- states predicted below 7 MeV are not yet found (Fig. 10). Already the comparison to the mSM configurations revealed the missing of at least two bound 1^- states [19]. The centroid energies calculated up to the 6720 1^-_{12} state, however, agree within 100 keV, similar to the global mean value (Table IX). The lower level density explains the lessened pushing down of the 1^- states, in contrast to the 3^- and 5^- states. For the 7^- states the level density is very low; hence, the excitation energies differ only slightly from the predicted energies (Fig. 15).

The 5659 5^-, 5705 5^-, and 5993 5^- states. The 5659 5^-, 5705 5^-, and 5993 5^- states are recognized to contain dominantly mSM configurations with $E_x^{\text{mSM}} > 6.20$ MeV (Fig. 14). Twelve of the lowest 5^- states ($3.1 < E_x < 5.7$ MeV) contain almost the complete strength of the lowest 12 mSM configurations [18]. The next 3 configurations are predicted at $E_x^{\text{mSM}} = 6279, 6371, 6373$ keV. Their near degeneracy explains their pushing down (Secs. II D and IV C 1, Fig. 14).

3. Unnatural parity states

Without any exception, for all unnatural parity states the gap at $E_x \approx 6.1$ MeV clearly shows up; see Figs. 3–8 for spins $1^+, 3^+, 5^+, 7^+, 9^+$, and 11^+ and Figs. 10–16 for spins $0^-, 2^-, 4^-, 6^-$, and 8^-. In many cases the dominant eSM configuration is close to the state with the same order number.

We especially note the remarkable difference in the sequence of 3^- and 4^- states: The number of eSM configurations at $E_x < 7.6$ MeV with more than 30 is almost identical. While the 4^- states are arranged with rather even spacing and the difference between the eSM energy and the corresponding experimental energy is less than 100 keV, the 3^- states are often shifted by several hundred keV, especially in the region $5.5 < E_x < 6.5$ MeV; the famous downshift of the yrast state by 1.6 MeV is the largest one.

The comparison of the level schemes for spins 1^- and 2^- and spins 3^- and 4^- demonstrates that the residual interaction among natural parity configurations is much stronger than among unnatural parity configurations.

The sSM configurations are essentially the same. The shift by the multiplet splitting described by the mSM is less than 200 keV, yet often in different directions. For each spin, additional sSM configurations are involved, but especially for negative parity most configurations are identical (Table II).

(i) Below $E_x^{\rm sSM} = 6594\,$keV, for the spin of $1^- s_{1/2}p_{1/2}$ and for 2^- $g_{9/2}f_{5/2}$, $d_{5/2}p_{1/2}$, $f_{7/2}d_{3/2}$, $s_{1/2}f_{5/2}$ are involved, but nine configurations are the same;

(ii) for the spins of 2^- and 3^- between the common configurations $d_{5/2}p_{1/2}$ and $s_{1/2}f_{5/2}$ and below $E_x^{\rm sSM} = 6594\,$keV, seven configurations are the same and only one configuration for each spin differs, namely $d_{3/2}p_{1/2}$ and $g_{7/2}p_{1/2}$(below $d_{5/2}p_{1/2}$ besides the common $d_{5/2}f_{5/2}$, there are four more configurations for the spin of 3^-);

(iii) below $E_x^{\rm sSM} = 6487\,$keV, for the spin of $3^- d_{5/2}p_{1/2}$ and $s_{1/2}f_{5/2}$ are involved additionally and for 4^- $g_{9/2}p_{1/2}$, $h_{9/2}s_{1/2}$, and $i_{11/2}p_{3/2}$ are involved additionally, but 11 configurations are the same.

The comparison of the level schemes for 1^-, 3^-, and 5^- to 2^-, 4^-, and 6^- clearly demonstrate the different strength of the configuration mixing (Figs. 10–16). While the unnatural parity states mostly are grouped into pairs or triples, the natural parity states follow a rather even spacing.

Only for natural parity is the large gap at $E_x = 6.20\,$MeV (Tables I and II) in the sequence of sSM configurations erased. For the spin of 1^- 6 configurations above the gap are shifted down by up to 0.5 MeV, for 3^- 14 configurations are shifted by up to 0.8 MeV, for 5^- 3 configurations are shifted by up to 0.7 MeV. The extreme downshift of the 1^-, 2^+, 3^-, 4^+, and 6^+ yrast states can be thus well understood.

4. Overall agreement

The main source of the agreement between the number of predicted states [Eqs. (37) and (38)] and the number of identified configurations [Eqs. (51) and (52)] is the presence of the large gap at $E_x \approx 6.1\,$MeV among both all predicted configurations and all identified states (Sec. III D).

A few states are uncertain both on the side of the model predictions and on the side of the experimental observation. The predictions by the eSM are uncertain by about 100 keV, especially for proton configurations [Eq. (5)]. Weak states are observed with difficulty, especially at higher energies close to strongly excited states (Secs. III F 5).

B. Centroid energies

In the following centroid energies are discussed. They may show that the agreement of the centroid energy for a group of states with that for the corresponding group of configurations verifies the correct identification. We do not discuss the composition of the states but just assume the same order numbers, M [Eq. (10)] $= m$ [Eq. (36)]; see, however, Sec. III C 1.

1. Centroid energies of ensembles of states

For each spin and parity, several large gaps are observed among the states and the particle-hole configurations (Fig. 2), large in comparison to the mean matrix element of the residual interaction of about 100 keV [87]. The gap at $6.11 < E_x < 6.19\,$MeV is the highest common one considered in this paper (Secs. II E 1 and III D, Fig. 2).

Figures 3–16 show level schemes for states with spins from 0^+ to 12^+ and from 0^- to 8^- and 14^-. Larger gaps define compartments marked by dotted lines at right. They contain ensembles of states considered to consist of the corresponding number of configurations; they mostly contain little admixtures of other configurations.

Table IX shows the centroid energies of these ensembles of states with spins from 1^+ to 12^+ and from 0^- to 8^-. The completeness of the subsystems is proven by the near coincidence of the centroid energies $\overline{E_x^{\rm exp}}$ of the states within a chosen compartment ($i_1 < i < i_M$) with the centroid energies of the corresponding configurations $\overline{E_x^{\rm eSM}}$,

$$\overline{E_x^{\rm exp}}(i_1,i_M) = \frac{1}{i_M - i_1 - 1}\sum_{i=i_1}^{i_M} E_x^{\rm exp}(i), \tag{53}$$

$$\overline{E_x^{\rm eSM}}(i_1,i_m) = \frac{1}{i_m - i_1 - 1}\sum_{i=i_1}^{i_m} E_x^{\rm eSM}(i),$$

$$\text{where } i_M = i_m. \tag{54}$$

In Figs. 3–16 the difference

$$\Delta E_x(i_1,i_M) = \overline{E_x^{\rm eSM}}(i_1,i_M) - \overline{E_x^{\rm exp}}(i_1,i_M) \tag{55}$$

is shown by the line connecting the values $\overline{E_x^{\rm exp}}$ and $\overline{E_x^{\rm eSM}}$ at the right side; it is raising for more than 40 compartments.

For nearly 50 compartments in total, the average value ΔE_x is about +80 keV (Table IX, Figs. 3–16, [Eq. (57)]); only for spins 7^-, 10^+, and 12^+ is the difference $\Delta E_x(i_1,i_M)$ slightly negative. Very large differences $\Delta E_x(i_1,i_M)$ are found for the first compartments of the natural parity states with spins 1^-, 2^+, 3^-, 4^+, and 6^+. The pushing down of the yrast state is explained by the analytical model of Brown (Fig. 10, Eq. (7.4) in Ref. [92]). The exceptional discrepancy for the two lowest 0^- states may be explained by the peculiar shape of the wave function for the spin of 0^- involving the particle in the $4s_{1/2}$ orbit.

Almost all mean values $\overline{E_x^{\rm exp}}(1,i_{\max})$ are less than the mean values $\overline{E_x^{\rm eSM}}(1,i_{\max})$. The mean value of the difference for all compartments calculated as

$$\langle \Delta E_x\rangle = \frac{1}{N}\sum_{n=1}^{N}\Delta E_x\left(i_1^n,i_M^n\right) \tag{56}$$

$$\begin{aligned}\text{yields}\quad \langle \Delta E_x(\text{negative parity})\rangle &= +100\text{ keV},\\ \langle \Delta E_x(\text{positive parity})\rangle &= +55\text{ keV},\\ \langle \Delta E_x(\text{unnatural parity})\rangle &= +80\text{ keV},\\ \langle \Delta E_x(\text{natural parity})\rangle &= +80\text{ keV}.\end{aligned} \tag{57}$$

We note that the most extreme values are found for unnatural parity with the spin of 0^- and for natural parity with the spin of 3^-, both with $\Delta E_x = 0.3\,$MeV. By ignoring negative values, the logarithmic distribution for unnatural parity and natural parity look alike. The median value for each parity is determined as 15 keV. The global downshift is explained by the cumulative influence of many weak admixtures from the large number of high-lying configurations.

TABLE IX. Centroid energies for groups of states in compartments with a range of order numbers from i_1 to i_M determined from experiment ($\overline{E_x^{\rm exp}}$ [Eq. (53)]) and by the mSM including the eSM ($\overline{E_x^{\rm eSM}}$ [Eq. (54)]). In Figs. 3–16, the ranges of the order numbers are marked by short thick arrows and the centroid energies are shown, with the global centroid energy for the full range of states at the bottom.

I^π	Centroid energy in compartment (keV)															
	All groups			ΔE_x [Eq. (55)] (keV)	1. group (5. group)			2. group (6. group)			3. group (7. group)			4. group (8. group)		
	i_1–i_M	$\overline{E_x^{\rm eSM}}$	$\overline{E_x^{\rm exp}}$		i_1–i_M	$\overline{E_x^{\rm eSM}}$	ΔE_x (keV)	i_1–i_M	$\overline{E_x^{\rm eSM}}$	ΔE_x (keV)	i_1–i_M	$\overline{E_x^{\rm eSM}}$	ΔE_x (keV)	i_1–i_M	$\overline{E_x^{\rm eSM}}$	ΔE_x (keV)
0^-	1–2	5757	5439	+318												
1^-	1–12	6135	6024	+111	1–5	5645	227	6–10	6249	57	11–12	6614	11			
2^-					2–3	4946	148	4–5	5744	149	6–7	5929	134	8–9	6081	76
2^-	1–14	5896	5800	+96	10–12	6540	20	13–14	6682	25						
3^-	1–23	5682	5366	+316	1–3	4123	483	4–6	4799	−70	7–13	5649	282	14–23	6551	386
4^-					2–3	4007	36	4–5	4328	18	6–7	4902	91	8–9	5267	10
4^-	1–14	4966	4943	+23	10–11	5575	−8	12–14	5953	−2						
5^-	1–12	4606	4572	+34	1–6	3944	−29	7–9	4970	−29	10–12	5567	98			
6^-	1–8	4807	4751	+56	1–4	4281	44	5–6	4965	44	7–8	5702	114			
7^-	1–5	4967	5007	−40	1–3	4549	−51	4–5	5595	−23						
8^-	1–2	5462	5377	+85												
0^+	1–2	5100	5054	+46												
1^+	1–2	5942	5890	+52												
2^+	1–8[a]	5670	5479	+191	1–3[a]	5164	360	4–8[a]	5923	106						
3^+	1–4	5613	5536	+87	1–2	5253	118	3–4[a]	5973	36						
4^+	1–7[a]	5559	5430	+129	1–3[a]	5132	158	4–7	6012	72						
5^+	1–6	5658	5618	+40	1-2	5200	123	3–6	5887	−2						
6^+	1–8[a]	5490	5444	+46	1–3[a]	5130	275	4–5	5384	−76	6–9	5814	−64			
7^+	1–8	5521	5487	+34	1–3	5099	80	4–5	5500	77	6–9	5849	−22			
8^+	1–8	5440	5431	+9	1–3	5079	103	4–8	5801	−86						
9^+	1–5	5492	5409	+83	1–3	5251	85	4–5	5855	80						
10^+	1–4	5311	5357	−46	1–3	5149	−18	3–4	5800	−128						
11^+	1–2	5544	5549	−5												
12^+	1–1	5776	5750	+26												

[a]Including eSM configurations (Secs. II D 1–II D 7).

2. *Centroid energies of unobservable configurations*

Several configurations are unobservable by experiment, especially $i_{11/2}i_{13/2}$, $i_{13/2}s_{1/2}$, and $i_{13/2}d_{3/2}$ (Table I) and $2^+\ 0^+_1$, $0^+\ 2^+$ [Eq. (20)], and $g_{9/2}p_{1/2}\ \otimes\ 3^-_1$ [Eq. (27)]; see Table III. In a one-to-one correspondence most members of the unobservable configurations are identified. The mean excitation energy is simply calculated as

$$E_x^{\rm avg} = \frac{1}{N}\sum_{M=1}^{N} E_x^{\rm exp}\big(I^\pi_M\big), \qquad (58)$$

where N is the number of states with the assumed configuration.

The mean centroid energies $E_x^{\rm avg}$ are close to the predicted eSM energies,

$$E_x^{\rm avg}(i_{11/2}i_{13/2}) - E_x^{\rm eSM}(i_{11/2}i_{13/2}) = +0.01\ {\rm MeV}$$
$$\text{for } I^\pi_M = 2^+_6,3^+_3,4^+_4,5^+_4,6^+_8,7^+_7,8^+_7,9^+_5,10^+_4 \qquad (59)$$

(the 1^+ member is predicted at $E_x^{\rm mSM} = 6543$ keV [16], but still unknown);

$$E_x^{\rm avg}(i_{13/2}s_{1/2}) - E_x^{\rm eSM}(i_{13/2}s_{1/2}) = +0.02\ {\rm MeV} \quad \text{for} \quad I^\pi_M = 6^+_5,7^+_5; \qquad (60)$$

$$E_x^{\rm avg}(i_{13/2}d_{3/2}) - E_x^{\rm eSM}(i_{13/2}d_{3/2}) = +0.14\ {\rm MeV} \quad \text{for} \quad I^\pi_M = 5^+_5,6^+_8,7^+_8,8^+_7; \qquad (61)$$

$$E_x^{\rm avg}(2^+_1\ 0^+_1,0^+_1\ 2^+_1) - E_x^{\rm eSM}(2^+_1\ 0^+_1,0^+_1\ 2^+_1) = -0.10\ {\rm MeV} \quad \text{for} \quad I^\pi_M = 2^+_4,2^+_7; \qquad (62)$$

$$E_x^{\rm avg}(g_{9/2}\,p_{1/2}\ 3^-_1) - E_x^{\rm eSM}(g_{9/2}\,p_{1/2}\ 3^-_1) = -0.05\ {\rm MeV} \quad \text{for} \quad I^\pi_M = 1^+_2,2^+_7,3^+_4,4^+_5,5^+_6,6^+_9,7^+_8,8^+_8. \qquad (63)$$

Structure information for the eSM configuration $g_{9/2}p_{1/2}\ \otimes\ 3^-_1$ may be derived, especially by the resonant ^{208}Pb(p,p')

reaction via the IARs at 17.6 MeV (Sec. V G 3), but the data are insufficient.

Evidently, the agreement between the centroid energies calculated by the eSM and the observed values for all five configurations is good. For the proton configurations $i_{13/2}s_{1/2}$ and $i_{13/2}d_{3/2}$ the estimate of the Coulomb energy [Eq. (5)] cannot be improved.

C. Structure information from the ^{208}Pb(d,d') reaction

Cross sections in the ^{208}Pb(d,d') reaction are weakly correlated with the spin and structure of the state (Table VI). Many yrast states but not all are strongly excited. There is a slight tendency to larger cross sections for states with natural parity and lower spins.

The cross sections for the ^{208}Pb(d,d') and the nonresonant ^{208}Pb(p,p') reactions are similar; both reactions were performed with the same bombarding energy of $E_d = 22$ MeV (this work) and $E_p = 22$ MeV [33,34]. For natural parity there is also a strong similarity to the ^{208}Pb(α,α') reaction; here the cross sections are about four times larger with $E_\alpha = 40$ MeV [33,34].

Several pairs of states are known to share almost the complete strengths of just two configurations. The product of the amplitudes $c^{I^\pi}_{M,i}$ [Eq. (10)] is derived from the analysis of the angular distributions and cross sections [5,6,11,12,18,19,88],

$$c_1 \equiv c^{I^\pi}_{1,1} \approx +c^{I^\pi}_{2,2},$$
$$c_2 \equiv c^{I^\pi}_{1,2} \approx -c^{I^\pi}_{2,1}, \quad 0 < |c_1 c_2| < \sqrt{2}/2. \qquad (64)$$

The ratio of the cross sections for the states in such pairs often deviate largely from unity (Table X); the shown cross section is the mean value $\sigma_{43} = \frac{d\sigma}{d\Omega}[^{208}\text{Pb}(d,d'),\Theta \approx 43°]$.

Evidently, the interference is constructive in one state and destructive in the other state, as shown by the sign of the product c_1c_2. In some cases the larger cross section exceeds those for natural parity states with a spin differing by one unit.

Clearly, there is no correlation of the cross section in the ^{208}Pb(d,d') reaction with the spin or nature of parity as opposed to the ^{208}Pb(α,α'), ^{206}Pb(t,p), and ^{210}Pb(p,t) reactions. The ^{208}Pb(d,d') reaction does not yield any good indication for spin or parity or structure of the state. However, the observation of a state verifies its existence (Figs. 17–20).

D. Structure information from ^{206}Pb(t,p) and ^{210}Pb(p,t)

The ^{206}Pb(t,p) and ^{210}Pb(p,t) reactions excite natural parity states essentially only, similar to the ^{208}Pb(α,α') reaction. Bjerregaard *et al.* [35] studied the ^{206}Pb(t,p) reaction at $E_t = 12$ MeV. Igo *et al.* [37] report 122 levels for the ^{206}Pb(t,p) reaction at $E_t = 20$ MeV up to $E_x = 8.5$ MeV; the ^{210}Pb(p,t) reaction was also studied at $E_t = 20$ MeV up to $E_x = 6.75$ MeV. NDS2007 shows more than 300 levels in the same region (Sec. V D 2).

1. Recalibration of excitation energies

The knowledge of ^{208}Pb states in 1971 was sparse [106]. Therefore, the calibration of the ^{206}Pb(t,p) and ^{210}Pb(p,t) data has to be reconsidered. The systematic uncertainties of the excitation energies are evidently included in Table I

TABLE X. Correlations of cross section for ^{208}Pb(d,d') between states sharing the complete strengths of two configurations $LJ\,lj$. The product of the amplitudes is $|c_1c_2|$ [Eq. (64)]. The sign indicates constructive (+) and destructive (−) interference; see Sec. V C.

1 state					$\|c_1c_2\|$	Ref.	2 state					Fig.
$\tilde{E}_x$	I^π_x	σ_{43} $\frac{\mu b}{sr}$	L_1J_1 l_1j_1	Sign			Sign	L_2J_2 l_2j_2	$\tilde{E}_x$	I^π_x	σ_{43} $\frac{\mu b}{sr}$	1 2
4262	4^-_4	6	$g_{9/2}$ $p_{3/2}$	−	0.46	[88]	+	$h_{9/2}$ $d_{3/2}$	4359	4^-_5	20	21(a) 21(b)
4383	6^-_3	4	$g_{9/2}$ $p_{3/2}$	−	0.32	[88]	+	$h_{9/2}$ $d_{3/2}$	4481	6^-_4	30	21(b) 21(b)
4611	8^+_1	12	$j_{15/2}$ $p_{1/2}$	+	0.44	[34]	−	$g_{9/2}$ $i_{13/2}$	4860	8^+_2	2	21(b) 21(c)
4680	7^-_2	2	$i_{11/2}$ $f_{5/2}$	−	0.10[a]	[5]	+	$i_{11/2}$ $p_{3/2}$	5085	7^-_3	20	21(c) 22(a)
4919	8^-_1	2	$i_{11/2}$ $f_{5/2}$	−	0.10[a]	[5,11]	+	$g_{9/2}$ $f_{7/2}$	5836	8^-_2	10	21(c) 23(b)
5280	0^-_1	5	$s_{1/2}$ $p_{1/2}$	−	0.34	[6]	+	$d_{5/2}$ $f_{5/2}$	5599	0^-_2	15	22(b) 22(c)
5292	1^-_2	8	$s_{1/2}$ $p_{1/2}$	−	0.33	[34]	+	$d_{5/2}$ $f_{5/2}$	5512	1^-_3	80	22(b) 22(c)
5482	5^-_{11}	70	$d_{5/2}$ $f_{5/2}$	+	0.60[a]	[18]	−	$g_{9/2}$ $f_{7/2}$	5659	5^-_{13}	10	22(c) 23(a)
5844	1^+_1	10	$h_{9/2}$ $h_{11/2}$	+	0.45[a]	[40]	−	[b]	5937	1^+_2	1	23(b) 23(c)

[a]This work.
[b]$g_{9/2}p_{1/2} \otimes 3^-_1$.

of Ref. [37]; they increase above $E_x = 4.0$ MeV by about 20 keV near $E_x = 6.0$ MeV. Apparently the experimental uncertainties are about 5 keV.

By identifying the levels shown by Igo *et al.* [37] with the states from Table VI the systematic uncertainty can be relieved by help of the linear function

$$E_x^{\text{calib}} = E_x^{tppt} - 0.007\big(E_x^{tppt} - 4000\big)\ \text{keV} \quad \text{for} \quad E_x^{tppt} > 4000\ \text{keV}, \tag{65}$$

where E_x^{tppt} is the reported excitation energy. Within the experimental uncertainty of about 5 keV mostly only one natural parity state is present.

Table XI shows the levels excited by the ^{206}Pb(t,p) and ^{210}Pb(p,t) reactions. Mean cross sections are determined from Figs. 3–9 in Ref. [37],

$$\sigma_{25}^{T} = \frac{d\sigma}{d\Omega}[^{206}\text{Pb}(t,p), \Theta \approx 25^\circ] \quad \text{and}$$
$$\sigma_{25}^{t} = \frac{d\sigma}{d\Omega}[^{210}\text{Pb}(p,t), \Theta \approx 25^\circ], \quad \text{respectively.} \tag{66}$$

The uncertainty is about 30%.

2. Excitement of natural parity states

In Table VI the states shown in Table XI are marked by footnotes T and t. The ^{206}Pb(t,p) and ^{210}Pb(p,t) reactions excite only natural parity states. The level number 46 presents the single exception, the 5615 state has unnatural parity. It may be explained by the fact that the $j_{15/2}$ particle coupled to the $p_{3/2}$ hole in the 5615 7^+ state is not a single-particle configuration, but contains about 25% of the configuration $3^-_1 \otimes g_{9/2}$ [Eq. (32)].

Remarkably, the 5615 7^+ state is also the single exception from the rule that the ^{208}Pb(α,α') reaction excites only natural parity states. It is observed in Fig. 1 in Ref. [44], but not identified; the cross section is weak.

Similar to the unexpected excitation of several states by the ^{207}Pb(d,p) reaction (Sec. V E), admixtures of multi-particle-hole eSM configurations are suggested as explanation; the weak excitation of the 5615 7^+_6 state may be explained by the eSM configuration $g_{9/2}p_{1/2} \otimes 3^-_1$ [Eq. (29)].

3. Structure information

Igo *et al.* [37] identified seven 2^+ states in their Table XIII. They suggested these states (and the levels 64, 65, 67 [apparently misprinted with the information from level 65], and 68) to have a two-particle–two-hole character based on their large cross sections.

Pairing configurations. The large ^{206}Pb(t,p) cross sections for the 5561 2^+_4 and 5819 2^+_6 states were explained by Igo *et al.* [36,37] with the two pairing vibration configurations 0^+2^+ and 2^+0^+ [Eq. (19)]. The recalibrated excitation energies yield $E_x^{\text{calib}} = 5560.9$ and 5813.6 keV (Table XI), in agreement with the values given in Table VI. The centroid energy of the two configurations agrees with the centroid energy of the two states within 25 keV.

Similarly, the strong cross sections for the 5918 4^+_6, 6099 4^+_7, 5989 6^+_8, and 6037 6^+_9 states may be explained by the eSM configurations 0^+I^+ [Eq. (19)] with predicted excitation energies $E_x = 6081$ and 6178 keV for spins $I^+ = 4^+$ and 6^+, respectively (Table III); however, they are certainly mixed with the configuration $g_{9/2}p_{1/2} \otimes 3^-_1$ [Eq. (27)] predicted at $E_x = 6045$ keV; see Figs. 3–6.

Remarkably, the sum of the cross sections for the even spins from 0^+ to 6^+ are similar within the large uncertainty (entries "sum" in Table XI). The sum of the cross sections for spins 0^+, 2^+, 4^+, and 6^+ yields about 200, 400, 500, and 300 μb/sr, respectively. [Some more levels at $E_x > 6.20$ MeV have considerable cross sections (Fig. 9 in Ref. [37]); they may contain not-yet-identified 6^+ and 8^+ states.] The spin assignments for the 5918 4^+ and 6099 4^+ states and the 5989 6^+, 6037 6^+ states are thus confirmed (Sec. IV C 1).

Interference effects. Similar to the ^{208}Pb(d,d') reaction (Sec. V C and Table X), interference effects may explain the striking differences in the cross sections of states with similar configuration mixing.

The 5292 1^-_2 and 5512 1^-_3 states share the essential strengths of the configurations $s_{1/2}p_{1/2}$ and $d_{5/2}f_{5/2}$ and contain little admixtures of other configurations. The ^{206}Pb(t,p) cross section for the 5512 1^-_3 state is very large, while the 5292 1^-_2 state is only weakly excited; the ratio is about 15:1 or even larger because the 5286 2^+ state is unresolved. The constructive interference in the two-neutron transfer with dominant neutron pairs $s_{1/2}p_{1/2}$ and $d_{5/2}f_{5/2}$ leading to the 5512 1^-_3 state and the destructive interference leading to the 5292 1^-_2 state explain the largely different cross sections.

The 4974 3^-_6 and 5245 3^-_8 states share the essential strengths of the configurations $d_{5/2}p_{1/2}$ and $d_{5/2}f_{5/2}$ [18]; they contain significant admixtures of proton particle-hole configurations which are irrelevant here. The interference between the two relevant components, $d_{5/2}p_{1/2}$ and $d_{5/2}f_{5/2}$, explains the large ratio of the ^{206}Pb(t,p) cross sections for the two 3^- states.

The structure of the lowest six 5^- states is known in detail [87,88]. While the 5^-_1 state contains 70% of the lowest particle-hole configuration, the 5^-_2 state contains six configurations with similar strengths. The large ratio of the ^{206}Pb(t,p) and ^{210}Pb(p,t) cross sections may be thus explained.

The 4180 5^-_4 and 4296 5^-_6 states consist essentially of three configurations: the proton configuration $h_{9/2}d_{3/2}$, which is irrelevant here, and the neutron configurations $g_{9/2}p_{3/2}$ and $i_{11/2}p_{1/2}$. Their opposite signs explain the large ratio of the ^{206}Pb(t,p) cross sections; the g.s. of ^{206}Pb contains besides the dominant pair ${p_{1/2}}^2$ admixtures of ${f_{5/2}}^2$ and ${p_{3/2}}^2$. In contrast, ^{210}Pb contains, besides the dominant pair ${g_{9/2}}^2$, a weak admixture of ${i_{11/2}}^2$. The similar ^{210}Pb(p,t) cross sections are explained by the similar $g_{9/2}p_{3/2}$ amplitudes.

The 5213 5^-_9 and 5482 5^-_{10} states share the essential strengths of the configurations $g_{9/2}f_{5/2}$ and $d_{5/2}f_{5/2}$ and contain little admixtures of other neutron configurations.

The 4037 7^-_1 and 5694 7^-_5 states consist essentially of the configurations $g_{9/2}f_{5/2}$ and $g_{9/2}f_{7/2}$, respectively; the weak amplitudes of the same configurations have opposite signs because no other configurations admix strongly (the $h_{9/2}d_{5/2}$ strength in the 5694 7^-_5 state is only 10%). Again the ratio of the ^{206}Pb(t,p) and

TABLE XI. By using Eq. (65), excitation energies determined by the ^{206}Pb(t,p) and ^{210}Pb(p,t) reactions [37] are recalibrated. For details, see Sec. V D.

Level	1. state		2. state		σ^T_{25}	σ^t_{25}		E_x^{calib} [a]	E_x^{org}	1. state			
[37]	$\tilde{E}_x$	I^π_M	$\tilde{E}_x$	I^π_M	μb/sr	μb/sr		(keV)	(keV)	Config.(1)	Config.(2)	Eq.	Ref.
g.s.	0	0^+_1			350	300	0						[36]
28*	4868	0^+_2	4860	8^+_2	150	300		4865.0±1.5	4859	0^+_ν		(17)	[36]
36*[b]	5241	0^+_3			60 [b]	30 [b]		5244.7±1.5[b]	5236	3^-3^-		(15)	[36]
sum		0^+			**210**	**330**							
26*	4842	1^-_1			[c]	60		4848.9[d]	4843	[e]			[19]
38*	5292	1^-_2	5286	2^+_3	50	5		5289.0±1.5	5280	$s_{1/2}p_{1/2}$	$d_{5/2}f_{5/2}$		[6]
43*	5512	1^-_3	5517	3^-_{11}	800	6		5515.5±1.5	5505	$s_{1/2}p_{1/2}$	$d_{5/2}f_{5/2}$		[6]
60*[f]	5947	1^-_5			50	30		5950.6±2.0	5937	$d_{3/2}$			[19]
65*[f]	6076	1^-_7			80	[c]		6072.4±2.0	6058	$d_{3/2}$			[g]
10	4086	2^+_1			[h]	15		4086.6±1.0	4086	[e]			
32	5042	2^+_2			10	[c]		5044.3±1.5	5037	[e]			
45* [f]	5561	2^+_4	5564	3^-_{12}	200	200		5560.9±1.5	5550	$2^+0^+_1$	$0^+2^+_1$	(20)	[36]
48* [f]	5642	2^+_5	5640	1^-_4	50	10		5640.4±1.5	5629	[e]			
51*	5715	2^+_6			20	8		5709.9±2.0	5698	[e]			
54* [f]	5819	2^+_7	5813	3^-_{14}	150	100		5813.6±2.0	5801	0^+2^+	2^+0^+	(20)	[36]
sum		2^+			**430**	**320**							
1*	2615	3^-_1			90	20		2614.0±0.5	2614	[e]			
17	4255	3^-_3			[h]	10		4251.8±1.2	4250	$g_{9/2}p_{3/2}$	$d_{5/2}p_{1/2}$		[87]
25*	4698	3^-_4			100	3		4697.9±1.5	4693	$g_{9/2}p_{3/2}$	$d_{5/2}p_{1/2}$		[87]
29	4937	3^-_5			10	40		4941.5±1.5	4935	$i_{11/2}f_{5/2}$	$d_{5/2}p_{1/2}$		[18]
31* [f]	4974	3^-_6			200	[h]		4974.8±1.5	4968	$i_{11/2}f_{5/2}$	$d_{5/2}p_{1/2}$		[18]
37[b]	5245	3^-_8			60 [b]	30 [b]		5244.7±1.5[b]		$i_{11/2}f_{5/2}$	$d_{5/2}p_{1/2}$		[18]
39*	5347	3^-_9			8	[c]		5347.4±1.5	5338	$g_{9/2}f_{7/2}$	$d_{5/2}f_{5/2}$		[18]
55* [f]	5874	3^-_{15}			30	[c]		5875.0±2.0	5862	$g_{9/2}f_{7/2}$	$d_{5/2}f_{5/2}$		[15]
68*[f]	6191	3^-_{19}	6193	2^+_8	4	5		6186.2±2.0	6171	[e]			
19	4324	4^+_1			100	5		4321.2±1.2	4319	[e]			
50*	5690	4^+_4	5694	7^-_4	3	2		5696.8±1.5	5685	[e]			
58*	5918	4^+_6			300	[c]		5918.3±2.0	5905	$0^+4^+_1$		(20)	[i]
67*[f]	6099	4^+_7			100	[c]		6103.6±2.0	6089	[e]		(20)	
sum		4^+			**500**	[c]							
2*	3198	5^-_1			40	50		3200.0±0.5	3200	$g_{9/2}p_{1/2}$	$i_{11/2}p_{1/2}$		[88,89]
4*	3708	5^-_2			8	[c]		3709.0±1.0	3709	$g_{9/2}p_{1/2}$	$i_{11/2}p_{1/2}$		[88,89]
6	3961	5^-_3			8	50		3961.0±1.0	3961	$g_{9/2}f_{5/2}$	$i_{11/2}p_{1/2}$		[88,89]
13	4180	5^-_5			[h]	4		4180.3±1.2	4179	$g_{9/2}p_{3/2}$	$i_{11/2}p_{1/2}$		[88,89]
18	4297	5^-_6			20	6		4295.1±1.2	4293	$g_{9/2}p_{3/2}$	$i_{11/2}p_{1/2}$		[88,89]
33	5075	5^-_8			[c]	1		5079.5±1.5	5072	$i_{11/2}p_{3/2}$	$d_{5/2}f_{5/2}$		[18]
35	5213	5^-_9	5214	6^+_3	10	3		5210.4±1.5	5202	$i_{11/2}p_{3/2}$	$d_{5/2}f_{5/2}$		[18]
42*	5482	5^-_{10}			50	[c]		5487.3±1.5	5477	$g_{9/2}f_{7/2}$	$d_{5/2}f_{5/2}$		[18]
22	4424	6^+_1			15	1		4427.0±1.2	4424	[e]			
62*[f]	5989	6^+_8			150	200		5986.8±2.0	5973	$0^+6^+_1$		(20)	[i]
64*[f]	6037	6^+_9			100	[c]		6033.1±2.0	6019	$0^+6^+_1$		(20)	[i]
sum		6^+			**265**	**200**							
46*	5615[j]	7^+_6			4	[c]		5606.2±1.5	5595	$j_{15/2}p_{3/2}$			[12]
8*	4037	7^-_1			40	5		4037.0±1.0	4037	$g_{9/2}f_{5/2}$			[87]
24*	4611	8^+_1			30	[c]		4609.2±1.5	4605	$g_{9/2}i_{13/2}$	$j_{15/2}p_{1/2}$		[12]

*Levels observed in the ^{206}Pb(t,p) reaction at $E_t = 12$ MeV by Bjerregaard *et al.* [35].
[a]The experimental uncertainty is about 5 keV.
[b]Data for level 36 and 37 are identical.
[c]No data.
[d]No uncertainty given.
[e]Unknown amplitudes.
[f]Revised identification (Sec. V D 2).
[g]This work (Sec. IV C 1).
[h]No angular distribution shown.
[i]This work (Sec. V D 3).
[j]Sec. V D 2.

^{210}Pb(p,t) cross sections may be explained by the interference between the two configurations for both pairs of states.

E. Weak ^{207}Pb(d,p) cross sections

Some states are clearly excited by the ^{207}Pb(d,p) reaction but are not expected as sSM configurations. The cross sections are between 1 and 10 μb/sr, as observed in up to two dozen runs; hence, the excitation energies are often determined with high precision.

The eSM may explain the excitation by the ^{207}Pb(d,p) reaction of

(i) the 5844 1^+_1 state,
(ii) the 4086 2^+_1 and 5715 2^+_5 states,
(iii) the 4324 4^+_1 and 5690 4^+_4 states,
(iv) the 5799 5^+_4 state,
(v) the 4424 6^+_1, 5721 6^+_6, and 6037 6^+_9 states

by the configuration $g_{9/2}p_{1/2} \otimes 3^-_1$ [Eq. (29)];

(vi) of the 6101 12^+_2 state

by the configuration $i_{11/2}p_{1/2} \otimes h_{9/2}d_{3/2}$ (Table IV); of

(vii) the 4037 7^-_1 state,
(viii) the 5836 8^-_2 state

by the configuration $j_{15/2}p_{1/2} \otimes 3^-_1$ [Eq. (29)].

There are more eSM configurations which may explain the observed excitation by ^{207}Pb(d,p).

The 6037 6^+_9, 6068 5^+_5, 6102 5^+_6, and 6193 2^+_9 states are observed by ^{207}Pb(d,p) with polarized deuterons [33]. The angular distributions of the analyzing power are remarkably similar; they were fitted assuming a transfer of $L = 5$ and $J = L + \frac{1}{2}$. The explanation by the eSM assumes the simultaneous Coulomb transition $0^+_{\text{g.s.}} \to 3^-_1$ together with the transfer $L = 4$ and $J = L + \frac{1}{2}$. The fits are in congruence with such an interpretation (Sec. II D 5).

F. Structure information from the ^{208}Pb(n,$n'\gamma$) reaction

About half of the γ rays observed by the ^{208}Pb(n,$n'\gamma$) reaction [1] are not placed. The knowledge of all states $E_x < 6.20$ MeV may allow to place some more γ rays.

1. *The 5040 2^+_2 state*

The 5038 2^- state deexcites to the 3^-_1 state with an extremely large intensity. A suggested transition of the 5040 2^+ state to the 3^-_1 state cannot be resolved if the distance between the two states is low and the ratio of the intensities large.

From Table VI the distance between the 5038 2^- and 5040 2^+ states is determined as 1.8 ± 0.3 keV [Eq. (49)]. No original ^{208}Pb(n,$n'\gamma$) data for this region have been published yet.

2. *The 5667 0^+_4 state*

Despite the low spin, the 5667 0^+ state is not reported to be observed by the ^{208}Pb(n,$n'\gamma$) experiment [1]. The inspection of the reported γ rays suggests the low intensity to be the reason. Presumable transitions are to the 2615 3^- and 4841 1^- states.

(i) Near the expected transition to the 2615 3^- state with $E_\gamma = 3052$ keV a strong γ ray (3061 keV) and a 30-times-weaker ray (3044 keV) are placed.
(ii) Near the expected transition to the 4841 1^- state with $E_\gamma = 852$ keV an extremely strong γ ray (861 keV) and a 70-times-weaker ray (849 keV) are placed.

Apparently, in both cases the intensity of the expected transition is very weak and below the detectability.

G. Structure information from ^{208}Pb(p,p') via IAR and ^{207}Pb(d,p)

1. *Particle-hole configurations*

As sketched in Sec. III G, amplitudes of many neutron particle-hole configurations can be determined from the analysis of the ^{207}Pb(d,p) reaction and from ^{208}Pb(p,p') via IAR in ^{209}Bi; similarly, amplitudes of many proton particle-hole configurations can be determined from ^{209}Bi(d,^{3}He). The knowledge of spin and parity is elementary to derive matrix elements of the residual interaction. Based on the present work, about 100 matrix elements may be determined in the future in a straightforward but tedious manner [87].

2. *Two-particle–two-hole configurations*

As suggested in Sec. II D 5, IARs are expected at $E_p \approx 17.5$ MeV, which may populate two-particle–two-hole configurations in ^{208}Pb described by Eq. (29). Indeed, the excitation functions of the 5937 1^+_2, 5989 6^+_2, 6054 4^+_6, 6068 5^+_5, and 6102 5^+_6 states exhibit a strong enhancement for $E_p = 17.6$ MeV with cross sections of about 4, 6, 5, 2.5, and 8 μb/sr, respectively, and off-resonance cross sections of about 0.5–1.0 μb/sr for $14.8 < E_p < 18.2$ MeV (Fig. 25).

Similarly, the excitation function for the 6054 4^+_6 state shows an enhancement near $E_p = 17.6$ MeV; in addition, however, a similar enhancement is observed near the $d_{5/2}$ IAR. There are no data for the $j_{15/2}$ IAR, but the Lorentzian tail of a resonance at the $j_{15/2}$ IAR ($E^{\text{res}} = 16.38$ MeV [12]) is still half of the maximum. A weak $j_{15/2}f_{7/2}$ admixture may explain the enhanced cross section because of the high penetrability of the $f_{7/2}$ proton [28], similar to the the $j_{15/2}f_{7/2}$ admixture in the 5235 11^+_1 state (Sec. IV B 2).

The interpretation of the 6068 5^+ and 6102 5^+_6 states to have dominant two-particle–two-hole configurations described by Eq. (29) is consistent with the findings from the ^{207}Pb(d,p) experiment with polarized deuterons (Sec. V E).

3. *New group of IARs in ^{209}Bi*

The excitation functions for the ^{208}Pb(p,p') reaction reveal a new IAR in ^{209}Bi near $E_p = 17.6$ MeV (Fig. 25). The new IAR is interpreted to correspond to the isobaric analogs of the multiplet $3^-_1 \otimes g_{9/2}$ with spins $\frac{3}{2}^-, \ldots, \frac{15}{2}^-$ in ^{209}Pb [Eq. (33)]. The width of the resonance is about 300 keV.

Despite the low values, the cross sections of the states shown in Fig. 25 are five times stronger than off-resonance. The centroid resonance energy for the five states is determined, in

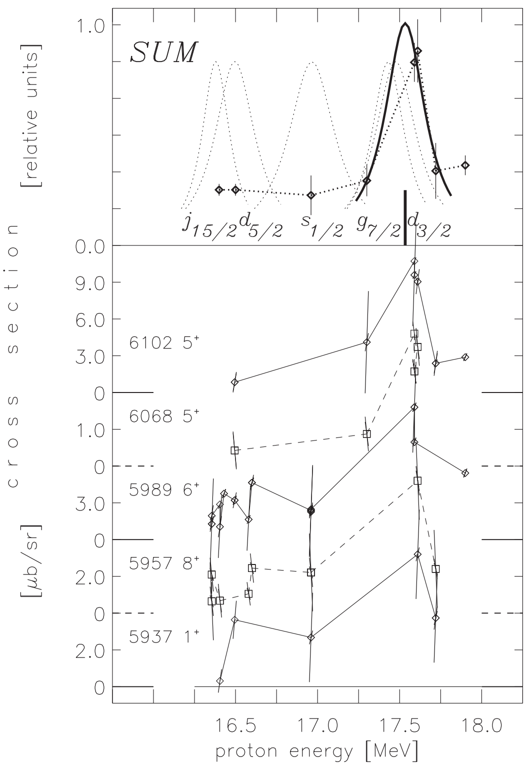

FIG. 25. Excitation functions for the ^{208}Pb(p,p') reaction showing a new IAR at $E^{\text{res}} = 17.60$ MeV with an assumed width of $\Gamma^{\text{tot}} = 300$ keV. Excitation functions for the individual states are shown at the bottom in a staggered manner (the base lines are marked at left and right) for the sum at top. The mean cross section is about 5 μb/sr near the new IAR and drops by a factor of five off-resonance. In the top frame, the Lorentzians for the known IARs at $E^{\text{res}} > 16.3$ MeV are shown with arbitrary height by dotted lines together with the values of LJ.

agreement with the predicted value ($E^{\text{res}} = 14.918$ MeV [25])

$$E^{\text{res}}(3^- \otimes g_{9/2}) = E^{\text{res}}_{g_{9/2}} + E_x(3^-_1),$$
$$E_p = 17.53 \text{ MeV}. \tag{67}$$

Some of the parent states assumed to have the structure $3^-_1 \otimes g_{9/2}$ and spins $\frac{3}{2}^-,\ldots,\frac{15}{2}^-$ are known [74]. Yet the excitation energies of the first six known members are spread over the range $2.3 < E_x < 3.3$ MeV. Assuming the same Coulomb displacement energy as for all other known IARs, the range would yield $17.2 < E_p < 18.3$ MeV; the analog of the $\frac{11}{2}^-$ member in ^{209}Pb is closest to the energy $E^{\text{res}}(3^- \otimes g_{9/2})$.

Apparently, the spread of the relevant IARs is less than 0.3 MeV, in contrast to the spread of the known parent states with spins $\frac{3}{2}^-,\ldots,\frac{15}{2}^-$. Yet for lack of sufficient data, no definite conclusion can be drawn.

H. Comparison to calculations

Many shell-model calculations were made in the past. We refer to three of them, the early calculations using the random phase approximation by Kuo and Brown [80–82], calculations using the OXBASH code and the M3Y force with one-particle–one-hole configurations by Maier [85,86], and calculations with the inclusion of two-particle–two-hole configurations by Brown [83,84].

TABLE XII. Excitation energies of the 11^+ and 12^+ yrast and yrare states in ^{208}Pb.

$\tilde{E}_x$	I^{π}_M	E_x (keV)	Note	
5235	11^+_1	5235.56 ± 0.10	Table VI	^{208}Pb(p,p')
		5235.31 ± 0.20	Table VI	^{208}Pb(d,d')
		5297	mSM	Eq. (6)
		5243	Refs. [83,84]	
		5230	Refs. [85,86]	
5864	11^+_2	5862.93 ± 0.35	Table VI	^{208}Pb(p,p')
		5862.80 ± 0.25	Table VI	^{208}Pb(d,d')
		5791	mSM	Eq. (6)
		5822	Refs. [83,84]	
		5853	Refs. [85,86]	
5750	12^+_1	5749.38 ± 0.30	Table VI	^{208}Pb(p,p')
		5750.45 ± 1.30	Table VI	^{208}Pb(d,d')
		5776	mSM	Eq. (6)
		5900	Refs. [83,84]	
		5787	Refs. [85,86]	
		5560	Ref. [109]	
6101	12^+_2	6101.90 ± 0.45	Table VI	^{208}Pb(p,p')
		6101.45 ± 0.50	Table VI	^{208}Pb(d,d')
		6101.70 ± 0.90	Table VI	^{207}Pb(d,p)
		8200	mSM	Eq. (6)
		7264	Refs. [83,84]	
		8386	Refs. [85,86]	

The calculations by Brown describe the excitation energies of positive-parity states with similar precision as the eSM (Sec. II D 7); the number of states at $E_x < 6.20$ MeV almost agrees for all spins and either parity. (Yet only the first ten states are communicated [84].)

We mention especially the two lowest 11^+ and 12^+ states (Table XII, Figs. 8 and 9, Sec. IV B 3). The excitation energies of the 11^+ yrast and yrare states agree with all calculations within 70 keV, the excitation energy of the natural parity 12^+ yrast state agrees within 150 keV. The excitation energy of the 12^+ yrare state is by more than 2 MeV lower than calculated in the space of one-particle–one-hole configurations and still 1 MeV lower than calculated by including two-particle–two-hole configurations.

The comparison to the calculations with one-particle–one-hole configurations only [85,86] elucidates the need for the inclusion of two-particle–two-hole configurations. For example, for the spin of 2^+ there are only four mSM configurations at $E_x < 6.20$ MeV, while in the eSM there are nine configurations (Fig. 3).

The excitation energies of negative-parity states are described by all calculations with similar precision as the mSM [16] because two-particle–two-hole configurations start for negative parity with the configuration $3^- \otimes 2^+$ (Table III). Only the excitation energies of the 1^- states deviate largely from the observations for all calculations [81–86]; the deviations generally increase with the excitation energy. However, the mSM reproduces the observed excitation energies quite well [19]; clearly at $E_x \gtrsim 6.5$ MeV not all 1^- states are identified.

The natural parity yrast states with spins 1^-, 2^+, 3^-, 4^+, and 6^+ are badly described by any calculation; the observed excitation energies are up to 1 MeV lower than calculated (Figs. 10, 3, 12, 4, and 5, respectively). We suggest that the description of the natural parity yrast states necessitates the inclusion of more configurations, say the extension of the configuration space [Eq. (1)], by including nucleons in other major shells and multi-particle-hole configurations with more nucleons (especially four-particle–four-hole configurations).

VI. SPURIOUS STATES

NDS2007 lists several levels which are questionable; we call such levels "spurious." In Table VI they are denoted by putting the energy labels in parentheses. Some levels are cited with a large uncertainty of the excitation energy; other levels belong to an unresolved doublet or an ensemble of states in ^{208}Pb. Still other levels represent a state listed by another level. Some levels with different spin and parity are identical and finally some levels do not represent a state in ^{208}Pb or are questionable. Secs. VI B 1–VI B 7 discuss the arguments.

Apparently [53], the highest neutron energy in the ^{208}Pb$(n,n'\gamma)$ reaction for the states shown in NDS2007 is 6.4 MeV, just above our chosen limit of investigation. Remarkably, almost all states observed by the ^{208}Pb$(n,n'\gamma)$ reaction are recognized to exist; some spin and parity assignments are revised. States additionally identified by other methods mostly have higher spins, from 5^+ up to 12^+ and from 5^- to 14^-. Some γ rays are placed twice or even three times.

A. Conditions

We consider levels listed by NDS2007 to be "spurious" under certain conditions discussed in the following. Certainly, the condition that some states are not observed with a significant cross section in a lot of spectra taken for the ^{207}Pb(d,p), the ^{208}Pb(d,d'), the off-resonance ^{208}Pb(p,p') reactions, and the ^{208}Pb(p,p') reaction via IARs in ^{209}Bi is vague and insufficient.

Contaminations from light nuclei are easily recognized by the kinematic broadening in the Q3D spectrograph. For nuclei with atomic weight $A \gtrsim 80$ the width of a peak is no criterion anymore, but still the kinematic shift with scattering angle and bombarding energy is. Yet lead isotopes cannot be distinguished in the (p,p') and (d,d') reactions and hardly in the (d,p) reaction; here the different Q values produce a weak shift in the excitation energy, as measured in the laboratory system. Targets with different isotopic composition make it possible to recognize states in ^{208}Pb.

Targets used in the ^{208}Pb(p,p') and ^{208}Pb(d,d') reactions had a purity of 99.98%. In the study of the ^{207}Pb(d,p) reaction, we used nine different targets in 2003–2013; for ^{208}Pb(d,d') two different targets were used (Table V).

In the study of the (d,p) reaction, four different compositions of the lead isotopes were used; the enrichments in ^{207}Pb were 0.2% (with an enrichment of 99.1% in ^{206}Pb and ^{208}Pb), 78.8%, 99.1%, and 99.92%. Remarkably, contaminations from lighter nuclei (^{1}H, ^{2}H, ^{12}C, ^{14}N, ^{16}O, ^{40}Ar) differed even with targets made from the same material.

Levels are considered to be spurious unless any of the following conditions are fulfilled.

(1) The peak should be observed in at least two different reactions: either
  (a) in the resonant ^{208}Pb(p,p') reaction via at least one of the seven known IARs in ^{209}Bi and off-resonance, or
  (b) in the resonant or nonresonant ^{208}Pb(p,p') and the ^{207}Pb(d,p) reactions, or
  (c) in the resonant or nonresonant ^{208}Pb(p,p') and the ^{208}Pb(d,d') reactions, or
  (d) in the resonant or nonresonant ^{208}Pb(p,p') and the ^{209}Bi$(d,{}^{3}$He$)$ reactions [40,41,47].

(2) The peak should show up in at least a few of the typically a dozen spectra with low background; the appearance in less than four spectra is doubted.

(3) The excitation energy obtained from the fit by GASPAN and the subsequent evaluation (Sec. III F) should yield at least three values that are consistent within an uncertainty of less than about 0.5 keV.

(4) The level should be reliably distinguished from K or L satellites. L satellites produce broader peaks in multiples of about 15 keV distance from the main peak. K satellites produce peaks in 88 and 176 keV distance which cannot be distinguished from peaks without the knockout of K-electrons (Table VII); K satellites are accompanied by L satellites (Fig. 17). The energies of the first L satellite fluctuate in a stochastic manner other than that of the energies of peaks from states in ^{208}Pb with a Gaussian distribution. Namely, the single L electron is accompanied by the simultaneous emission of M,N,O,P electrons; the distribution of these energies is quantized. Fitting the peak by GASPAN with a broader width yields a distribution of the energies different from a normal Gaussian distribution.

(5) The shape of the peak, especially the width of the peak, should be similar to neighboring peaks. Note that the width increases with the position in the detector of the Q3D spectrograph from the beginning to the end by a factor of two due to the changing dispersion along the focal plane.

(6) In case of the ^{208}Pb(p,p') reaction, either
  (a) the excitation function across the IARs in ^{209}Bi should be smooth, indicating a nonresonant reaction, or
  (b) a resonance effect should be seen near at least one of the seven known IARs in ^{209}Bi [25] or near the newly discovered IAR (Sec. V G 3).

(7) In case of the ^{207}Pb(d,p) reaction, the angular distribution should have a shape well described by one L value or the incoherent sum for two L values consistent with the assigned spin. The angular distribution for the analyzing power in the ^{207}Pb(d,p) reaction with polarized deuterons [33,34] should be consistent with the assigned spin.

(8) In the ^{207}Pb(d,p) reaction, no contamination from ^{206}Pb or ^{208}Pb should be present near the observed peak. The shift by the correction from the different relativistic kinematics by up to 20 keV has to be taken into account.

(9) The (d,d') reaction should excite the state with a significant cross section. Because of too few data, this condition cannot be always met.

(10) If NDS2007 has strong arguments from other experiments, especially for spins 2^+, 10^+, 11^+, 12^+, and 14^-, they are accepted (see Sec. IV B 2).

B. Specific eliminations

1. Data from ^{209}Bi(d,^{3}He)

Some levels from the study of the ^{209}Bi(d,^{3}He) experiment [40] listed in NDS2007 suffer from the low resolution (12–15 keV) and low statistics. The levels reported by Grabmayr *et al.* [40] at $E_x = 4144(5)$ {questionable [1]}, 4447(5) {questionable [1]}, 5867(4), 6071(5) keV have low statistics and are not reliably fitted in the four spectra [41]. In the spectra taken with the Q3D spectrograph at the ten aforementioned reactions no evidence for either state is present; see also Figs. 21–23.

(i) The level at $E_x = 5084(2)$ keV {$E_x =$ 5087.9 keV [1]} is interpreted by the unresolved 5085 7^- and 5093 8^+ states as reported by Schramm *et al.* [47] (see also Sec. VI B 7),
(ii) the level at $E_x = 5234(5)$ keV by the 5239 4^- state,
(iii) the level at $E_x = 5352(6)$ keV by the unresolved 5347 3^- and 5374 7^+ states,
(iv) the level at $E_x = 5378(3)$ keV {$E_x =$ 5380.6 keV [1]} by the unresolved 5374 7^+, 5383 4^+, and 5385 3^- states (see also Secs. VI B 4 and VI B 2),
(v) the level at $E_x = 5524(9)$ keV by the unresolved 5516 3^- and 5546 10^+ states (see also Sec. VI B 7),
(vi) the level at $E_x = 5581(6)$ keV {denoted as 5576.6 and 5579.0 [1]} by the 5587 5^+ state (see also Secs. VI B 7 and VI B 6),
(vii) the level at $E_x = 5627(5)$ keV by the unresolved 5615 7^+ and 5642 2^+ states,
(viii) the level at $E_x = 5727(6)$ keV by the unresolved 5721 6^+ and 5741 8^+ states,
(ix) the level at $E_x = 5821(3)$ keV by the unresolved 5819 2^+ and 5825 8^+ state,
(x) the level at $E_x = 5996(5)$ keV by the 5993 5^- state,
(xi) the level at $E_x = 6183(5)$ keV {denoted as 6179 [1]} by the 6191 3^- and 6193 2^+ states.

2. Data from ^{208}Pb(e,e')

The group of Heisenberg [48–52] reported levels from the study of the ^{208}Pb(e,e') experiment at $E_x = 4830$, 5260, 5270, 5291, and 5565 keV [1]. The resolution was improved over the time from 60 to 15 keV. The excitation energies of high spin levels are now determined with higher precision (Table VI).

(i) The level reported at $E_x = 4830$ keV is identified with the 4861 8^+ state,
(ii) the levels at $E_x = 5260$, 5270, and 5291 keV with the high-spin doublet consisting of the 5235 11^+ and 5326 9^+ states,
(iii) the level at $E_x = 5565$ keV with the 5564 3^- and 5587 5^+ states,
(iv) the level at $E_x = 5954$ keV with the 5957 8^+ state.

3. Data from ^{208}Pb(α,α')

All levels from the study of the ^{208}Pb(α,α') experiment [33,34,42,44] listed (see Sec. IV B 2) in NDS2007 are matched with natural parity states (Table VI).

The 5.04-MeV level consists of the 5038 2_2^- and 5040 2_2^+ states (Secs. III F 5 and III G). The cross section in the ^{208}Pb(α,α') reaction is determined to be rather high in a convincing manner. The spectra taken in 1991 (Sec. III B) reveal the existence of the 5040 2_2^+ state [Eq. (48)]. Despite the low resolution of about 11 keV (about 15 keV in the spectra from 1991 [43]), it is well resolved from the next neighbors (4974 3_6^-, 5069 10_2^+).

The level reported at $E_x = 5640.8(0.8)$ keV [33,34] is identified with the 5640 1_4^- and 5642 2_5^+ states.

The 5667 state is recognized as the proton pairing vibration state [20].

The 5835 level is identified with the 5819 2^+ and 5825 8^+ states (Sec. IV B 2).

The level reported at $E_x = 5490(2)$ keV [33,34] is identified with the 5502 6_5^+ state not well resolved from the strong 5482 5_{10}^- state; Atzrott reports a level at $E_x = 5487.4 \pm 1.7$ keV [42]. The level reported at $E_x = 5544(2)$ keV [33,34] is identified with the 5546 5_{12}^- state; admixtures from the 5537 10_3^+ and 5543 7_4^- states are not resolved.

Both levels, however, are deteriorated by the presence of L satellites from the 5482 5_{12}^- state and 5512 1_3^- state, respectively; these states are excited with extremely large cross sections. The 3^- and 5^- yrast states at $E_x < 3.5$ MeV clearly show the presence of L satellites, as observed in the ^{208}Pb(α,α') spectra taken by Atzrott *et al.* in 1991 (Sec. III B).

4. Data from ^{207}Pb(d,$p\,\gamma$) and ^{208}Pb(p,$p'\,\gamma$)

The 5075 and 5076 levels. NDS2007 assumes two states at $E_x = 5.075$ keV: the 5075 and 5076 levels. We consider the two levels to be identical. The arguments of NDS2007 are based on the comparison of γ transitions from the 5075 level, the 5195, 5196 doublet levels, and the 5490, 5492 doublet levels with spins 3^-, 7^+ and 4^-, 6^-, respectively. Transitions in ^{208}Pb(n,$n'\,\gamma$) with $E_\gamma = 868$ keV are placed twice, but transitions in ^{207}Pb(d,$p\,\gamma$) and ^{209}Bi(t,$\alpha\,\gamma$) with $E_\gamma = 869$ keV may be placed twice similarly; the 5.49-MeV doublet was not recognized before 2007 [1,12].

The 5254 level. The 5254 level is doubted by NDS2007. In both ^{207}Pb(d,$p\,\gamma$) and ^{209}Bi(t,$\alpha\,\gamma$), the transitions with $E_\gamma =$ 1781.5 and 1779.06 keV may be the assumed to start from the 5490 4^-, 5492 6^- doublet; the transition with $E_\gamma = 178$ keV is placed once starting from the 4359 4^- state; again, in the analysis of ^{207}Pb(d,$p\,\gamma$) the 5.49-MeV doublet was not yet recognized.

The 5565 level. In ^{207}Pb($d,p\gamma$) and ^{209}Bi($t,\alpha\gamma$), the transition with $E_\gamma = 2090.3 \pm 1.0$ keV may be placed as 5799 $5^+_4 \rightarrow$ 3708 5^-_2.

The 5783 level. The transition with $E_\gamma = 1398.8 \pm 0.6$ keV observed in ^{207}Pb($d,p\gamma$) and ^{209}Bi($t,\alpha\gamma$) and with $E_\gamma = 1399.93 \pm 0.06$ keV observed in ^{208}Pb($n,n'\gamma$) may be placed as 5721 $6^+_6 \rightarrow$ 4324 4^+_1, 5694 $7^-_5 \rightarrow$ 4296 5^-_6, or 5347 $3^-_{10} \rightarrow$ 3946 4^-_2.

The 5966 level. In ^{207}Pb($d,p\gamma$), the transition with $E_\gamma = 749.63 \pm 0.40$ keV may be placed as 5836 $8^-_2 \rightarrow$ 5085 7^-_3. The 5836 8^-_2 state is populated by ^{207}Pb(d,p), as explained by the eSM (Sec. V E).

The 6103 level. At $E_x = 6104$ keV no level from ^{207}Pb(d,p) is observed; hence, the reported γ transitions must be placed otherwise. The transition with $E_\gamma = 538.0 \pm 0.5$ keV may be placed as 6099 $4^+_7 \rightarrow$ 5561 2^+_4. The transition with $E_\gamma = 1807.6 \pm 0.6$ keV may be placed as 5517 $3^-_{12} \rightarrow$ 3708 5^-_2.

5. Data from ^{208}Pb($n,n'\gamma$)

For the 5075, 5076, 5254, and 5783 levels, see Sec. VI B 4. The 6147 level considered to be uncertain [1] is not confirmed.

6. Data from ^{207}Pb(d,p)

The 4992 level is certainly a L satellite in about 15 keV distance to the 4974 3^- state, the 5261 and 5266 levels are certainly L satellites in about 15 keV distance to the 5245 3^- state, the 5307 level is certainly a L satellite in about 15 keV distance to the 5292 1^- state, and the 5572 and 5579 levels are certainly L satellites in about 15 keV distance to the 5564 3^- state.

The 5557 level is created as a L^3 satellite to the 5512 1^- and 5517 3^- states. It could not be confirmed within the ensemble of five states from the 5537 10^+ to the 5564 3^- state.

In the ^{208}Pb(p,p') spectra the 5557 level shows up near the $d_{5/2}$ IAR; yet it is interpreted as the superposition of a L^3 satellite to the 5512 1^- and 5517 3^- states and a K^2 satellite from the strongly excited 5385 3^- state. (Valnion *et al.* [33,34] report the level as 5554(2) keV.)

The 5056 level is certainly a L satellite (Sec. III F 5) to the peculiar 5.04-MeV doublet (Sec. III G). For the 5075 and 5076 levels, see Sec. VI B 4.

7. Data from ^{208}Pb(p,p') at $E_p = 22$ and 35 MeV

Wagner *et al.* [58] observe most levels listed in Table VI with the ^{208}Pb(p,p') reaction at $E_p = 35$ MeV and a resolution of 5–8 keV. They recognized the doublets at $E_x = 4.256$ (now 4255 3^- and 4262 4^-), 4.480 (now 4481 6^-), 4.863 (now 4861 8^+ and 4867 7^+), 5.514 (now 5512 1^- and 5517 3^-), 5.642 (now 5640 1^-, 5642 2^+, and 5643 2^-), 5.720 (now 5715 2^+ and 5721 6^+), 5.777 (now 5765 $^-$ and 5778 2^-), 5.842 (now 5836 8^- and 5844 1^+), and also the 5.872 MeV state (now 5874 3^-).

The 4909 level [33,34] is identified with the 4911 4^- state; the 5835 level is identified with the 5836 8^- state. The 4878, 5401, 5531, 5737 levels are not confirmed. The level reported at $E_x = 5966 \pm 4$ keV [58] is identified with the 5957 8^+ and 5969 4^- states.

The following states at $E_x < 6.20$ MeV are considered to be spurious: $E_x = 4.106$, 4.141, 4.159, 4.403, 4.444, 4.577, 5.444, and 6.170 MeV.

Valnion *et al.* [33,34] observe the following levels in the ^{208}Pb(p,p') reaction with cross sections less than 3 μb/sr and an uncertainty of $0.6 < \delta E_x < 3$ keV: 4878, 5103, 5364, 5401, 5524, 5531, 5554, 5576, 5737, and 6033. They are not confirmed by our data taken since 2003.

The 5087.9(15) and 5094.3(15) levels correspond to the single 5092 8^+_3 state as the last member of a dense ensemble of five states within 33 keV. The levels at $E_x = 6020.4(20), 6025.1(20)$ keV are identified with the 6023 7^+ and 6026 8^+ states.

VII. SUMMARY

We investigated states in the doubly magic nucleus ^{208}Pb with excitation energies restricted to $E_x < 6.2$ MeV as a clear border. The region $6.1 < E_x < 6.3$ MeV in ^{208}Pb is remarkably void. Within 0.15 MeV only the 6.19-keV doublet with spins 2^+ and 3^- is known, while the mean distance between the states at $4.8 < E_x < 6.0$ MeV is 11 keV. Above 6.20 MeV the knowledge of spins drops. The chosen limit in excitation energy is owed to the outstanding observation of the $3^-/2^+$ doublet at $E_x = 6.19$ MeV in most spectra together with the fact that among the next three dozen states only few spins are firmly known although for many of them admixtures of the configurations $g_{7/2}f_{5/2}$ or $d_{3/2}f_{5/2}$ are known.

From 2003 to 2013 experiments on ^{208}Pb were performed using the Q3D magnetic spectrograph of the MLL at Garching (Germany). Peak-to-valley ratios of typical a few hundred were achieved. In total, 300 spectra were taken for ^{208}Pb(p,p') with a typical length of 0.9 MeV. For both the ^{208}Pb(d,d') and the ^{207}Pb(d,p) reactions about 100 spectra with a length of 1.5 and 2.0 MeV were taken.

We studied ten different particle-exchange reactions, namely the ^{208}Pb(p,p') reaction via the seven known IARs in ^{209}Bi, which is equivalent to the neutron pickup reaction on a target of ^{209}Pb in excited states or in the ground state, the ^{208}Pb(d,d'), ^{207}Pb(d,p), and off-resonance ^{208}Pb(p,p') reactions.

A typical resolution of 3 keV was obtained. Yet the peak shape is asymmetric, mostly the half-width at half-maximum is 1.5 keV on the low energy side, but on the high-energy side it is generally up to three times worse. Excitation energies are determined with a median uncertainty of 70 eV for ^{208}Pb(p,p') and starting with uncertainties of 20 eV, and 150 eV for ^{208}Pb(d,d') and 250 eV for ^{207}Pb(d,p). The uncertainty for about 50 states is better than that obtained by NDS2007 [1], but within the statistical uncertainty of 2σ. More than 20 doublets are resolved where the states have distances less than 2 keV.

Spin, parity assignment, and structure information are predominantly obtained from the study of the inelastic proton scattering on ^{208}Pb via the seven known IARs in ^{209}Bi; here the particle of a particle-hole configuration is chosen by adjusting the bombarding energy to a certain IAR. The investigation of the ^{207}Pb(d,p) reaction is important because of the high sensitivity of the Q3D magnetic spectrograph; admixtures of a particle-hole configuration can be determined down to 0.1% in strength.

Most states at $E_x < 6.20$ MeV are well described by one-particle–one-hole configurations; however, already around 5.0 MeV collective states are found which consist dominantly of two-particle–two-hole configurations. We extend the schematic shell model without residual interaction by including the coupling of one-particle–one-hole configurations to the lowest collective states with low spins, to each other, and the coupling of the lowest collective states to each other.

Some states with spins of 7^- and 8^-, from 1^+ to 6^+, 9^+, 10^+, and 12^+ are excited by the ^{207}Pb(d,p) reaction; the excitation can be explained by admixtures of two-particle–two-hole configurations. A newly discovered IAR in ^{209}Bi at $E^{\mathrm{res}} = 17.6$ MeV populates states which contain two-particle–two-hole configurations.

The ^{208}Pb(d,d') reaction clearly identifies states in ^{208}Pb which ^{208}Pb(p,p') and ^{207}Pb(d,p) are unable to recognize because of neighboring states with extremely large cross cross sections; its cross sections do not show any correlation with spin and parity of the state within the range of scattering angles at $\Theta \approx 45^\circ$. Interference effects between pairs of states with similar configuration mixing were noted. Similar interference effects are recognized in the ^{206}Pb(t,p) and ^{210}Pb(p,t) reactions after recalibrating the excitation energies.

Half of the states belong to doublets where the states are separated by less than 6 keV; still every fourth state belongs to 2-keV doublets. The possibility of the ^{208}Pb(p,p') reaction via IAR in ^{209}Bi to choose the particle in the particle-hole configuration dissolved some of these doublets, even with vanishing distances.

We identify 151 states at $E_x < 6.20$ MeV while the extended schematic shell model (eSM) predicts around 146 states. The spin and parity assignments are derived in a plausible, consistent manner. Four new states are identified, 22 spins are newly assigned, half a dozen spins suggested by NDS2007 are confirmed.

Since the publication of NDS2007 spin or parity was newly assigned to nearly sixty states. More than 40 levels listed by NDS2007 at $E_x < 6.20$ MeV are suggested to be spurious. Many of these levels are listed twice because of limitations in the resolution or calibration in experiments performed before 2007.

Needless to say that the demonstrated completeness of the level scheme for ^{208}Pb at $E_x < 6.2$ MeV does not exclude some incorrect spin or parity assignment or a missing state.

The paper discusses essentially only the identification, spin, and parity of each state at $E_x < 6.20$ MeV but not the full structure information. Many states are known to contain up to a dozen particle-hole components with good precision [6,18,87,88]. Matrix elements of the residual interaction among the particle-hole configurations in the modified schematic shell model (mSM) can be determined by future work.

ACKNOWLEDGMENTS

We thank T. von Egidy for discussions. We thank F. Riess for several privatissima on GASPAN. We remember the late K. H. Maier with whom we discussed the shell model around ^{208}Pb for many years.

[1] M. J. Martin, Nucl. Data Sheets **108**, 1583 (2007).
[2] M. Löffler, H. J. Scheerer, and H. Vonach, Nucl. Instrum. Methods Phys. Res. B **111**, 1 (1973).
[3] J. Ott, H. Angerer, T. von Egidy, R. Georgii, and W. Schauer, Nucl. Instr. Methods A **367**, 280 (1995).
[4] H.-F. Wirth, Ph.D. thesis, Technische Universität München, 2001; http://mediatum.ub.tum.de/?id=602907.
[5] A. Heusler, G. Graw, R. Hertenberger, F. Riess, H.-F. Wirth, T. Faestermann, R. Krücken, J. Jolie, D. Mücher, N. Pietralla, and P. von Brentano, Phys. Rev. C **74**, 034303 (2006).
[6] A. Heusler, G. Graw, R. Hertenberger, R. Krücken, F. Riess, H.-F. Wirth, and P. von Brentano, Phys. Rev. C **75**, 024312 (2007).
[7] A. Heusler, P. von Brentano, T. Faestermann, G. Graw, R. Hertenberger, J. Jolie, R. Krücken, K. H. Maier, D. Mücher, N. Pietralla, F. Riess, V. Werner, and H.-F. Wirth. In A. Covello, editor, *Proceedings of the 9th International Spring Seminar on Nuclear Physics: Changing Facets of Nuclear Structure* (World Scientific, Singapore, 2008), p. 293.
[8] A. Heusler, P. von Brentano, T. Faestermann, G. Graw, R. Hertenberger, J. Jolie, R. Krücken, K. H. Maier, D. Mücher, N. Pietralla, F. Riess, V. Werner, and H.-F. Wirth. In *Proceedings of the 23th International Nuclear Physics Conference (INPC2007), Tokyo* (2007), Vol. 2, p. 254, http://inpc2007.riken.jp/F/F4-heusler.pdf
[9] A. Heusler and P. von Brentano, Eur. Phys. J. A **38**, 6 (2008).
[10] A. Heusler, T. Faestermann, R. Hertenberger, R. Krücken, H.-F. Wirth, and P. von Brentano, Eur. Phys. J. A **46**, 17 (2010).
[11] A. Heusler, G. Graw, T. Faestermann, R. Hertenberger, H.-F. Wirth, R. Krücken, C. Scholl, and P. von Brentano, Eur. Phys. J. A **44**, 233 (2010).
[12] A. Heusler, G. Graw, R. Hertenberger, F. Riess, H.-F. Wirth, T. Faestermann, R. Krücken, Th. Behrens, V. Bildstein, K. Eppinger, C. Herlitzius, O. Lepyoshkina, M. Mahgoub, A. Parikh, S. Schwertel, K. Wimmer, N. Pietralla, V. Werner, J. Jolie, D. Mücher, C. Scholl, and P. von Brentano, Phys. Rev. C **82**, 014316 (2010).
[13] A. Heusler, J. Phys.: Conf. Ser. **267**, 012038 (2011).
[14] A. Heusler, T. Faestermann, G. Graw, R. Hertenberger, R. Krücken, H.-F. Wirth, and P. von Brentano, Eur. Phys. J. A **47**, 22 (2011); **47**, 29 (2011).
[15] A. Heusler, T. Faestermann, R. Hertenberger, R. Krücken, H.-F. Wirth, and P. von Brentano, J. Phys. G (London) **38**, 105102 (2011).
[16] A. Heusler, R. V. Jolos, and P. von Brentano, Yad. Fiz. **76**, 860 (2013) [Phys. At. Nuclei **76**, 807 (2013)].
[17] A. Heusler, T. Faestermann, R. Hertenberger, H.-F. Wirth, and P. von Brentano, EPJ Web Conf. **66**, 02049 (2014).
[18] A. Heusler, T. Faestermann, R. Hertenberger, H.-F. Wirth, and P. von Brentano, Phys. Rev. C **89**, 024322 (2014).

[19] A. Heusler, J. Phys.: Conf. Ser. **580**, 012021 (2015).
[20] A. Heusler, T. Faestermann, R. Hertenberger, H.-F. Wirth, and P. von Brentano, Phys. Rev. C **91**, 044325 (2015).
[21] C. F. Moore, L. J. Parish, P. von Brentano, and S. A. A. Zaidi, Phys. Lett. **22**, 616 (1966).
[22] P. Richard, W. G. Weitkamp, W. Wharton, H. Weiman, and P. von Brentano, Phys. Lett. B, **26**, 8 (1967).
[23] C. F. Moore, J. G. Kulleck, P. von Brentano, and F. Rickey, Phys. Rev. **164**, 1559 (1967).
[24] S. A. A. Zaidi, L. J. Parish, J. G. Kulleck, C. F. Moore, and P. von Brentano, Phys. Rev. **165**, 1312 (1968).
[25] W. R. Wharton, P. von Brentano, W. K. Dawson, and P. Richard, Phys. Rev. **176**, 1424 (1968).
[26] P. Richard, P. von Brentano, H. Weiman, W. Wharton, W. G. Weitkamp, W. W. McDonald, and D. Spalding, Phys. Rev. **183**, 1007 (1969).
[27] H.-J. Glöckner, Master's thesis, Universität Heidelberg, 1972, http://www.mpi-hd.mpg.de/personalhomes/hsl/HJG_diplom/
[28] A. Heusler, H.-J. Glöckner, E. Grosse, C. F. Moore, J. Solf, and P. von Brentano, Eur. Phys. J. A **50**, 92 (2014).
[29] A. Heusler, H. L. Harney, and J. P. Wurm, Nucl. Phys. A **135**, 591 (1969).
[30] A. Heusler, Nucl. Phys. A **141**, 667 (1970).
[31] A. Heusler, Original and processed data for ^{208}Pb, taken with the Q3D magnetic spectrograph, (1) computer garching.physik.uni-muenchen.de, directory /o/expt/polar/HsL/Blei208_Q3D, (2) computer lfs1.mpi-hd.mpg.de, directory /d1/hfm/ctgroup/hsl/Blei208_Q3D; ask computer staff for accessing the data.
[32] P. B. Vold, J. O. Andreassen, J. R. Lien, A. Graue, E. R. Cosman, W. Dünnweber, D. Schmitt, and F. Nüsslin, Nucl. Phys. A **215**, 61 (1973).
[33] B. D. Valnion. Ph.D. thesis, Universität München, 1998, Herbert Utz Verlag, München.
[34] B. D. Valnion, V. Yu. Ponomarev, Y. Eisermann, A. Gollwitzer, R. Hertenberger, A. Metz, P. Schiemenz, and G. Graw, Phys. Rev. C **63**, 024318 (2001).
[35] J. H. Bjerregaard, Ole Hansen, O. Nathan, and S. Hinds, Nucl. Phys. **89**, 337 (1966).
[36] G. J. Igo, P. D. Barnes, and E. R. Flynn, Phys. Rev. Lett. **24**, 470 (1970).
[37] G. Igo, P. D. Barnes, and E. R. Flynn, Ann. Phys. (N. Y.) **66**, 60 (1971).
[38] G. Mairle, K. Schindler, P. Grabmayr, G. J. Wagner, U. Schmidt-Rohr, G. P. A. Berg, W. Hürlimann, S. A. Martin, J. Meissburger, J. G. H. Römer, B. Styczen, and J. L. Tain, Phys. Lett. B **121**, 307 (1983).
[39] G. Mairle and P. Grabmayr, Z. Phys. A **325**, 243 (1986).
[40] P. Grabmayr, G. Mairle, U. Schmidt-Rohr, G. P. A. Berg, J. Meissburger, P. von Rossen, and J. L. Tain, Nucl. Phys. A **469**, 285 (1987).
[41] P. Grabmayr (private communication).
[42] U. Atzrott, Ph.D. thesis, Universität Tübingen, 1995.
[43] U. Atzrott (private communication).
[44] B. D. Valnion, W. Oelmaier, D. Hofer, E. Zanotti-Müller, G. Graw, U. Atzrott, F. Hoyler, and G. Staudt, Z. Phys. A **350**, 11 (1994).
[45] J. G. Cramer, P. von Brentano, G. W. Phillips, H. Ejiri, S. M. Ferguson, and W. J. Braithwaite, Phys. Rev. Lett. **21**, 297 (1968).
[46] E. Radermacher, M. Wilhelm, S. Albers, J. Eberth, N. Nicolay, H. G. Thomas, H. Tiesler, P. von Brentano, R. Schwengner, S. Skoda, G. Winter, and K. H. Maier, Nucl. Phys. A **597**, 408 (1996).
[47] M. Schramm, K. H. Maier, M. Rejmund, L. D. Wood, N. Roy, A. Kuhnert, A. Aprahamian, J. Becker, M. Brinkman, D. J. Decman, E. A. Henry, R. Hoff, D. Manatt, L. G. Mann, R. A. Meyer, W. Stoeffl, G. L. Struble, and T.-F. Wang, Phys. Rev. C **56**, 1320 (1997).
[48] J. Lichtenstadt, J. Heisenberg, C. N. Papanicolas, C. P. Sargent, A. N. Courtemanche, and J. S. McCarthy, Phys. Rev. C **20**, 497 (1979).
[49] J. Lichtenstadt, C. N. Papanicolas, C. P. Sargent, J. Heisenberg, and J. S. McCarthy, Phys. Rev. Lett. **44**, 858 (1980).
[50] D. Goutte, J. B. Bellicard, J. M. Cavedon, B. Frois, M. Huet, P. Leconte, Phan Xuan Ho, S. Platchkov, J. Heisenberg, J. Lichtenstadt, C. N. Papanicolas, and I. Sick, Phys. Rev. Lett. **45**, 1618 (1980).
[51] J. Heisenberg, J. Lichtenstadt, C. N. Papanicolas, and J. S. McCarthy, Phys. Rev. C **25**, 2292 (1982).
[52] J. P. Connelly, D. J. DeAngelis, J. H. Heisenberg, F. W. Hersman, W. Kim, M. Leuschner, T. E. Milliman, J. Wise, and C. N. Papanicolas, Phys. Rev. C **45**, 2711 (1992).
[53] Minfang Yeh, P. E. Garrett, C. A. McGrath, S. W. Yates, and T. Belgya, Phys. Rev. C **54**, 942 (1996).
[54] M. Yeh, P. E. Garrett, C. A. McGrath, S. W. Yates, and T. Belgya, Phys. Rev. Lett. **76**, 1208 (1996).
[55] M. Yeh, P. E. Garrett, C. A. McGrath, S. W. Yates, and T. Belgya, Phys. Rev. C **57**, R2085 (1998).
[56] T. Belgya, B. Fazekas, Zs. Kasztovszky, Zs. Revay, G. Molnár, M. Yeh, P. E. Garrett, and S. W. Yates, Phys. Rev. C **57**, 2740 (1998).
[57] J. N. Orce, T. Kibédi, G. D. Dracoulis, R. Julin, and S. W. Yates, J. Phys. (London) G **31**, S1705 (2005).
[58] W. T. Wagner, G. M. Crawley, G. R. Hammerstein, and H. McManus, Phys. Rev. C **12**, 757 (1975).
[59] G. S. Adams, A. D. Bacher, G. T. Emery, W. P. Jones, D. W. Miller, W. G. Love, and F. Petrovich, Phys. Lett. B **91**, 23 (1980).
[60] A. D. Bacher, G. T. Emery, W. P. Jones, D. W. Miller, G. S. Adams, F. Petrovich, and W. G. Love, Phys. Lett. B **97**, 58 (1980).
[61] A. D. Bacher, G. T. Emery, W. P. Jones, D. W. Miller, G. S. Adams, F. Petrovich, and W. G. Love, Annual Report IUCF (Bloomington), p. 38 (1988–1989).
[62] F. Petrovich, W. G. Love, G. S. Adams, A. D. Bacher, G. T. Emery, W. P. Jones, and D. W. Miller, Phys. Lett. B **91**, 27 (1980).
[63] D. Cook, N. M. Hintz, M. M. Gazzaly, G. Pauletta, R. W. Fergerson, G. W. Hoffmann, J. B. McClelland, and K. W. Jones, Phys. Rev. C **35**, 456 (1987).
[64] Y. Fujita, T. Yanagihara, M. Fujiwara, I. Katayama, K. Hosono, S. Morinobu, T. Yamazaki, S. I. Hayakawa, K. Katori, K. Muto, and H. Ikegami, Phys. Lett. B **247**, 219 (1990).
[65] I. Talmi, *Contemporary Concepts in Physics*, Simple Models of Complex Nuclei (Harwood Academic Publishers, Chur, Switzerland, 1993), Vol. 7.
[66] C. Ellegaard, J. Kantele, and P. Vedelsby, Nucl. Phys. A **129**, 113 (1969).

[67] A. Bohr, in *Nuclear Structure: Dubna Symposium* (International Atomic Energy Agency, Vienna, 1968), p. 179.
[68] R. V. Jolos, A. Heusler, and P. von Brentano, Phys. Rev. C **92**, 011302(R) (2015).
[69] M. Rejmund, K. Maier, R. Broda, B. Fornal, M. Lach, J. Wrzesiński, J. Blomqvist, A. Gadea, J. Gerl, M. G'orska, H. Grawe, M. Kaspar, H. Schaffner, Ch. Schlegel, R. Schubart, and H. Wollersheim, Eur. Phys. J. **8**, 161 (2000).
[70] J. Wrzesiński, K. H. Maier, R. Broda, B. Fornal, W. Królas, T. Pawlat, D. Bazzacco, S. Lunardi, C. Rossi Alvarez, G. de Angelis, A. Gadea, J. Gerl, and M. Rejmund, Eur. Phys. J. A **10**, 259 (2001).
[71] R. Broda, B. Fornal, W. Królas, T. Pawłat, J. Wrzesiński, D. Bazzac, G. Arngel, S. Lunard, and C. Rossi-Alvarez, Eur. Phys. J. A **20**, 145 (2003).
[72] G. Audi, A. H. Wapstra, and C. Thibault, Nucl. Phys. **729**, 337 (2003).
[73] M. Wang, G. Audi, A. H. Wapstra, F. G. Kondev, M. MacCormick, X. Xu, and B. Pfeiffer, Chin. Phys. C **36**, 1603 (2012).
[74] National Nuclear Data Center, Brookhaven, Evaluated Nuclear Structure Data File, http://ie.lbl.gov/ensdf/
[75] V. M. Slipher, Astron. Nachr. **189**, 5 (1911).
[76] H. J. Wollersheim, P. Egelhof, H. Emling, J. Gerl, W. Henning, R. Holzmann, R. Schmidt, R. S. Simon, N. Martin, G. Eckert, Th. W. Elze, K. Stelzer, R. Kulessa, G. Duchene, B. Haas, J. C. Merdinger, J. P. Vivien, J. de. Boer, E. Hauber, K. Kaiser, P. von Brentano, R. Reinhardt, R. Wirowski, R. Julin, C. Fahlander, I. Thorslund, and H. Kluge, Z. Phys. A **341**, 137 (1992).
[77] L. W. Nordheim, Phys. Rev. **78**, 294 (1950).
[78] A. de-Shalit, Phys. Rev. **91**, 1479 (1953).
[79] J. P. Schiffer, Ann. Phys. (NY) **66**, 798 (1971).
[80] T. T. S. Kuo and G. E. Brown, Nucl. Phys. **85**, 40 (1966).
[81] T. T. S. Kuo, J. Blomqvist, and G. E. Brown, Phys. Lett. B **31**, 93 (1970).
[82] T. T. S. Kuo and G. E. Brown (private communication).
[83] B. A. Brown, Phys. Rev. Lett. **85**, 5300 (2000).
[84] B. A. Brown (private communication).
[85] K. H. Maier, Acta Phys. Pol. B **32**, 899 (2001).
[86] K. H. Maier (private communication).
[87] A. Heusler and P. von Brentano, Ann. Phys. (NY) **75**, 381 (1973).
[88] A. Heusler, http://www.mpi-hd.mpg.de/personalhomes/hsl/208Pb_eval/appendix_a.pdf
[89] A. Heusler, http://www.mpi-hd.mpg.de/personalhomes/hsl/208Pb_eval/update2013.pdf
[90] A. Bohr and B. R. Mottelson. *Nuclear Structure* (W. A. Benjamin, New York, 1969), Vol. I.
[91] J. H. D. Jensen and M. Goeppert-Mayer, *Elementary Theory of Nuclear Shell Structure* (Wiley, New York, 1955).
[92] G. E. Brown. *Unified Theory of Nuclear Models and Forces* (North Holland, Amsterdam, 1964).
[93] J. Blomqvist, Phys. Lett. B **33**, 541 (1970).
[94] A. Bohr and B. R. Mottelson, *Nuclear Structure* (W. A. Benjamin, New York, 1975), Vol. II.
[95] D. J. Decman, J. A. Becker, J. B. Carlson, R. G. Lanier, L. G. Mann, G. L. Struble, K. H. Maier, W. Stöffl, and R. K. Sheline, Phys. Rev. C **28**, 1060 (1983).
[96] M. Anselment, W. Faubel, S. Göring, A. Hanser, G. Meisel, H. Rebel, and G. Schatz, Nucl. Phys. A **451**, 471 (1986).
[97] O. Häusser, T. K. Alexander, J. R. Beene, E. D. Earle, A. B. McDonald, F. C. Khanna, and I. S. Towner, Nucl. Phys. A **273**, 253 (1976).
[98] T. Bastuğ, B. Fricke, M. Finkbeiner, and W. R. Johnson, Z. Phys. D **37**, 281 (1996).
[99] I. Hamamoto and P. Siemens, Nucl. Phys. A **269**, 199 (1976).
[100] W. Dünnweber, E. R. Cosman, E. Grosse, and W. R. Hering, Nucl. Phys. A **247**, 251 (1975).
[101] P. Mukherjee, I. Mukherjee, and R. Majumdar, Nucl. Phys. A **294**, 73 (1978).
[102] R. A. Broglia and P. F. Bortignon, Phys. Lett. B **65**, 221 (1976).
[103] M. Rejmund, M. Schramm, and K. H. Maier, Phys. Rev. C **59**, 2520 (1999).
[104] F. Riess, http://www.it.physik.uni-muenchen.de/dienste/software/gaspan/index.html, Gamma-ray and particle spectra interactive and automatic analysis, GASPAN.
[105] Experimental Nuclear Reaction Data (EXFOR), data sets O1860, O1861, O1866, O2171 (Heusler), http://www.nndc.bnl.gov/exfor/exfor.htm.
[106] M. B. Lewis, Nucl. Data Sheets **5**, 243 (1971).
[107] M. J. Martin, Nucl. Data Sheets **47**, 797 (1986).
[108] A. v. d. Decken, M. Goldschmidt, A. Heusler, H. V. Klapdor, W. Reiter, D. Rieck, W. Saathoff, C. A. Wiedner, and D. Dehnhard, Z. Phys. **260**, 247 (1973).
[109] E. Weber, W. Knüpfer, E. Grecksch, and M. G. Huber, Phys. Lett. B **65**, 189 (1976).